5-2007

Preparation, Characterization and Reactivities of Early Transition Metal Silyl Compounds

He Qiu
University of Tennessee - Knoxville

To the Graduate Council:

I am submitting herewith a dissertation written by He Qiu entitled "Preparation, Characterization and Reactivities of Early Transition Metal Silyl Compounds." I have examined the final electronic copy of this dissertation for form and content and recommend that it be accepted in partial fulfillment of the requirements for the degree of Doctor of Philosophy, with a major in Chemistry.

Ziling Xue, Major Professor

We have read this dissertation and recommend its acceptance:

Jamie L. Adcock, Richard M. Pagni, Xuemin Xu

Accepted for the Council:

Carolyn R. Hodges

Vice Provost and Dean of the Graduate School

(Original signatures are on file with official student records.)

To the Graduate Council:

I am submitting herewith a dissertation written by He Qiu entitled “Preparation, Characterization and Reactivities of Early Transition Metal Silyl Compounds.” I have examined the final electronic copy of this dissertation for form and content and recommend that it be accepted in partial fulfillment of the requirements for the degree of Doctor of Philosophy, with a major in Chemistry.

Ziling Xue
Major Professor

We have read this dissertation
and recommend its acceptance:

Jamie L. Adcock

Richard M. Pagni

Xuemin Xu

Accepted for the Council:

Linda R. Painter
Interim Dean of Graduate Studies

(Original Signatures are on file with official student records)

PREPARATION, CHARACTERIZATION AND REACTIVITIES OF EARLY-TRANSITION-METAL SILYL COMPOUNDS

A Dissertation

Presented for the

Doctor of Philosophy Degree

The University of Tennessee, Knoxville

He Qiu

May 2007

DEDICATION

This dissertation is dedicated to

my parents: Shilun Qiu and Nanjie Liu.

ACKNOWLEDGMENTS

Many people have been instrumental in allowing this dissertation to be completed. I would first like to thank especially Dr. Ziling Xue, my Ph.D. advisor at the University of Tennessee, for his patience and guidance throughout the duration of my Ph.D. studies. The door to Dr. Xue's office was always open whenever I ran into a trouble or a question about my research. His words of encouragement, quiet urgings and careful reading of all of my writings will never be forgotten.

I also want to thank my committee members, Dr. Jamie Adcock, Dr. Richard Pagni, and Dr. Xuemin Xu, who agreed to serve on my dissertation committee and to review my Ph.D. research.

I would like to thank the following individuals who have given me assistance to complete the work: Dr. Xiaobin Feng at the University of Tennessee for his help in setting up a mathematical model to understand the kinetic process in Chapter 4, Minyoung Lee, Jason Clark and Dr. Hongjun Pan at the University of Tennessee for the help on the 400 MHz NMR spectrometer, Dr. Al Tuinman at the University of Tennessee for his help on mass spectrometric analyses, Xianghua Yu at the University of Tennessee and Dr. Ilia A. Guzei at the University of Wisconsin, Madison, for help with X-ray crystallography.

Let me also say "thank you" to some of the past and present members of Dr. Xue's group: Dr. Hu Cai, Dr. Ruitao Wang, Dr. Shujian Chen, Dr. Li Yong, Cheri Clavier, Tianniu Chen, Hee-Jung Im, Jaime Blanton, Andy Canada,

Xianghua Yu, Laurie Morton, Lynn Rodman, Nathan Carrington, Kristie Armstrong, Brenda Dougan, Julia Covington, Royce Dansby-Sparks, and Tara Williams. I will miss the lunch time conversations and debate. I own special thanks to Xianghua Yu for training me in single crystal X-ray diffraction and Dr. Hu Cai for helping me start my research.

Finally I would like to thank the National Science Foundation and the Camille Dreyfus Teacher-Scholar program for supporting my graduate research in the past five years.

ABSTRACT

This dissertation focuses on syntheses, characterization and reactivities of Groups 4 and 5 metal amide silyl complexes free of anionic π-ligands.

A summary of the research in this dissertation is provided in Chapter 1. Chapter 2 reports an unusual reaction between $Ta(NMe_2)_4SiBu^tPh_2$ (**1**) and O_2. Three products $(Me_2N)_4Ta(OSiBu^tPh_2)$ (**2**), $(Me_2N)_3Ta(ONMe_2)(OSiBu^tPh_2)$ (**3**) and $(Me_2N)_2(Ph_2Bu^tSiO)_2(Me_2NCH_2NMe)_2Ta_2(\mu\text{-}O)_2$ (**4**) were isolated from the reaction.

Preparation and characterization of Hf and Ta disilyl complexes are presented in Chapter 3. Novel exchange processes of Zr and Hf amides with silyl ligands were are described in this Chapter.

Chapter 4 describes the kinetics studies of complex $(Me_2N)_3Ta[Si(SiMe_3)_3]_2$ (**11**) complexes with $LiSiBu^tPh_2$ (**7**). The reaction mechanism was found to follow a dissociative pathway. Tetrahydrofuran (THF) was found to promote the substitution.

Chapter 5 reports the studies of the thermal decomposition of $(Me_2N)_3Ta(SiBu^tPh_2)_2$ (**15**) and $(Me_2N)_3Ta(SiBu^tPh_2)[Si(SiMe_3)_3]$ (**16**). First-order kinetics was observed and the activation parameters $\Delta H^{\neq}$, $\Delta S^{\neq}$, and $\Delta G^{\neq}_{298\,K}$ for the reaction have been obtained. Heating the mixture of $W(CH_2SiMe_3)_3(\equiv CSiMe_3)(PMe_2Ph)$ (**18a**) and its bis(alkylidene) tautomer $W(CH_2SiMe_3)_2(=CHSiMe_3)_2(PMe_2Ph)$ (**18b**) in the presence of excess PMe_2Ph

leads to the formation of $W(CH_2SiMe_3)(=CHSiMe_3)(\equiv CSiMe_3)(PMe_2Ph)_2$ (**19**). The reaction process was found to follow first-order kinetics, and the rate constant is independent of the concentrations of PMe_2Ph. A possible mechanistic pathway is discussed.

TABLE OF CONTENTS

LIST OF TABLES

LIST OF FIGURES

LIST OF SCHEMES

NUMBERING SCHEME FOR COMPOUNDS IN THE TEXT

1	$(Me_2N)_4Ta(SiBu^tPh_2)$
2	$(Me_2N)_4Ta(OSiBu^tPh_2)$
3	$(Me_2N)_3Ta(ONMe_2)(OSiBu^tPh_2)$
4	$(Me_2N)_2(Ph_2Bu^tSiO)_2(Me_2NCH_2NMe)_2Ta_2(\mu\text{-}O)_2$
5	$(Me_2N)_4TaCl$
6	$LiOSiBu^tPh_2$
7	$Li(THF)_2SiBu^tPh_2$
8	$(Me_2N)_3HfCl$
9	$[K(18\text{-crown-}6)]_2[(Me_3Si)_2Si\text{-}(CH_2)_2\text{-}Si(SiMe_3)_2]$
10	$K(18\text{-crown-}6)_{3/2}\{(Me_2N)_3Hf[\eta^2\text{-}(Me_3Si)_2Si(CH_2)_2Si(SiMe_3)_2]\}$
11	$(Me_2N)_3Ta[Si(SiMe_3)_3]_2$
12	$(Me_2N)_3Ta[Si(SiMe_3)_3]Cl$
13	$Li(THF)_3Si(SiMe_3)_3$
14	$(Me_2N)_3TaCl_2$
15	$(Me_2N)_3Ta(SiBu^tPh_2)_2$
16	$(Me_2N)_3Ta(SiBu^tPh_2)[Si(SiMe_3)_3]$
17	$(Me_2N)_3Ta(SiBu^tPh_2)Cl$
18a	$W(CH_2SiMe_3)_3(\equiv CSiMe_3)(PMe_2Ph)$
18b	$W(CH_2SiMe_3)_2(=CHSiMe_3)_2(PMe_2Ph)$
19	$W(CH_2SiMe_3)(=CHSiMe_3)(\equiv CSiMe_3)(PMe_2Ph)$

20 $(Me_2N)_4Ta\text{-}Si(SiMe_3)_3$

21 $(Me_2N)_3Ta(\eta^2\text{-}ONMe_2)[OSi(SiMe_3)_3]$

22 $Ta(NMe_2)_4(\eta^2\text{-}NMeCH_2NMe_2)$

23 $K(18\text{-crown-}6)_{3/2}\{(Me_2N)_3Zr[\eta^2\text{-}(Me_3Si)_2Si(CH_2)_2Si(SiMe_3)_2]\}$

24 $[K(18\text{-crown-}6)]_2[(Me_3Si)_2Si\text{-}(CH_2)_3\text{-}Si(SiMe_3)_2]$

25a $W(CH_2SiMe_3)_3(\equiv CSiMe_3)(PMe_3)$

25b $W(CH_2SiMe_3)_2(=CHSiMe_3)_2(PMe_3)$

26 $W(CH_2SiMe_3)(=CHSiMe_3)(\equiv CSiMe_3)(PMe_3)_2$

27 $Zr(NMe_2)_3[N(SiMe_3)_2]$

CHAPTER 1

Introduction

1.1. Foreword

Silyl derivatives of transition metals are of intense current interest for their unique structures, reactivities and catalytic applications.[1] Early-transition-metal silyl chemistry is of intense current interest. In particular, catalytic hydrosilylation of olefins and the polymerization of hydrosilanes (Scheme 1.1) have been actively investigated.[2] Early-transition-metal silyl complexes are precursors to dehydropolymerization catalysts.[3] For example, Tilley's group has reported that the reaction of Cp*(ArN=)Ta[Si(SiMe$_3$)$_3$]H (Cp* = η^5-C$_5$Me$_5$; Ar = 2,6-diisopropylphenyl) with PhSiH$_3$ gives two dimeric products Cp*$_2$(ArN=)Ta$_2$H$_2$(μ-ArNSiHPh) and Cp*$_2$Ta$_2$H$_2$(μ-ArNSiHPh)$_2$ containing bridging silanimine ligands (Scheme 1.2).[3d] These complexes are probably formed from σ-bond metathesis reactions. Our interest has focused on the development of d^0 early-transition-metal silyl amide complexes free of cyclopentadienyl groups.[4]

Most of the previously reported early-transition-metal silyl complexes contain cyclopentadienyl (Cp) or analogous anionic π-ligands.[1] We have been interested in Cp-free transition metal silyl amide complexes as they are related to molecular approaches to microelectronic metal silicides and metal silicate (M-Si-O) ternary materials. Only a few Cp-free early-transition-metal silyl complexes have been reported.[4-9] This area of early-transition-metal chemistry is

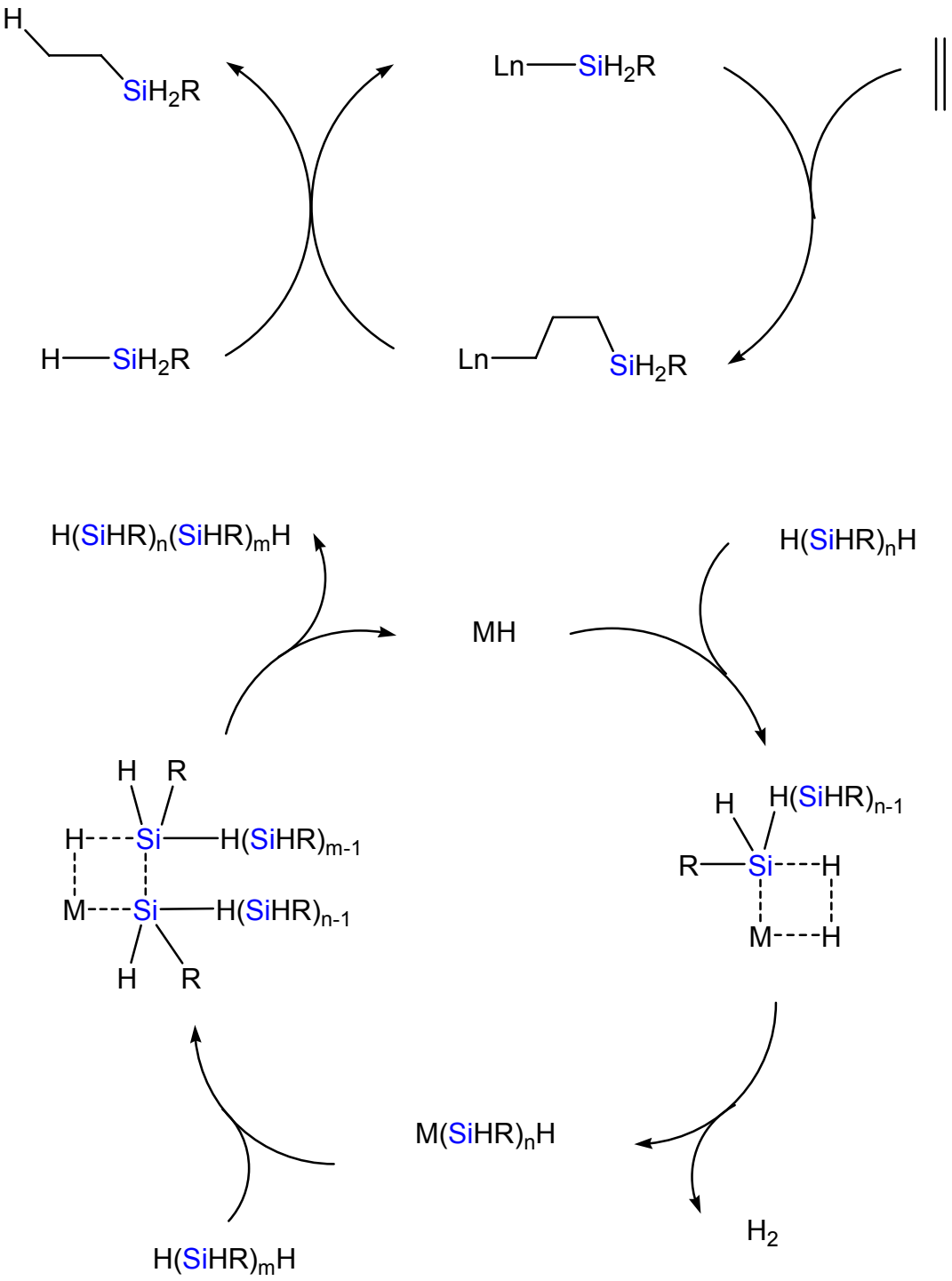

Scheme 1.1. Mechanistic pathways for catalytic hydrosilylation of olefins[2] and the polymerization of hydrosilanes

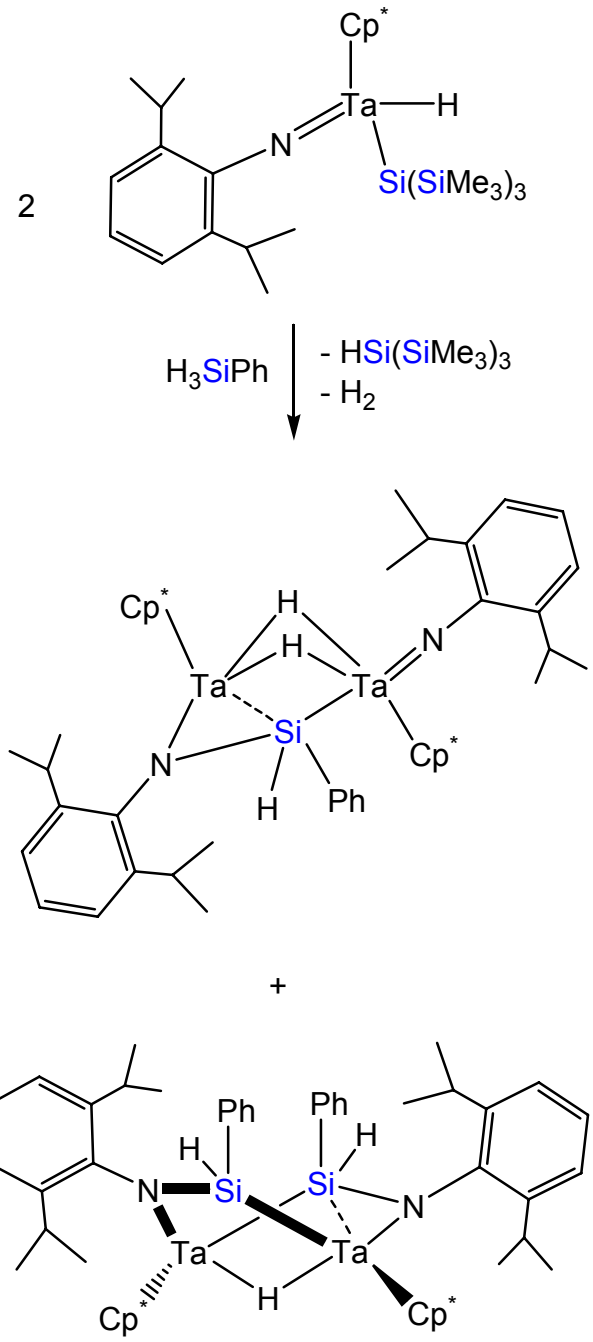

Scheme 1.2. The reaction of Cp*(ArN=)Ta[Si(SiMe$_3$)$_3$]H (Cp* = η^5-C$_5$Me$_5$) with PhSiH$_3$ [3d]

thus relatively new. Our work has been focused on the preparation, structures, characterization, and reactivities of Cp-free early-transition-metal silyl amide complexes. New silyl complexes have been prepared and characterized by NMR spectroscopy, elemental analysis, and single-crystal X-ray crystallography. In the reactivities of these silyl complexes, we are particularly interested in their reactions with O_2 and substitution reactions. Nearly all early-transition-metal silyl complexes investigated in this dissertation are in high oxidation states of the metals, and have no valence *d* electrons. They are thus d^0 transition metal complexes.

Reactions of O_2 with d^0 transition metal complexes are key steps in the chemical vapor deposition (CVD) processes. CVD is an important technique widely used in the microelectronic industry and in research laboratories to prepare thin films of metal silicides, metal oxide (MO_n), and metal silicate (M-Si-O) ternary materials in very-large-scale-integration (VLSI) devices.[10] The mechanistic pathways in the formation of these materials are largely unexplored. An understanding of the pathways is important in the design of the precursor compounds and CVD processes. The mechanistic pathways in the reactions of O_2 with d^0 transition metal complexes are also of fundamental interest as analyzed below:

(a) Early-transition-metal complexes are known to be air-sensitive – They readily react with oxygen (or moisture) in air. However the nature of such reactivity is often not understood.

(b) The d^0 transition metal complexes that are used as precursors in the preparation of microelectronic materials have no valence *d* electrons. The metals in the complexes thus cannot undergo oxidation by O_2, as often is the case in the reactions of d^n transition metal complexes with O_2.[11-13] *Ligand oxidation* is thus required for the reactions of O_2 with d^0 transition metal complexes to proceed. Such reactions involving d^0 transition metal complexes are expected to proceed through pathways fundamentally different from those of d^n transition metal complexes.

(c) O_2 is a di-radical in its ground state, and its reactions with d^0 transition metal complexes are thus radical in nature. This feature however adds to the challenges in probing the reactivities here.

As demonstrated in this dissertation, the preparation of new transition-metal silyl complexes is nearly exclusively conducted through substitution reactions by silyl anions for, e.g., halide or amide ligands in the starting materials. The substitution reactions of amide and silyl ligands by incoming silyl anions or dianions (or silyl exchanges in the cases of the substitution of silyl ligands by incoming silyl anions) have been investigated.

1.2. Current Dissertation

This Ph.D. dissertation focuses on the preparation and characterization of novel Cp-free, Groups 4 and 5 silyl complexes, mechanistic pathways in the formation of these compounds, and studies of their reactions with O_2. In addition, the conversion of an equilibrium tautomic mixture of bis(alkyl) bis(alkylidene) tungsten ⇌ tris(alkyl) alkylidyne tungsten to an alkyl alkylidene alkylidyne complex was investigated to obtain a rate constant of the conversion.

1.2.1. *Chapter 2*

Transition-metal silyl amide complex $(Me_2N)_4Ta(SiBu^tPh_2)$ (**1**) was found to react with O_2 to give three new products $(Me_2N)_4Ta(OSiBu^tPh_2)$ (**2**), $(Me_2N)_3Ta(ONMe_2)(OSiBu^tPh_2)$ (**3**) and $(Me_2N)_2(Ph_2Bu^tSiO)_2(Me_2NCH_2NMe)_2Ta_2(\mu\text{-}O)_2$ (**4**). The structure of **4** containing two bridging oxo ligands and chelating Me_2NCH_2NMe(-) ligands was confirmed by single crystal X-ray diffraction. Complex **2** was also prepared from the reaction between $(Me_2N)_4TaCl$ (**5**) and $LiOSiBu^tPh_2$ (**6**). The reaction of **2** with O_2 leads to **3** and **4** as well. This observation suggests that **2** may be an intermediate in the reaction of **1** with O_2 to give **3** and **4**. In another words, an oxygen atom first inserts into the Ta-Si bond in **1** to give $(Me_2N)_4Ta(OSiBu^tPh_2)$ (**2**), followed by a second oxygen insertion into a Ta-N bond leading to **3**. The formation of the chelating Me_2NCH_2NMe(-) ligand in **4** is particularly interesting, although how it is formed in the reaction of $(Me_2N)_4Ta(SiBu^tPh_2)$ (**1**) or $(Me_2N)_4Ta(OSiBu^tPh_2)$ (**2**) with O_2 is not clear.

1.2.2. *Chapter 3*

The reaction of $(Me_2N)_3HfCl$ with $[K(18\text{-crown-}6)]_2[(Me_3Si)_2Si\text{-}(CH_2)_2\text{-}Si(SiMe_3)_2]$ in toluene was found to give chelating disilyl complexes $K(18\text{-crown-}6)_{3/2}\{(Me_2N)_3Hf[\eta^2\text{-}(Me_3Si)_2Si(CH_2)_2Si(SiMe_3)_2]\}$ (**10**). No exchange between the chelating silyl ligands in **10** and excess $Li(THF)_3SiBu^tPh_2$ (**7**) was observed after the two species were mixed in toluene-d_8 for 24 h. This is perhaps not surprising, as the substitution of the chelating $[(Me_3Si)_2Si(CH_2)_2Si(SiMe_3)_2]^{2-}$ ligand in **10** by mono silyl $SiBu^tPh_2^-$ anion is thermodynamically unfavorable.

The tantalum disilyl complex $(Me_2N)_3Ta[Si(SiMe_3)_3]_2$ (**11**) was readily prepared either by the reactions of the silyl chloride complex $(Me_2N)_3Ta[Si(SiMe_3)_3]Cl$ (**12**) with one equiv of $Li(THF)_3Si(SiMe_3)_3$ (**13**) or by the reaction of $(Me_2N)_3TaCl_2$ (**14**) with two equiv of $Li(THF)_3Si(SiMe_3)_3$ (**13**). $(Me_2N)_3Ta(SiBu^tPh_2)_2$ (**15**), an analog of **11**, was similarly prepared. The mixed bis(silyl) complex $(Me_2N)_3Ta(SiBu^tPh_2)[Si(SiMe_3)_3]$ (**16**) was prepared from the reaction of $(Me_2N)_3Ta(SiBu^tPh_2)Cl$ (**12**) with one equiv of $Li(THF)_3Si(SiMe_3)_3$ (**13**).

1.2.3. *Chapter 4*

Tantalum disilyl complex $(Me_2N)_3Ta[Si(SiMe_3)_3]_2$ (**11**) was found to undergo a silyl exchange with $Li(THF)_3SiBu^tPh_2$ to give $(Me_2N)_3Ta(SiBu^tPh_2)_2$ (**15**) and $(Me_2N)_3Ta(SiBu^tPh_2)[Si(SiMe_3)_3]$ (**16**). Kinetic and mechanistic studies of this silyl substitution reaction reveal that it follows a dissociative pathway. The dissociation of the $-Si(SiMe_3)_3$ ligand was found to be the first step, forming a four coordinated Ta species. Then the $-SiBu^tPh_2$ ligands were added to the four

coordinated Ta intermediate to give **16**. In the presence of excess $LiSiBu^tPh_2$, the disappearance of **10** follows pseudo first-order kinetics. Tetrahydrofuran (THF), a polar solvent, was found to promote the substitution with 1.7(0.3) order on THF. The kinetic studies of this THF effect are probed by the change in observed rate constants k_{obs} with different THF concentrations.

1.2.4. *Chapter 5*

Both $(Me_2N)_3Ta(SiBu^tPh_2)_2$ (**15**) and $(Me_2N)_3Ta(SiBu^tPh_2)[Si(SiMe_3)_3]$ (**16**) are thermally unstable, and decompose at 23 °C to give $HSiBu^tPh_2$, $HSiBu^tPh_2$ and $HSi(SiMe_3)_3$, respectively, as well as other unknown Ta species. First-order kinetic plots of the decomposition reactions suggest that they are intramolecular process. Kinetic studies of the decomposition of **16** give the activation parameters of the decomposition of **16**: $\Delta H^{\neq}$ = 22.8(1.3) kcal/mol, $\Delta S^{\neq}$ = –3(5) eu and $\Delta G^{\neq}_{298\,K}$ = 24(3) kcal/mol. Compared with **7** [k = 4.33(0.16) $\times$ 10^{-5} s^{-1}], **15** was found to decompose faster [k =7.2(0.2) $\times$ 10^{-5} s^{-1}] at 303 K.

Heating a mixture of alkyl alkylidyne $W(CH_2SiMe_3)_3(\equiv CSiMe_3)(PMe_2Ph)$ (**18a**) and its bis(alkylidene) tautomer $W(CH_2SiMe_3)_2(=CHSiMe_3)_2(PMe_2Ph)$ (**18b**) in the presence of excess PMe_2Ph leads to an α-hydrogen abstraction reaction and conversion of **18a-b** to alkyl alkylidene alkylidyne $W(CH_2SiMe_3)(=CHSiMe_3)(\equiv CSiMe_3)(PMe_2Ph)_2$ (**19**). The kinetic studies of this reaction are reported in this chapter. The reaction process was found to follow

first-order kinetics, and the rate constant is independent of the concentrations of PMe_2Ph. A possible mechanistic pathway is discussed.

CHAPTER 2

Reaction of a Tantalum Silyl Complex with Oxygen

2.1. Introduction

Reactions of d^0 early-transition-metal complexes with O_2 are among the most important processes in the preparation of metal oxide thin films as microelectronic gate materials.[14-16] Silicon oxide with a dielectric constant of 4.3 has been the gate material of choice for many generations of microelectronic devices over other dielectrics because of its good physical properties and ease of preparation from silicon wafers (through oxidation of silicon). In the next generation of ultra-large scale (ULS) integrated metal–oxide–semiconductor field effect transistor (MOSFET) devices (Figure 2.1), the scaling of gate material thickness is one of the most challenging issues. In order to meet the requirements for sub-100 nm MOSFET devices, an oxide thickness of less than 15 Å is necessary. However, when the SiO_2 thin film is scaled to below 20 Å, the gate leakage current becomes unacceptably high. In other words, SiO_2 is not adequate as the gate material. To satisfy the requirements for sub-100 nm MOSFET devices with a small, acceptable gate leakage current, thin films of metal oxides with large dielectric constants are needed. Much research has been conducted to prepare oxide thin films of early transition metals such tantalum, zirconium and hafnium.[14-16] Reactions of O_2 with d^0 metal amides such as $Ta(NR_2)_5$ (R = Me, Et) and $M(NR_2)_4$ (M = Zr, Hf; R = Me, Et) have been used

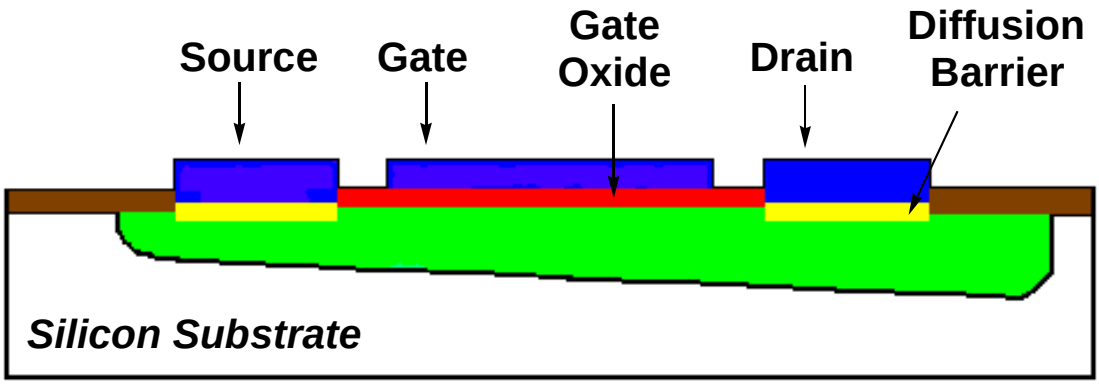

Figure 2.1. Schematic of gate materials in microelectronic devices

to yield thin films of Ta_2O_5 (ε = 26), ZrO_2 (ε = 25) and HfO_2 (ε = 25) as gate insulating materials.[14a-d,17,18]

Reactions of O_2 with late-transition-metal complexes have been widely studied in fundamental biological processes and design of oxidation catalysts. Most studies of these reactions involve d^n complexes.[11-13] The presence of the valence *d* electrons in the metal centers often leads to the oxidation of the metals by O_2, and this oxidation is believed to be a driving force of the reactions. There are fewer studies of the reactions of d^0 complexes with O_2, however, because the d^0 metal atoms at their highest oxidation states are unlikely to be oxidized.[19-30] In the reactions of O_2 with d^0 alkyl complexes, oxygen insertion into M-alkyl bond has been reported.[19-21] A similar M-Si bond insertion was observed in the reaction of $Cp_2Zr(SiMe_3)Cl$ with O_2.[22] We recently reported that reactions of amides $M(NMe_2)_4$ (M = Zr, Hf) and $(Me_2N)_4Ta\text{-}Si(SiMe_3)_3$ (**20**) with O_2 yield oxo aminoxo complexes $M_3(NMe_2)_6(\mu\text{-}NMe_2)_3(\mu_3\text{-}O)(\mu_3\text{-}ONMe_2)$[31] and O_2-stable $(Me_2N)_3Ta(\eta^2\text{-}ONMe_2)[OSi(SiMe_3)_3]$ (**21**),[29] respectively (Scheme 2.1). However the fundamental chemistry of the reactions of d^0 amides with O_2 is a still largely unexplored area.

In the current studies, $Ta(NMe_2)_4SiBu^tPh_2$ (**1**), an analog of $(Me_2N)_4Ta\text{-}Si(SiMe_3)_3$ (**20**), was treated with O_2 in order to compare the reactivity of different silyl ligands. This reaction gives $(Me_2N)_4Ta(OSiBu^tPh_2)$ (**2**), $(Me_2N)_3Ta(ONMe_2)(OSiBu^tPh_2)$ (**3**), and the unusual oxo amino $(Me_2N)_2(Ph_2Bu^tSiO)_2(Me_2NCH_2NMe)_2Ta_2(\mu\text{-}O)_2$ (**4**) containing a novel chelating

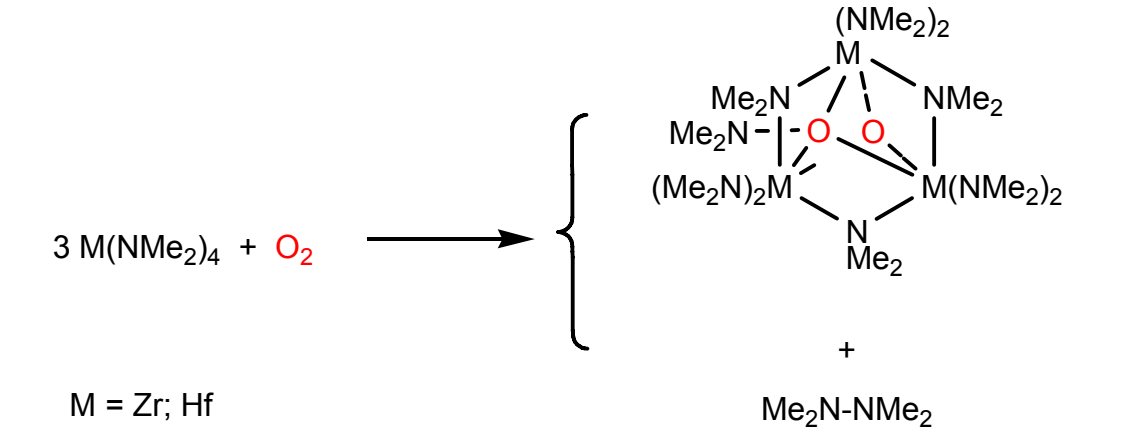

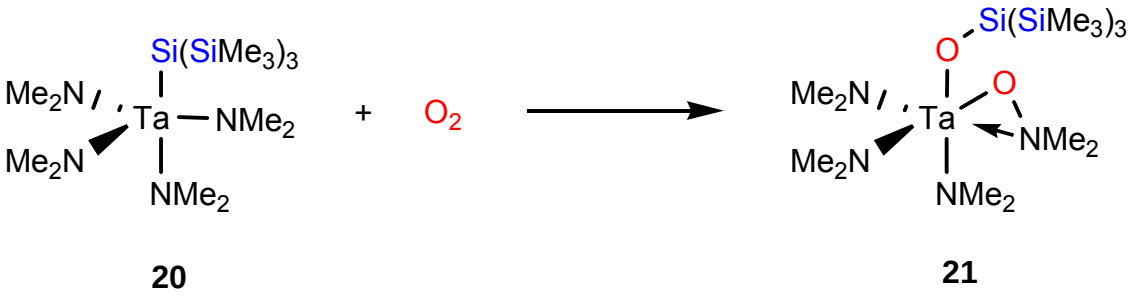

20 **21**

Scheme 2.1. Reactions of d^0 complexes with oxygen[29,31]

(aminomethyl)amide -N(Me)CH_2NMe_2 ligand (Scheme 2.2). $(Me_2N)_4Ta(OSiBu^tPh_2)$ (**2**) has been prepared from the reaction between $(Me_2N)_4TaCl$ (**5**) and $LiOSiBu^tPh_2$ (**6**) (Section 2.2.3). The reaction between **2** and O_2 has also been investigated. Surprisingly both **3** and **4** were found to be the products in this reaction as well. In this chapter, preparation and characterization of **2**, **3** and **4** and our mechanistic studies of the reaction are reported.

2.2. Results and Discussion

2.2.1. *Preparation of $(Me_2N)_4Ta(OSiBu^tPh_2)$ (2), $(Me_2N)_3Ta(ONMe_2)(OSiBu^tPh_2)$ (3) and $(Me_2N)_2(Ph_2Bu^tSiO)_2(Me_2NCH_2NMe)_2Ta_2(\mu\text{-}O)_2$ (4) from the reaction of 1 with O_2*

d^0 Ta amide silyl complex $Ta(NMe_2)_4SiBu^tPh_2$ (**1**) was first reported in 2002, and it was prepared from the reaction of **5** with 1 equiv $Li(THF)_2SiBu^tPh_2$ (**7**) in Et_2O.[29] After **1** was extracted from the reaction mixture by pentane, it was directly used in the reaction of **1** with O_2. The pentane solution was exposed to 1.5 equiv of O_2 at –60 °C, and the deep brown solution of **1** slowly turned to light yellow. A white precipitate was observed at the bottom of the flask. After removal of the volatiles and extraction of the residue by CH_2Cl_2, the solution in CH_2Cl_2 at –32 °C gave colorless crystals of **4** in 4.1% yield. Complex **4** could also be prepared from the reaction of $(Me_2N)_4Ta(OSiBu^tPh_2)$ (**2**) with O_2, as

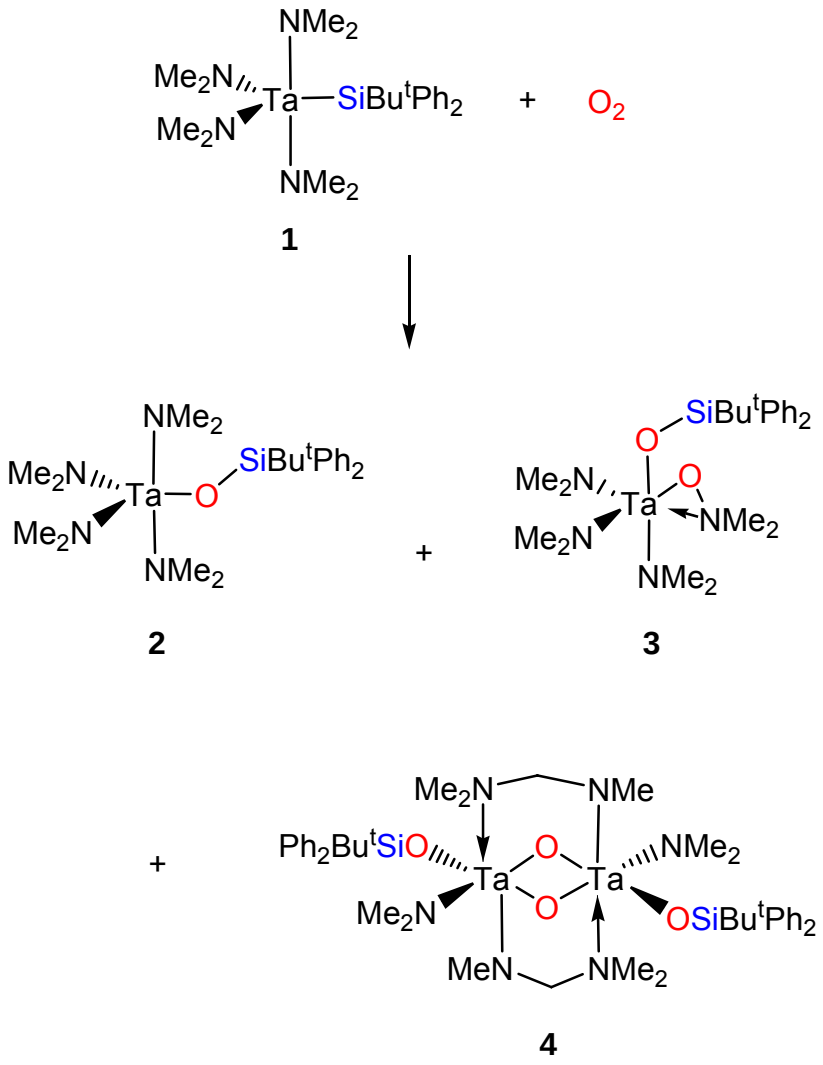

Scheme 2.2. Formation of **2**, **3** and **4** from the reaction of **1** with O_2

discussed below. Crystals of **4** in 5.3% isolated yield were obtained from a solution in CH_2Cl_2.

When the mixture after the reaction was analyzed by ^{1}H NMR in benzene-d_6, and it was mostly $(Me_2N)_4Ta(OSiBu^tPh_2)$ (**2**), $(Me_2N)_3Ta(ONMe_2)(OSiBu^tPh_2)$ (**3**) and $HSiBu^tPh_2$. The presence of $(Me_2N)_2(Ph_2Bu^tSiO)_2(Me_2NCH_2NMe)_2Ta_2(\mu\text{-}O)_2$ (**4**) was not clear based on the ^{1}H NMR spectrum. If it was present in the reaction mixture, its ^{1}H NMR peaks were probably below the base line. The solubility of **4** in non-polar solvents is apparently low, as discussed below. The solubilities of both **2** and **3** are high. In fact, **2** is apparently a liquid at 23 °C. Crystallization yields only **4**. The characterization of **2** and **3** will be discussed in Sections 2.2.3 and 2.2.4.

When the reaction was conducted with less than one equiv of O_2, it was not possible to obtain **4** through crystallization. An excess of O_2 (1.5 equiv) is important for the preparation of **4**.

The reaction of $Ta(NMe_2)_4SiBu^tPh_2$ (**1**) with less than one equiv of O_2 was monitored by NMR. Complex **1** was prepared *in situ* from $Ta(NMe_2)_4Cl$ (**5**) and $Li(THF)_2SiBu^tPh_2$ (**7**) in benzene-d_6 in a Young NMR tube. The solution was frozen at –60 °C to remove the gases in the headspace of the NMR tube. O_2 (ca. 0.9 equiv) was added, and the NMR tube was subsequently warmed to room temperature, and shaken for 10 min. The color of the solution gradually turned from brown to light yellow during this period. ^{1}H and ^{13}C NMR spectra of the mixture after 20 min of reaction showed it was a mixture of **2** (34.3% yield), **3** (5.2% yield) and unreacted $(Me_2N)_4TaSiBu^tPh_2$ (**1**, 16.0%). It is not clear if the

$(Me_2N)_2(Ph_2Bu^tSiO)_2(Me_2NCH_2NMe)_2Ta_2(\mu\text{-}O)_2$ (**4**) was produced from this reaction involving excess starting tantalum complex **1**. If it was present in the reaction mixture, its ^{1}H NMR peaks were probably below the base line.

2.2.2. *Characterization and crystal and molecular structure of $(Me_2N)_2(Ph_2Bu^tSiO)_2(Me_2NCH_2NMe)_2Ta_2(\mu\text{-}O)_2$ (4)*

The ^{1}H NMR spectrum of $(Me_2N)_2(Ph_2Bu^tSiO)_2(Me_2NCH_2NMe)_2Ta_2(\mu\text{-}O)_2$ (**4**) at 23 °C is consistent with the structural assignment. There is an inversion center in **4**. The two H atoms in the $–CH_2$- group are diastereotopic, and the $–MeNCH_aH_bNMe_2$ ligand thus gives three methyl peaks and two doublets for H_a and H_b, respectively. These two doublets were found at 5.49 and 4.87 ppm in the ^{1}H NMR spectrum ($^3J_{H\text{-}H}$ = 9.8 Hz) (Figure 2.2). The two methyl groups in

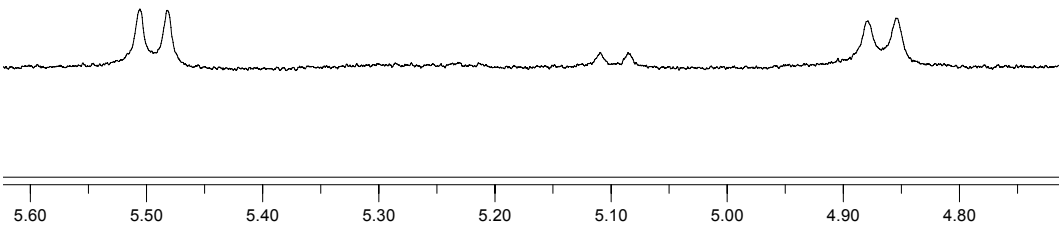

Figure 2.2. ^{1}H NMR spectrum of **4** showing two doublets

–NMe_2 in the –$MeNCH_aH_bNMe_cMe_d$ ligand are inequivalent, thus giving three methyl resonances at 3.36 (*Me*$NCH_aH_bNMe_cMe_d$), 2.88 ($MeNCH_aH_bN$*Me*$_cMe_d$) and 2.78 ppm ($MeNCH_aH_bNMe_c$*Me*$_d$) in a 1:1:1 ratio for the ligand. The Ta–NMe_2 amide ligand does not undergo a free rotation around the Ta-N bond. Thus the two methyl groups in Ta–NMe_2 are not chemical equivalent, and they were observed at 3.75 (s, 6H, Ta-N*Me*$_e$Me$_f$) and 3.62 (s, 6H, Ta-NMe$_e$*Me*$_f$) ppm. A peak at 1.35 ppm was assigned to the butyl group of the siloxy Ph_2Bu^tSiO-ligand.

The dimeric complex $(Me_2N)_2(Ph_2Bu^tSiO)_2(Me_2NCH_2NMe)_2Ta_2(\mu\text{-}O)_2$ (**4**) was characterized by single crystal X-ray diffraction. The crystals were obtained from both CH_2Cl_2 and toluene solutions. They were found to contain solvent molecules. Molecular drawing, packing diagram, crystallographic data, selected bond distances and angles of **4·CH_2Cl_2** are given in Figures 2.3 and 2.4 and Tables 2.1 and 2.2, respectively. The crystallographic data of **4·toluene** is listed in Table 2.3. Complete lists of crystallographic data are given in Appendix. The dimeric **4** consists of two oxo atoms as bridging ligands between Ta centers. Each Ta center is coordinated by six ligands in a pseudo octahedral geometry. The –$OSiBu^tPh_2$ and –NMe_2 ligands and the two bridging oxo atoms are in equatorial positions. The chelating –$MeNCH_2NMe_2$ ligands are in axial positions. In the chelating –$MeNCH_2NMe_2$ ligand, the –NMe– unit is bound to a Ta atom with a regular σ bond, and the NMe_2 group in the ligand forms a dative N$\rightarrow$Ta bond through the lone pair electrons on the N atom. The Ta(1)-N(1) and Ta(1)-

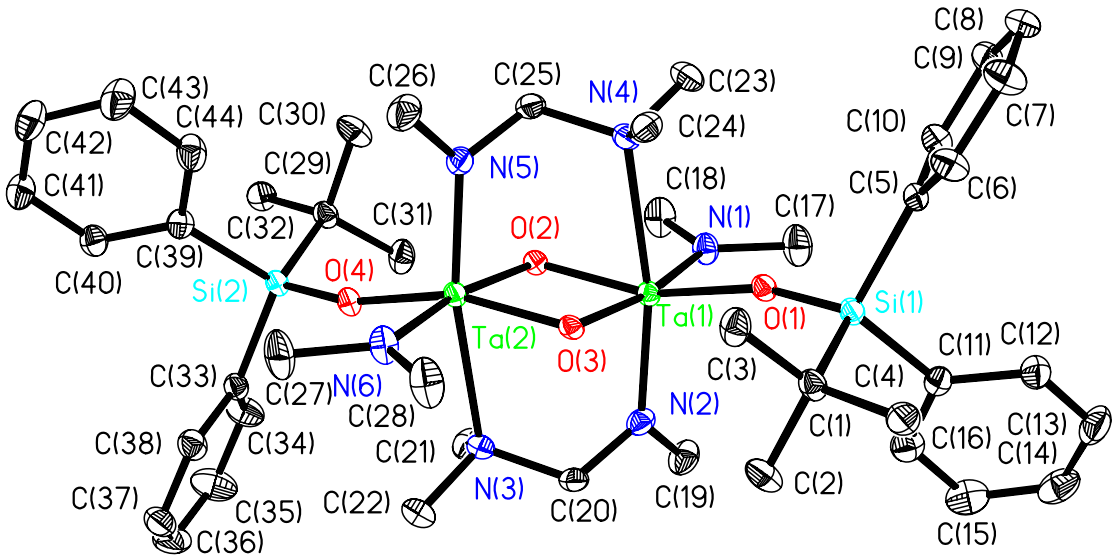

Figure 2.3. Molecular drawing of **4** in **4·CH_2Cl_2** showing 30% probability thermal ellipsoids

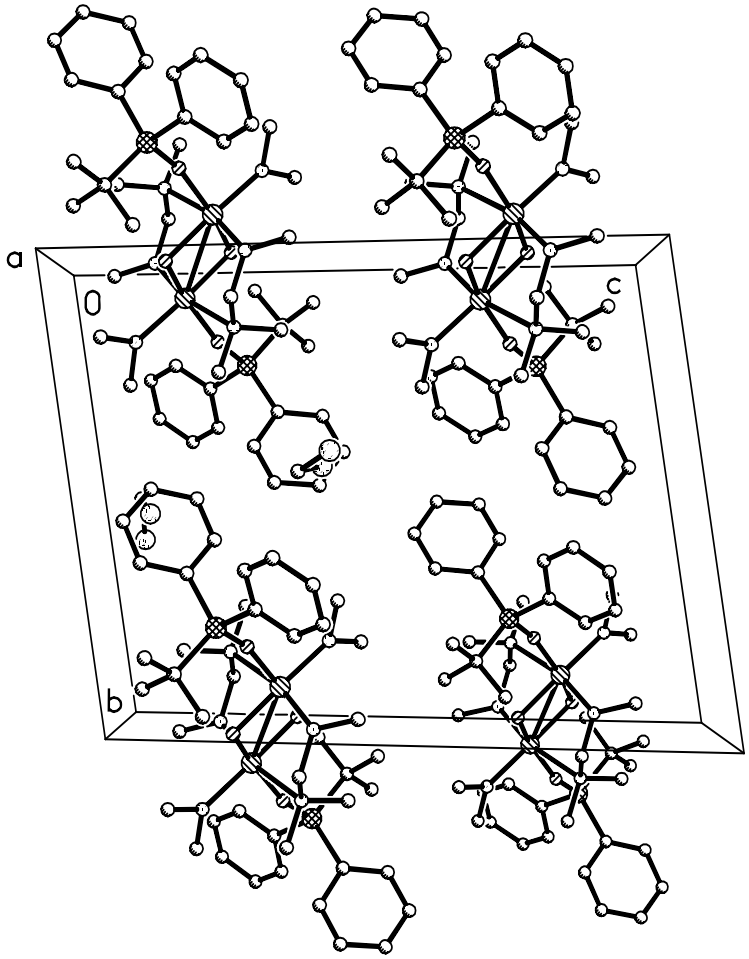

Figure 2.4. Packing diagram of **4·CH_2Cl_2** along the *a* axis

Table 2.1. Crystal data and structure refinement for **4·CH_2Cl_2**

Compound No.	**4·CH_2Cl_2**	
Empirical formula	$C_{46}H_{76}Cl_4N_6O_4Si_2Ta_2$	
Formula weight	1337.01	
Temperature	100(2) K	
Wavelength	0.71073 Å	
Crystal system	Triclinic	
Space group	*P*-1	
Unit cell dimensions	*a* = 10.965(3) Å	α = 82.008(4)°
	b = 14.209(3) Å	β = 75.331(3)°
	c = 18.356(4) Å	γ = 89.577(3)°
Volume	2738.6(11) $Å^3$	
Z	2	
Density (calculated)	1.621 Mg/m^3	
Absorption coefficient	4.276 mm^{-1}	
F(000)	1336	
Crystal size	0.38 x 0.27 x 0.10 mm^3	
θ range for data collection	1.16 to 26.38°	
Index ranges	$-13 \le h \le 13$, $-17 \le k \le 17$, $-22 \le l \le 22$	

Table 2.1. Continued

Compound No.	**4·CH_2Cl_2**
Reflections collected	26822
Independent reflections	10988 [*R*(int) = 0.0297]
Completeness to θ = 26.38°	98.0%
Absorption correction	Semi-empirical from equivalents
Max. and min. transmission	0.6744 and 0.2933
Refinement method	Full-matrix least-squares on F^2
Data / restraints / parameters	10988 / 0 / 593
Goodness-of-fit on F^2	0.978
Final *R* indices [$I > 2\sigma(I)$]	*R*1 = 0.0281, w*R*2 = 0.0661
R indices (all data)	*R*1 = 0.0435, w*R*2 = 0.0733
Largest diff. peak and hole	1.619 and -0.650 e.Å^{-3}

[a]w*R2* = $[\Sigma w(F_o^2 - F_c^2)^2/\Sigma w(F_o^2)^2]^{1/2}$; $R = \Sigma||F_o| - |F_c||/\Sigma|F_o|$;

$w = 1/[\sigma^2(F_o^2) + (aP)^2 + bP]$; $P = [2F_c^2 + \text{Max}(F_o^2, 0)]/3$

Table 2.2. Selected bond distances (Å) and angles (deg) in **4·CH_2Cl_2**

Distances			
Ta(1)-O(2)	1.925(3)	Ta(1)-N(4)	2.511(3)
Ta(1)-O(1)	1.965(3)	N(2)-C(20)	1.454(6)
Ta(1)-N(2)	1.978(3)	Si(1)-O(1)	1.621(3)
Ta(1)-N(4)	2.014(3)	N(3)-C(20)	1.506(5)
Ta(1)-N(1)	2.034(4)	N(2)-C(19)	1.476(5)
N(3)-C(21)	1.478(5)	N(3)-C(22)	1.467(6)
Si(1)-C(1)	1.895(4)		
Angles			
O(2)-Ta(1)-O(1)	160.95(11)	O(1)-Ta(1)-N(4)	82.99(11)
O(2)-Ta(1)-O(3)	80.84(11)	O(3)-Ta(1)-N(4)	81.75(11)
O(1)-Ta(1)-O(3)	95.13(11)	N(2)-Ta(1)-N(4)	166.64(13)
O(1)-Ta(1)-N(2)	102.78(12)	N(1)-Ta(1)-N(4)	92.84(13)
O(3)-Ta(1)-N(2)	85.71(13)	O(2)-Ta(1)-Ta(2)	41.02(8)
O(2)-Ta(1)-N(1)	90.18(13)	O(1)-Ta(1)-Ta(2)	132.32(8)
O(3)-Ta(1)-N(1)	170.30(12)	N(2)-Ta(1)-Ta(2)	90.61(10)
N(2)-Ta(1)-N(1)	98.90(15)	N(1)-Ta(1)-Ta(2)	131.11(10)
O(2)-Ta(1)-N(4)	78.01(11)	N(2)-C(20)-N(3)	113.3(3)
Si(1)-O(1)-Ta(1)	162.53(18)		

Table 2.3. Crystal data and structure refinement for **4·toluene**

Compound No.	**4·toluene**	
Empirical formula	$C_{51}H_{80}N_6O_4Si_2Ta_2$	
Formula weight	1259.30	
Temperature	173(2) K	
Wavelength	0.71073 Å	
Crystal system	Triclinic	
Space group	*P*-1	
Unit cell dimensions	*a* = 9.029(4) Å	α = 105.007(6)°
	b = 10.540(4) Å	β = 93.067(7)°
	c = 15.746(6) Å	γ = 102.871(7)°
Volume	1401.3(10) $Å^3$	
Z	4	
Density (calculated)	1.931 Mg/m^3	
Absorption coefficient	7.915 mm^{-1}	
F(000)	784	
Crystal size	0.27 x 0.22x 0.16 mm^3	
θ range for data collection	1.35 to 28.32°	
Index ranges	$-11 \le h \le 11$, $-13 \le k \le 14$, $-20 \le l \le 20$	

Table 2.3. Continued

Compound No.	**4·toluene**
Reflections collected	14564
Independent reflections	6510 [*R*(int) = 0.0388]
Completeness to θ = 28.32°	93.5%
Refinement method	Full-matrix least-squares on F^2
Data / restraints / parameters	6510 / 0 / 296
Goodness-of-fit on F^2	1.166
Final R indices [I > 2σ(*I*)]	*R*1 = 0.0335, w*R*2 = 0.0868
R indices (all data)	*R*1 = 0.0450, w*R*2 = 0.1162
Largest diff. peak and hole	1.621 and -1.320 e.Å^{-3}

[a]w*R2* = $[\Sigma w(F_o^2 - F_c^2)^2/\Sigma w(F_o^2)^2]^{1/2}$; $R = \Sigma||F_o| - |F_c||/\Sigma|F_o|$;

$w = 1/[\sigma^2(F_o^2) + (aP)^2 + bP]$; $P = [2F_c^2 + \text{Max}(F_o^2, 0)]/3$

N(2) σ bond distances of 2.034(4)–2.014(3) Å are similar to those of Ta-NMe_2 bonds in $(Me_2N)_4TaSiBu^tPh_2$ (**1**) [1.979(10)–2.029(10) Å] and $(Me_2N)_3TaCl(SiBu^tPh_2)$ [1.926(11)–1.989(11) Å].[29] The dative Ta(1)-N(4) bond length of 2.511(3) Å is significantly larger than the Ta-N dative bonds in $(Me_2N)_3Ta(\eta^2\text{-}ONMe_2)[OSi(SiMe_3)_3]$ (**21**) [2.254(9) Å][29] and $[TaCl(\mu\text{-}Cl)(NBu^t)(NHBu^t)(NH_2Bu^t)]_2$ [2.23(3) Å].[32] It is not clear why the dative Ta(1)-N(4) bond is longer than other reported N→Ta bonds. The Ta-O bonds lengths [1.925(3)-1.978(3) Å] are close those reported in other Ta complexes: $Ta(CH_2SiMe_3)(O_2CNMe_2)_4$ [1.932(5)-2.132(5) Å],[33a] $[(Me_2N)_2(Me_2NH)TaCl_2]_2O$ [1.917(6)-1.928(6) Å][33b] and $(Me_2N)_3Ta(\eta^2\text{-}ONMe_2)[OSi(SiMe_3)_3]$ (**21**) [1.991(8) Å].[29] The Ta(1)-O(2)-Ta(2) angle of 99.24(12)° in the Ta(1)-O(2)-Ta(2)-O(3) four-member ring is much larger than the O(2)-Ta(1)-O(3) bond angle of 80.84(11)°.

4 was found to be thermally unstable in solution at room temperature, but stable in the solid state. Decomposition of **4** gave $Me_2NCH_2NMe_2$ and unknown Ta species (Eq. 2.1). The formation of $Me_2NCH_2NMe_2$ was confirmed by ^1H and ^{13}C NMR. The observation of $Me_2NCH_2NMe_2$ strongly suggests that **4** contains -$MeNCH_2NMe_2$ ligand. But the pathway and driving force of the decomposition are still unknown.

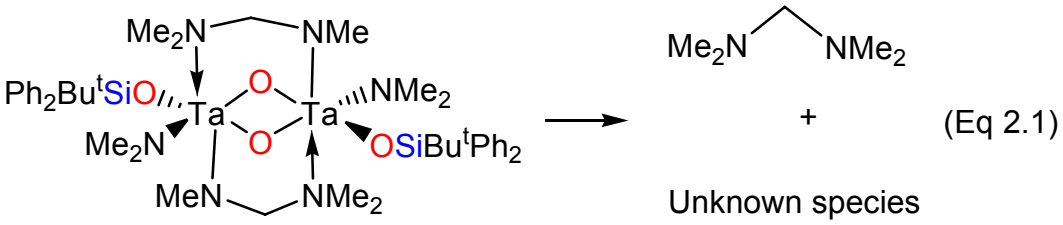

(Eq 2.1)

4

The formation of the chelating -$MeNCH_2NMe_2$ ligand in **4** is particularly significant. Our search of the literature revealed that only one theoretical paper in 2001 reported the calculations of its parent amine $MeNHCH_2NMe_2$.[34] To our knowledge, the formation of the chelating -$MeNCH_2NMe_2$ ligand has not been reported. As discussed earlier, the X-ray crystal structure of **4** revealed that the –$NMeCH_2NMe_2$ ligand forms one σ bond and one dative bond with a Ta atom. The former uses the N atom in the –NMe-CH_2– group, and the latter involves the lone pair electrons on the –NMe_2 group.

2.2.3. *Characterization of $(Me_2N)_4Ta(OSiBu^tPh_2)$ (2) and its preparation from the reaction of $Ta(NMe_2)_4Cl$ (5) with $LiOSiBu^tPh_2$ (6)*

$(Me_2N)_4Ta(OSiBu^tPh_2)$ (**2**) was also prepared from the reaction of $Ta(NMe_2)_4Cl$ (**5**) with $LiOSiBu^tPh_2$ (**6**, Scheme 2.3). $LiOSiBu^tPh_2$ was synthesized earlier in our group and used to give $(Bu^tCH_2)_2W(\equiv CBu^t)(OSiBu^tPh_2)$ in a study of the tungsten siloxide complex.[30] In the current work, **2** was directly prepared from **5** and **6** so that it can be characterized, thus confirming its formation in the reaction of $Ta(NMe_2)_4(SiBu^tPh_2)$ (**1**) with O_2, and study its reactivities.

After stirring $Ta(NMe_2)_4Cl$ (**5**) and $LiOSiBu^tPh_2$ (**6**) in Et_2O at –60 °C, the mixture was warmed to room temperature and stirred overnight. This substitution reaction was found to be relatively slow, and requires overnight stirring at room temperature. After removal of the volatiles and LiCl, an oil of **2** was obtained in

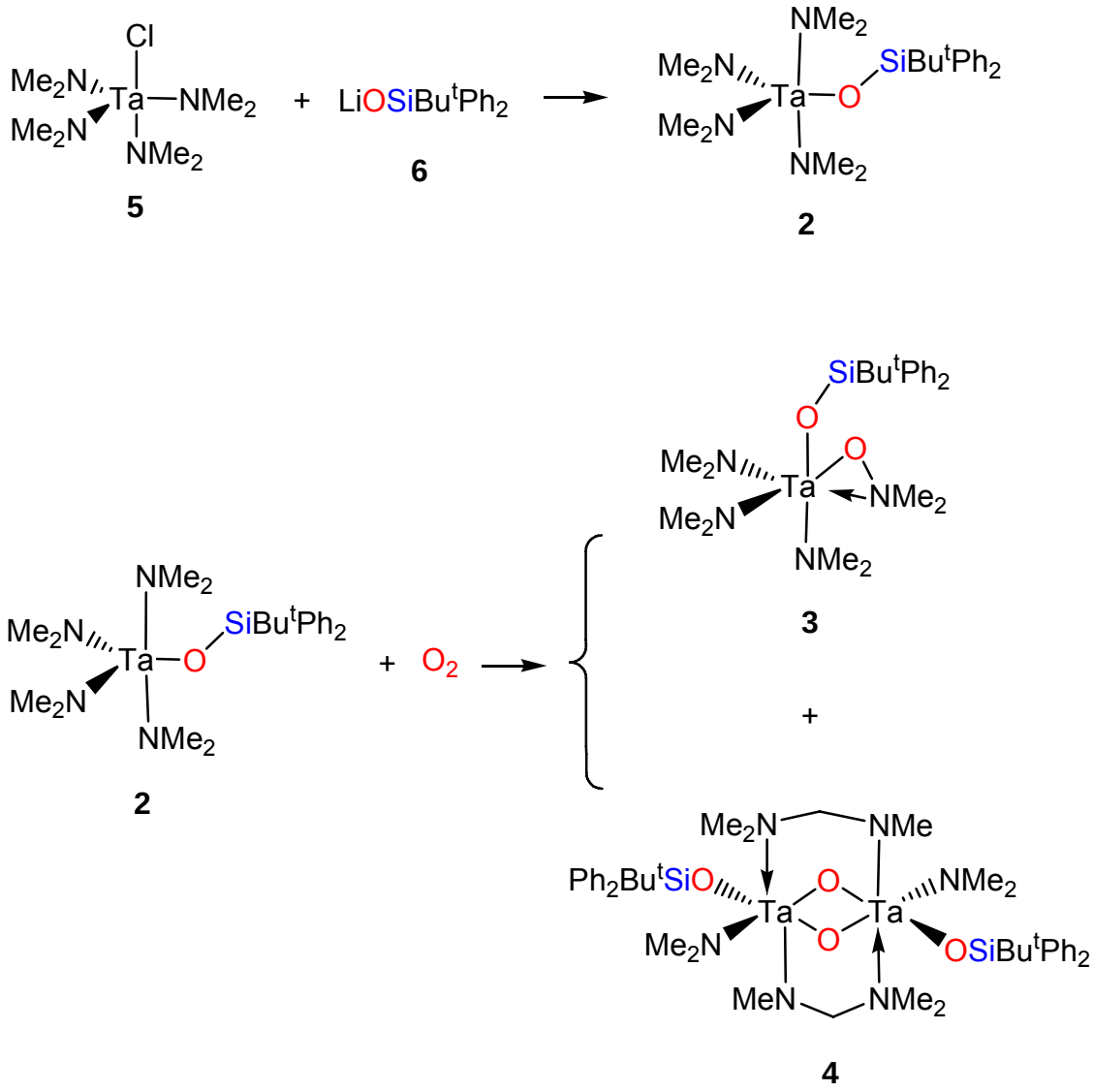

Scheme 2.3. Direct preparation of **2** from the reaction of $Ta(NMe_2)_4Cl$ (**5**) with $LiOSiBu^tPh_2$ (**6**) and the reaction of **2** with O_2

77.1% yield. **2** was found to be a liquid at room temperature with a high solubility in non-polar solutions such as pentane and benzene.

The NMR spectra of $(Me_2N)_4Ta(OSiBu^tPh_2)$ (**2**) are consistent with the structural assignment of the complex. The ^1H NMR spectrum of **2** shows only one resonance for the four $–NMe_2$ ligands at 3.17 ppm and one signal for the tert-butyl group of the silyloxy ligand at 1.21 ppm. The $^{13}C\{^1H\}$ NMR spectrum shows a single amide resonance at 45.98 ppm and the tert-butyl resonances at 27.88 (CMe_3) and 20.02 (CMe_3) ppm. These observations suggest that **2** perhaps adopts a trigonal bipyramidal (TBP) structure with the silyloxy ligand in the equatorial position. A similar structure was observed for its silyl analog $(Me_2N)_4Ta(SiBu^tPh_2)$ (**1**).[29]

The reaction of $(Me_2N)_4Ta(OSiBu^tPh_2)$ (**2**) with O_2 is discussed in Section 2.2.5. This reaction was used in the mechanistic studies of the reaction between **1** and O_2.

2.2.4. *Characterization of $(Me_2N)_3Ta(ONMe_2)(OSiBu^tPh_2)$ (3)*

We reported earlier that the reaction of tantalum silyl complex $(Me_2N)_4TaSi(SiMe_3)_3$ (**20**) with O_2 gave an O_2-stable complex $(Me_2N)_3Ta(\eta^2\text{-}ONMe_2)[OSi(SiMe_3)_3]$ (**21**, Scheme 2.1).[29] Complex **3**, an analog of **20**, was initially prepared from the reaction of $Ta(NMe_2)_4SiBu^tPh_2$ (**1**) with O_2. As discussed earlier, both $(Me_2N)_4Ta(OSiBu^tPh_2)$ (**2**) and $(Me_2N)_2(Ph_2Bu^tSiO)_2(Me_2NCH_2NMe)_2Ta_2(\mu\text{-}O)_2$ (**4**) are products from this reaction as well. Reaction of $(Me_2N)_3TaCl_2$ (**14**) with $LiOSiBu^tPh_2$ (**6**) and

$LiONMe_2$ (Scheme 2.4) or the reaction of $(Me_2N)_4Ta(OSiBu^tPh_2)$ (**2**) with O_2 also led to the formation of **3** (Scheme 2.3).

^1H and $^{13}C\{^1H\}$ NMR spectra of **3** are consist with the molecular structure, and chemical shifts are listed in Table 2.4. These spectra suggest that the structure of **3** is similar to that of $(Me_2N)_3Ta(\eta^2\text{-}ONMe_2)[OSi(SiMe_3)_3]$ (**21**). Three resonances were observed in the ^1H NMR spectrum of **3**. The $-NMe_2$ resonance (3.28 ppm) and $-ONMe_2$ signal (2.36 ppm) are only slightly upfield-shifted from those in **21**. In the $^{13}C\{^1H\}$ NMR spectrum of **3**, the $-NMe_2$ and $-ONMe_2$ resonances at 47.05 and 49.55 ppm are close to those in $(Me_2N)_3Ta(\eta^2\text{-}ONMe_2)[OSi(SiMe_3)_3]$ (**21**). Both ^1H and ^{13}C resonances of the methyl groups in the $-OSiBu^tPh_2$ ligand in **3** are close to those in **2**.

Unlike its analog $(Me_2N)_3Ta(\eta^2\text{-}ONMe_2)[OSi(SiMe_3)_3]$ (**21**), $(Me_2N)_3Ta(ONMe_2)(OSiBu^tPh_2)$ (**3**) is not stable to O_2, and the reaction gives unknown species. One interpretation is that the $-OSiBu^tPh_2$ ligand in **3** is not as bulky as the $-OSi(SiMe_3)_3$ ligand in **21**, and is thus not effective in protecting the metal center in **3** from O_2 attack.

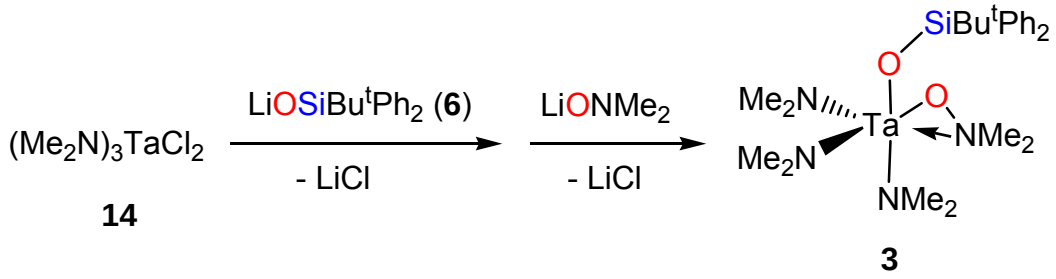

Scheme 2.4. Preparation of **3** from the reaction of **14** with **6** and $LiONMe_2$

Table 2.4. NMR resonances of **2**, **3** and **21** in benzene-d_6

Complex	^{1}H NMR	^{13}C NMR
$(Me_2N)_4Ta(OSiBu^tPh_2)$ (**2**)	3.17 (N*Me*$_2$) 1.22 (C*Me*$_3$)	45.98 (N*Me*$_2$) 27.88 (C*Me*$_3$) 20.02 (*C*Me$_3$)
$(Me_2N)_3Ta(ONMe_2)$- $(OSiBu^tPh_2)$ (**3**)	3.28 (N*Me*$_2$) 2.36 (ON*Me*$_2$) 1.25 (C*Me*$_3$)	49.37 (ON*Me*$_2$) 46.85 (N*Me*$_2$) 27.42 (C*Me*$_3$) 28.72 (*C*Me$_3$)
$(Me_2N)_3Ta(\eta^2$- $ONMe_2)[OSi(SiMe_3)_3]$ (**21**)	3.30 (N*Me*$_2$) 2.49 (ON*Me*$_2$) 0.33 (Si*Me*$_3$)	49.06 (ON*Me*$_2$) 47.10 (N*Me*$_2$) 1.00 (Si*Me*$_3$)

2.2.5. *Mechanistic studies of the reaction between $(Me_2N)_4TaSiR_3$ [R_3 = $(SiMe_3)_3$, 20; Bu^tPh_2, 1] and O_2*

We recently reported the formation of $(Me_2N)_3Ta(\eta^2\text{-}ONMe_2)[OSi(SiMe_3)_3]$ (**21**) from the reaction of $(Me_2N)_4Ta\text{-}Si(SiMe_3)_3$ (**20**, Scheme 2.1) with O_2. As a part of our studies of the mechanistic pathways in the reactions between metal amide silyl complexes and O_2, we investigated this reaction in the current work.

Density functional theory (DFT) quantum mechanical calculations were conducted by Professor Yun-Dong Wu's research group at the Hong Kong University of Science and Technology. These calculations suggest a pathway shown in Scheme 2.5. One O_2 molecule was first inserted into the Ta-Si bond, forming a Ta peroxide species. Then the O atom bound to the Ta atom migrates into a neighboring Ta-N bond, leading to the formation of a Ta-ONR'_2 and a Ta-$OSiR_3$ ligand.

If this mechanism operates, the two O atoms in a molecule of $(Me_2N)_3Ta(\eta^2\text{-}ONMe_2)[OSi(SiMe_3)_3]$ (**21**) are from the same O_2 molecule. Thus, if a mixture of $^{16}O_2/^{18}O_2$ is used to react with $(Me_2N)_4Ta\text{-}Si(SiMe_3)_3$ (**20**), the formation of a mixture of $(Me_2N)_3Ta(\eta^2\text{-}^{16}ONMe_2)[^{16}OSi(SiMe_3)_3]$ (**21-$^{16}O_2$**) and $(Me_2N)_3Ta(\eta^2\text{-}^{18}ONMe_2)[^{18}OSi(SiMe_3)_3]$ (**21-$^{18}O_2$**) is expected (**Path I**, Scheme 2.6).

If the two oxygen atoms are from two different O_2 molecules, a test using a mixture of $^{16}O_2/^{18}O_2$ and **20** is expected to follow **Path II** in Scheme 2.6 and to give a mixture of isotopomers $(Me_2N)_3Ta(\eta^2\text{-}^{16}ONMe_2)[^{16}OSi(SiMe_3)_3]$ (**21-$^{16}O_2$**),

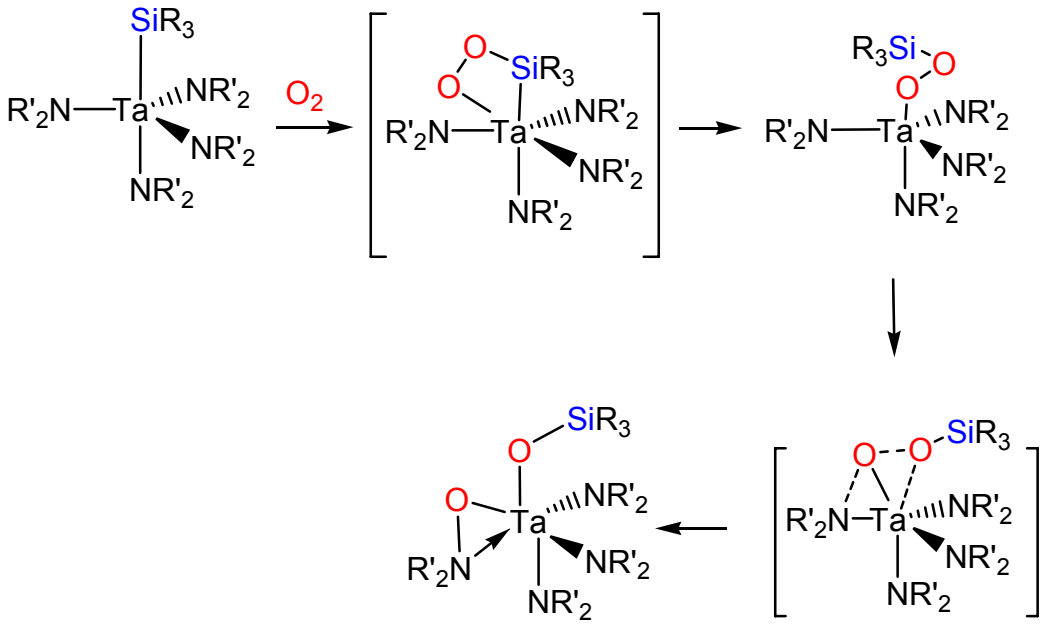

Scheme 2.5. Pathways in the reaction of $(R'_2N)_4Ta(SiR_3)$ with O_2 suggested by DFT calculations

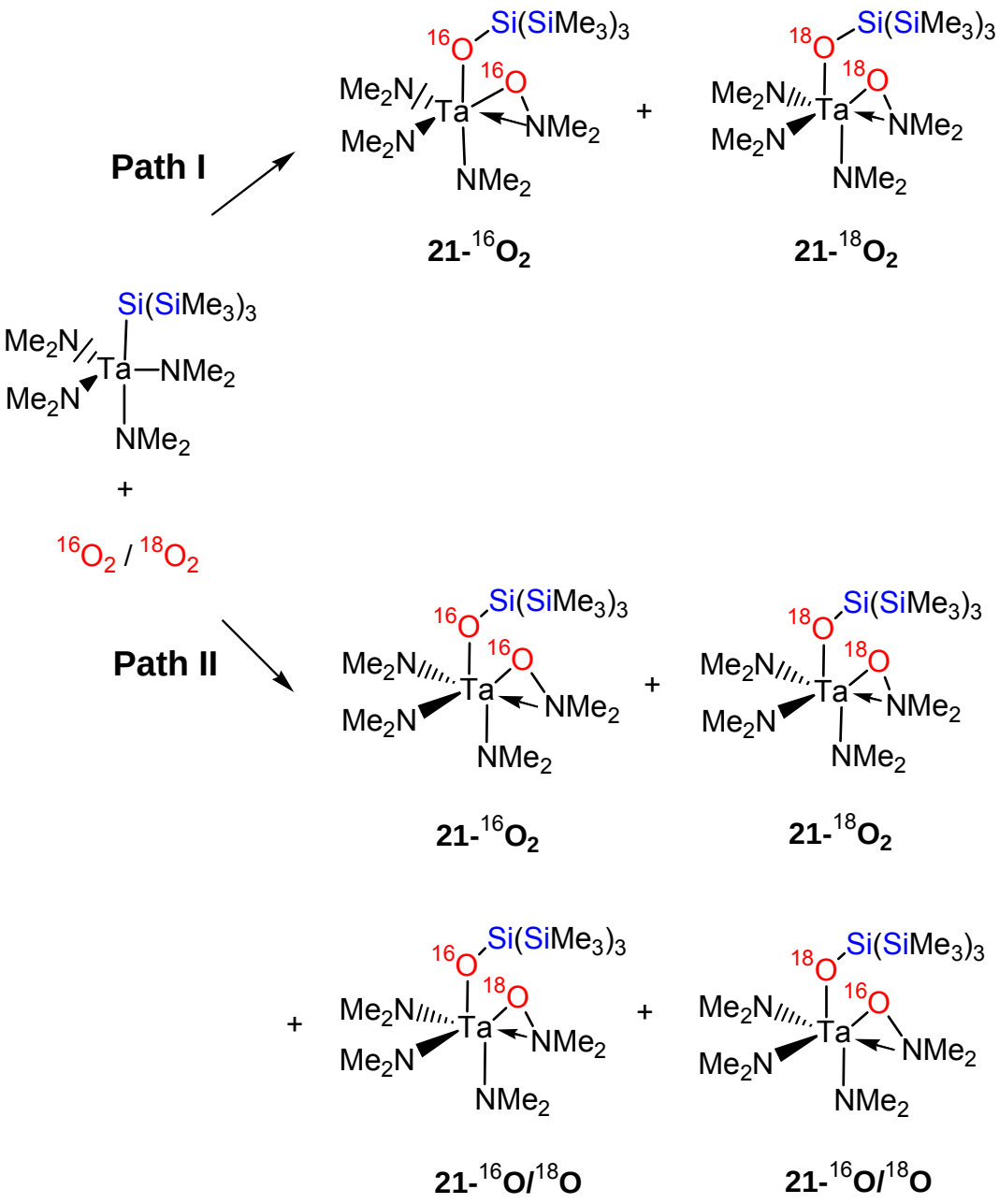

Scheme 2.6. Attempted mechanistic study of the reaction between $(Me_2N)_4Ta[Si(SiMe_3)_3]$ (**20**) and O_2

$(Me_2N)_3Ta(\eta^2\text{-}^{18}ONMe_2)[^{18}OSi(SiMe_3)_3]$ (**21-$^{18}O_2$**), $(Me_2N)_3Ta(\eta^2\text{-}^{16}ONMe_2)[^{18}OSi(SiMe_3)_3]$ (**21-$^{16}O/^{18}O$**) and $(Me_2N)_3Ta(\eta^2\text{-}^{18}ONMe_2)[^{16}OSi(SiMe_3)_3]$ (**21-$^{16}O/^{18}O$**).

Thus an analysis of the mixture by mass spectrometry (MS) would give the parent ion peaks of both isotopomers, if the following conditions are met: (1) The molecules of $(Me_2N)_3Ta(\eta^2\text{-}ONMe_2)(OSiR_3)$ do not defragment in the MS studies to the extent that no parent ion peaks could be observed; (2) The molecules of $(Me_2N)_3Ta(\eta^2\text{-}ONMe_2)(OSiR_3)$ do not undergo exchanges of the $–ONMe_2$ or $–OSiR_3$ ligands; (3) The molecules of $(Me_2N)_3Ta(\eta^2\text{-}ONMe_2)(OSiR_3)$ are stable to O_2 for the Electron Ionization (EI) MS studies. In the tests, the MS probe containing a very small amount of $(Me_2N)_3Ta(\eta^2\text{-}ONMe_2)(OSiR_3)$ needs to be briefly exposed to air.

In order to test whether the first condition was met, several MS techniques [Electron Ionization (EI) at 70.0 eV, Electrospray Ionization (ESI), and Matrix Assisted Laser Desorption Ionization (MALDI)] were used to obtain the mass spectra of **21**. In all the tests we have conducted, no molecular ion peaks were observed in the mass spectra. The heaviest fragment peaks were observed at 494 (EI) and 495 (MALDI), and the structures of the fragments were not clear from the mass spectra. Since the Si-Si bonds in $(Me_2N)_4Ta\text{-}Si(SiMe_3)_3$ (**20**) are weak, it is likely they fragment in the MS studies.

$(Me_2N)_3Ta(ONMe_2)(OSiBu^tPh_2)$ (**3**) without a Si-Si bond appears to be a better candidate for MS studies, but **3** was found not to be stable to air. No MS

probe test has been conducted because it is likely to decompose on the MS probe when the probe was exposed briefly to air before being inserted in the EI MS chamber. Moreover complex **3** is hard to be isolated from the reaction mixture due to its high solubility in both polar solvents and non polar solvents.

Studies were conducted to see if $(Me_2N)_4Ta(OSiBu^tPh_2)$ (**2**) was an intermediate to give **3** and $(Me_2N)_2(Ph_2Bu^tSiO)_2(Me_2NCH_2NMe)_2Ta_2(\mu\text{-}O)_2$ (**4**) in the reaction of $(Me_2N)_4Ta\text{-}SiBu^tPh_2$ (**1**) with O_2. **2** was prepared directly from $(Me_2N)_4Ta\text{-}Cl$ (**5**) and $LiOSiBu^tPh_2$ (**6**) and isolated from the reaction mixture (Scheme 2.3). Complex **2** was then exposed to O_2. This reaction was found to give both $(Me_2N)_3Ta(ONMe_2)(OSiBu^tPh_2)$ (**3**) and **4** (Scheme 2.3). In addition, unlike the reaction of silyl complex **1** with O_2 that yields ca. 19 mol% of silane $HSiBu^tPh_2$, this reaction involving a siloxy complex did not give a detectable amount of the silane. The yields of **3** at 77.1% and **4** at 5.3% are higher than 5.2% and 4.1% yields, respectively, in the reaction of **1** with O_2.

Attempts to isolate **3** from the reaction mixture were unsuccessful. Recrystallization yields **4** as crystals. This is perhaps not surprising, as the complex **3** was found to have high solubility in most organic solvents.

The formation of **3** and **4** from the reaction of $(Me_2N)_4Ta(OSiBu^tPh_2)$ (**2**) and O_2 shed some light on the mechanistic pathways in reaction between **1** and O_2. At least it indicates that, once **2** is formed, it may proceed to react with O_2 to yield **3** and **4**. However it is not clear: (1) How **2** is formed, including whether it is formed from **1** in a single step. (2) Whether there are other pathways to give **3** and **4**. (3) What process(es) leads to the formation of the chelating –NMe-CH_2-

NMe_2 ligand in **4**. We have recently isolated and characterized $Ta(NMe_2)_4(\eta^2$-$NMeCH_2NMe_2)$ (**22**) containing the same chelating $–NMe\text{-}CH_2\text{-}NMe_2$ ligand.[35] This complex was produced from the reaction of $TaCl_5$ with $LiNMe_2$. Studies of $Ta(NMe_2)_4(\eta^2$-$NMeCH_2NMe_2)$ (**22**) suggest that the formation of the chelating $–NMe\text{-}CH_2\text{-}NMe_2$ ligand may involve a β-hydrogen elimination between two $–NMe_2$ ligands to generate an imine CH_2=NMe ligand and a Ta(III) species. The imine ligand then undergoes a coupling reaction with a $–NMe_2$ ligand to give the chelating $–NMe\text{-}CH_2\text{-}NMe_2$ ligand. Subsequent oxidation by adventitious molecular oxygen perhaps returns the Ta(III) complex back to d^0 Ta(V) $Ta(NMe_2)_4(\eta^2$-$NMeCH_2NMe_2)$ (**22**). A similar pathway *may* operate here, as shown in Scheme 2.7. Among the four $\text{-}NMe_2$ ligands, two undergo a β-hydrogen elimination reaction to give a Ta(III) imine species **A**. The imine ligand on **A** then couples with a $\text{-}NMe_2$ ligand to give the chelating $–NMe\text{-}CH_2\text{-}NMe_2$ ligand in **B**. O_2 oxidizes Ta(III) **B** to Ta(V) **C** containing an oxo ligand which subsequently dimerizes to give **4**. Alternatively, **A** may directly go to **C** through an O_2-induced coupling reaction between the imine CH_2=NMe and amide $–NMe_2$ ligands.

It should be noted that the ground state of O_2 at room temperature is a triplet with two unpaired electrons. In other words, it is a diradical, and the proposed pathway in Scheme 2.7 may involve radical processes. Additional work is needed to elucidate the mechanistic pathways in the formation of **2-4** in the reaction of $(Me_2N)_4Ta\text{-}SiBu^tPh_2$ (**1**) with O_2.

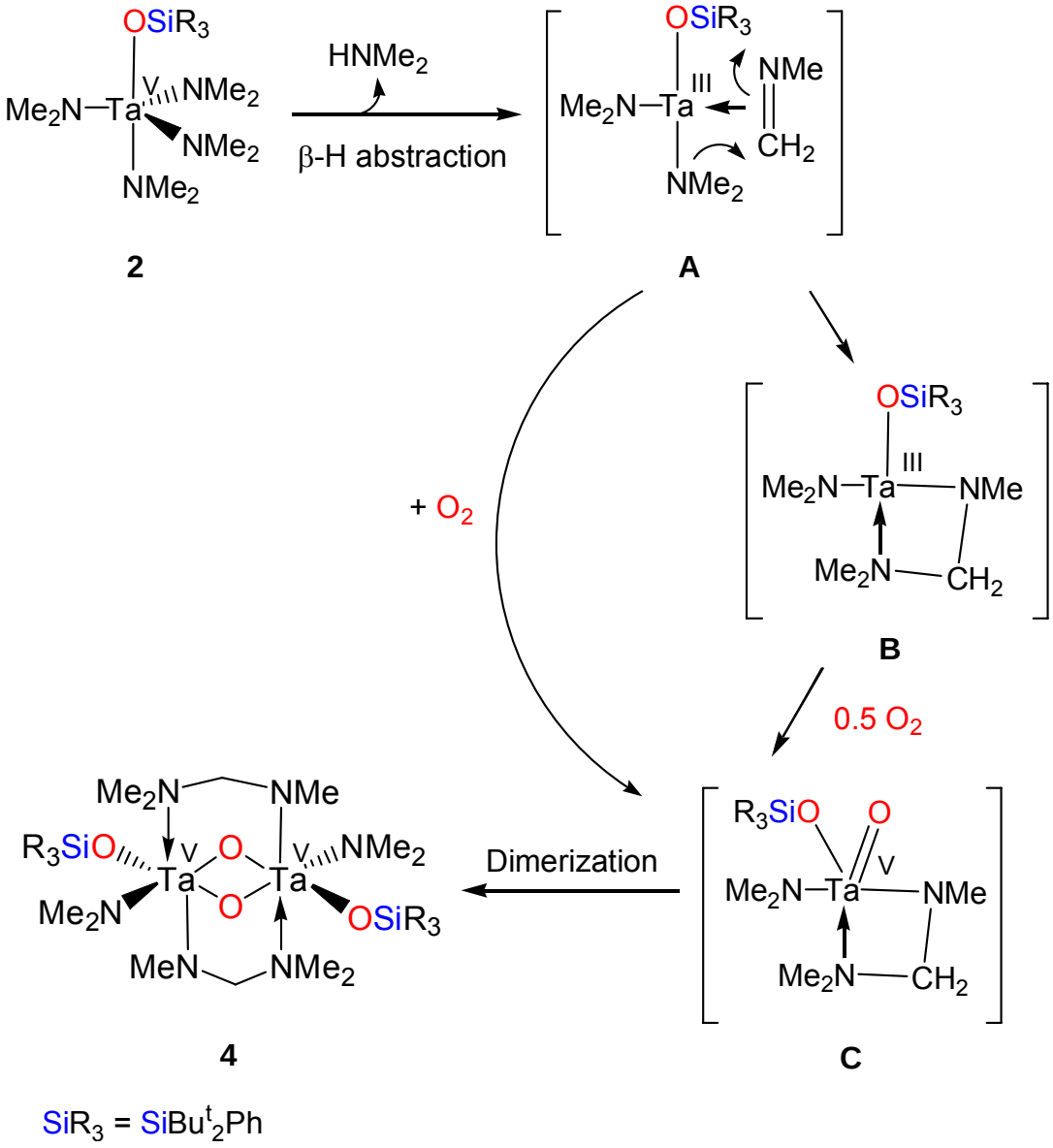

Scheme 2.7. Proposed pathway for the formation of **4** from **2** and O_2

2.3. Conclusions

Silyl complex $(Me_2N)_4Ta(SiBu^tPh_2)$ (**1**) was found to react with O_2 to give three complexes $(Me_2N)_4Ta(OSiBu^tPh_2)$ (**2**), $(Me_2N)_3Ta(ONMe_2)(OSiBu^tPh_2)$ (**3**) and $(Me_2N)_2(Ph_2Bu^tSiO)_2(Me_2NCH_2NMe)_2Ta_2(\mu\text{-}O)_2$ (**4**). In all three products **2-4**, the silyl ligands are oxidized with an oxygen insertion, suggesting a preferential silyl oxidation in the reaction. The oxidation of complex **2** by O_2 and formation of **3** and **4** in the reaction suggest that **2** may be the intermediate in the reaction of **1** with O_2.

2.4. Experimental Section

2.4.1. *General procedures*

All manipulations were performed under a dry nitrogen atmosphere with the use of either a dry box or standard Schlenk techniques. Solvents were purified by distillation from potassium/benzophenone ketyl. Benzene-d_6 and toluene-d_8 were dried over activated molecular sieves and stored under N_2. $TaCl_5$ (Strem) was freshly sublimed under vacuum. O_2 (National Welders Supply Co.) was dried by P_2O_5 before use. $Ta(NMe_2)_4Cl$ (**5**)[33a], $LiOSiBu^tPh_2$ (**6**)[30] and $Li(THF)_2SiBu^tPh_2$ (**7**)[36a] were prepared by the literature procedures. ^1H and $^{13}C\{^1H\}$ NMR spectra were recorded on a Bruker AC-250 or AMX-400 spectrometer and referenced to solvent (residual protons in the ^1H spectra). Elemental analyses were performed by Complete Analysis Laboratories Inc., Parsippany, New Jersey.

2.4.2. *Observation of $(Me_2N)_4Ta(OSiBu^tPh_2)$ (2) and $(Me_2N)_3Ta(ONMe_2)(OSiBu^tPh_2)$ (3) in the reaction of $(Me_2N)_4TaSiBu^tPh_2$ (1) with O_2 conducted in an NMR tube*

$Li(THF)_2SiBu^tPh_2$ (**7**) (0.0469 g, 0.12 mmol) and $Ta(NMe_2)_4Cl$ (**5**) (0.0409 g, 0.11 mmol) were mixed in a Young NMR tube containing ca. 0.6 mL of benzene-d_6 to yield *in situ* $(Me_2N)_4TaSiBu^tPh_2$ (**1**). Bibenzyl (0.0182 g, 0.10 mmol) was used as an internal standard. The solution was frozen at –60 °C, and the headspace in the Yong's NMR tube was evacuated for 10 min. O_2 (0.10 mmol) was then added, and the NMR tube was subsequently warmed to room temperature, and shaken for 10 min. The brown solution gradually turned into light yellow during this period. ^1H and ^{13}C NMR spectra of the mixture after 20 min of the reaction showed that it was a mixture of **2** (34.3% yield), **3** (5.2% yield) and unreacted $(Me_2N)_4TaSiBu^tPh_2$ (**1**, 16.0%). The NMR chemical shifts of these two new complexes are given in Sections 2.2.3 and 2.2.4. It is not clear if the $(Me_2N)_2(Ph_2Bu^tSiO)_2(Me_2NCH_2NMe)_2Ta_2(\mu\text{-}O)_2$ (**4**) was produced from this reaction involving excess starting tantalum complex **1**. If it was present in the reaction mixture, its ^1H NMR peaks were probably very weak.

2.4.3. *Preparation of $(Me_2N)_4Ta(OSiBu^tPh_2)$ (2), $(Me_2N)_3Ta(ONMe_2)(OSiBu^tPh_2)$ (3) and $(Me_2N)_2(Ph_2Bu^tSiO)_2(Me_2NCH_2NMe)_2Ta_2(\mu\text{-}O)_2$ (4) from the reaction of $(Me_2N)_4TaSiBu^tPh_2$ (1) with O_2*

$Li(THF)_2SiBu^tPh_2$ (**7**) (1.622, 4.16 mmol) in Et_2O (20 mL) at –30 °C was added dropwise to $Ta(NMe_2)_4Cl$ (**5**) (1.502, 3.83 mmol) in Et_2O (30 mL) –30 °C. The mixture was warmed with stirring to room temperature in 2 h. The volatiles were removed. Pentane (20 mL) was added and the solution was then filtered. After filtration, the pentane solution was cooled to –60 °C, and O_2 (5.52 mmol) was added. The yellow solution was stirred overnight at room temperature. A white precipitate was observed in the mixture. All volatiles were removed *in vacuo* to leave a yellow oil containing a white solid. This mixture was then dissolved in CH_2Cl_2, and the solution was cooled to –30 °C to grow colorless crystals of $(Me_2N)_2(Ph_2Bu^tSiO)_2(Me_2NCH_2NMe)_2Ta_2(\mu\text{-}O)_2$ (**4**) (0.0916 g, 0.078 mmol, 4.1%). ^1H NMR (benzene-d_6, 399.87 MHz, 23 °C) δ 8.0-6.80 (m, C_6H_5), 5.49 (d, 2H, $MeNCH_aH_bNMe_2$, $^3J_{H\text{-}H}$ = 9.8 Hz), 4.87 (d, 2H, $MeNCH_aH_bNMe_2$, $^3J_{H\text{-}H}$ = 9.8 Hz), 3.75 (s, 6H, NMe_eMe_f), 3.62 (s, 6H, NMe_eMe_f), 3.36 (s, 6H, $MeNCH_2NMe_2$) 2.88 (s, 6H, $MeNCH_2NMe_cMe_d$), 2.78 (s, 6H, $MeNCH_2NMe_cMe_d$) 1.35 (s, 9H, CMe_3). $^{13}C\{^1H\}$ NMR (benzene-d_6, 100.57 MHz, 7 °C) δ 115-135 (C_6H_5), 87.62 ($MeNCH_2NMe_2$), 48.67 (NMe_eMe_f), 48.61 (NMe_eMe_f), 46.80 ($MeNCH_2NMe_cMe_d$), 46.63 ($MeNCH_2NMe_cMe_d$), 38.83 ($MeNCH_2NMe_2$) 27.52 (CMe_3), 22.72 (CMe_3). In obtaining crystals of high purity for elemental analysis,

toluene was also used to grow the colorless crystals. The X-ray structure of these crystals showed that there are toluene molecules in the unit cell of the crystals in a 1:1 ratio with **4**. The crystallographic data of **4·toluene** are given in Table 2.3. Anal. Calcd for **4·toluene** $C_{51}H_{80}N_6O_4Si_2Ta_2$: C, 48.64; H, 6.40. Found: C, 48.56; H, 6.29.

In a separate, similar test, a ^{1}H NMR spectrum of the mixture (after the reaction) in benzene-d_6 showed that it was mostly $(Me_2N)_4Ta(OSiBu^tPh_2)$ (**2**), $(Me_2N)_3Ta(ONMe_2)(OSiBu^tPh_2)$ (**3**) and $HSiBu^tPh_2$. The presence of $(Me_2N)_2(Ph_2Bu^tSiO)_2(Me_2NCH_2NMe)_2Ta_2(\mu\text{-}O)_2$ (**4**) was not clear based on the ^{1}H NMR spectrum. If it was present in the reaction mixture, its ^{1}H NMR peaks were probably below the base line.

It should be noted that an excess of O_2 is important for the preparation of **4**. When the reaction was conducted with less than one equiv of O_2, no **4** was obtained through crystallization.

2.4.4. *Preparation of $(Me_2N)_4Ta(OSiBu^tPh_2)$ (2) from the reaction of $Ta(NMe_2)_4Cl$ (5) with $LiOSiBu^tPh_2$ (6)*

A mixture of $LiOSiBu^tPh_2$ (**6**) (0801 g, 3.05 mmol) and $Ta(NMe_2)_4Cl$ (**5**) (1.281 g, 3.26 mmol) was placed in a flask at 0 °C. Cold Et_2O (30 mL) at 0 °C was added to the mixture. Then the yellow solution was slowly warmed to room temperature, and stirred overnight. After all volatiles were removed *in vacuo*, pentane (2 × 20 mL) was added, and the solution was filtered. Then volatiles in the filtrate were removed *in vacuo* again to give a yellow oil of

$(Me_2N)_4Ta(OSiBu^tPh_2)$ (**2**) (1.438 g, 2.35 mmol, 77.1% yield). ^1H NMR (benzene-d_6, 300.09 MHz, 23 °C) δ 8.0-6.80 (m, C_6H_5), 3.17 (s, 24H, NMe_2), 1.22 (s, 9H, CMe_3). $^{13}C\{^1H\}$ NMR (benzene-d_6, 75.46 MHz, 23 °C) δ 135-127 (C_6H_5), 45.98 (NMe_2), 27.88 (CMe_3), 20.02 (CMe$_3$). Anal. Calcd for $C_{24}H_{43}N_4SiOTa$: C, 47.05; H, 7.07. Found: C, 47.02; H, 6.85.

2.4.5. *Preparation of $(Me_2N)_3Ta(ONMe_2)(OSiBu^tPh_2)$ (3) from the reaction of $(Me_2N)_3TaCl_2$ (14) with $LiOSiBu^tPh_2$ (6) and $LiONMe_2$ or the reaction of $(Me_2N)_4Ta(OSiBu^tPh_2)$ (2) with O_2*

Method 1. $LiOSiBu^tPh_2$ (**6**, 0.322 g, 1.23 mmol) in THF (15 mL) was added to $(Me_2N)_3TaCl_2$ (**14**, 0.472 g, 1.23 mmol) in THF (10 mL) at -78 °C with vigorous stirring. The mixture was stirred for 22 h. $LiONMe_2$ (0.082 g, 1.23 mmol) was then added to this solution at -18 °C. After stirring for 24 h, all volatiles were removed *in vacuo*. The residue was dissolved in hexanes and filtrated. The volatiles in the filtrate were removed *in vacuo* to give light yellow powders of $(Me_2N)_3Ta(ONMe_2)(OSiBu^tPh_2)$ (**3**, 0.434 g, 0.690 mmol, 56.2% yield). ^1H NMR (benzene-d_6, 400.04 MHz) δ 8.0-70 (m, 4H, C_6H_5), 3.28 (s, 18H, NMe_2), 3.36 (s, 6H, ONMe_2) 1.25 (s, 9H, CMe_3). ^{13}C NMR (benzene-d_6, 100.59 MHz) δ 147.0-127.0 (C_6H_5), 49.37 (ONMe_2), 46.85 (NMe_2), 27.42 (CMe_3), 28.72 (CMe$_3$). Anal. Calcd for $C_{24}H_{43}N_4SiO_2Ta$: C, 45.85; H, 6.89. Found: C, 45.68; H, 6.79.

Method 2. A solution of $(Me_2N)_4Ta(OSiBu^tPh_2)$ (**2**) (1.0377 g, 1.70 mmol)

in pentane (30.0 mL) was frozen in liquid nitrogen. The Schlenk flask was then pumped for 10 min to remove gases in the headspace of flask. After the solution slowly melted, O_2 (1.02 mmol) was added to the solution. The yellow solution was vigorously stirred overnight. A white precipitate was observed. Volatiles were then removed *in vacuo*. Pentane (2 × 20 mL) was added to extract the solution, and the solution was filtered. After removal of the volatiles, crude **3** was obtained as a yellow solid (0.8254 g, 1.31 mmol, 77.1% yield).

It should be noted that in a few times when **3** was prepared by this reaction, a white precipitate formed from the pentane solution. ^{1}H NMR spectra of the white precipitate revealed that it was $(Me_2N)_2(Ph_2Bu^tSiO)_2(Me_2NCH_2NMe)_2Ta_2(\mu\text{-}O)_2$ (**4**).

2.4.6. *Preparation of $(Me_2N)_2(Ph_2Bu^tSiO)_2(Me_2NCH_2NMe)_2Ta_2(\mu\text{-}O)_2$ (4) from the reaction of $(Me_2N)_4TaOSiBu^tPh_2$ (2) with O_2*

A solution of $(Me_2N)_4Ta(OSiBu^tPh_2)$ (**2**, 1.369 g, 2.36 mmol) in pentane (30.0 mL) was frozen in liquid nitrogen. The Schlenk flask containing the solid was then pumped for 10 min to remove gases in the flask. The solution was slowly warmed so that pentane melted. O_2 (2.51 mmol) was added to the solution. The yellow solution was vigorously stirred overnight. A white precipitate was observed. Then all volatiles were removed under vacuum. Pentane (2 × 20 mL) was added to extract the solution, and the solution was filtered. Pentane was removed *in vacuo*, and the residue was dissolved in

CH_2Cl_2 (3 mL). Recrystallization at –30 °C yielded colorless crystals of $(Me_2N)_2(Ph_2Bu^tSiO)_2(Me_2NCH_2NMe)_2Ta_2(\mu\text{-}O)_2$ (**4**, 0.0735 g, 0.062 mmol, 5.3% yield).

2.4.7. *Determination of the structure of $(Me_2N)_2(Ph_2Bu^tSiO)_2(Me_2NCH_2NMe)_2Ta_2(\mu\text{-}O)_2$ (4) by single crystal X-ray diffraction*

The data for the X-ray crystal structures of **4·toluene** and **4·CH_2Cl_2** were collected on a Bruker AXS Smart 1000 X-ray diffractometer equipped with a CCD area detector and a graphite-monochromated Mo source (K_α radiation, 0.71073 Å) and fitted with an upgraded Nicolet LT-2 low temperature device. A suitable crystal was coated with paratone oil (Exxon) and mounted on a hairloop under a stream of nitrogen at –100(2) °C. The structures of **4·toluene** and **4·CH_2Cl_2** were solved by direct methods in triclinic space group *P*-1. Non-hydrogen atoms were anisotropically refined. All hydrogen atoms were treated as idealized contributions. Empirical absorption correction was performed with SADABS.[37a] In addition, the global refinements for the unit cells and data reductions of the two structures were performed using the Saint program (version 6.02).[37a] All calculations were performed using SHELXTL (version 5.1) proprietary software package.[37b]

CHAPTER 3

The Synthesis and Characterization of Disilyl Complexes of Hafnium and Tantalum

3.1. Introduction

Silyl derivatives of transition metals are of intense interest for their unique structures, reactivities and catalytic applications.[1-3] Many early-transition-metal silyl complexes contain the cyclopentadienyl (Cp) ligand or analogous anionic π-ligands,[1] and there are relatively few Cp-free d^0 silyl complexes, especially those with two silyl ligands (Scheme 3.1).[2d,4-9] In comparison, multi-alkyl complexes of these transition metals are well known including peralkyl complexes $M(CH_2R)_n$ (n = 4; M = Ti, Zr, Hf; n = 5, M = Ta; n = 6, M = W).[38] Persilyl complexes $M(SiR_3)_n$ are very difficult to prepare and isolate, and have been one of the major challenges in synthetic inorganic and organometallic chemistry. The preparation of early-transition-metal complexes by the reactions of MCl_n with n equivalents of silyl reagents could have two major decomposition pathways: (a) The metal centers are reduced to form disilanes and reduced metal species; (b) The M-Si bonds could undergo a homolytic cleavage to produce silyl radicals which combine to give disilanes. A report of $Ti(SiPh_3)_4$, prepared from $TiCl_4$ and $KSiPh_3$, was later refuted, and this compound was reformulated as $Ti(OSiPh_3)_4$.[6] It has also been reported to be difficult to prepare silyl complexes from the

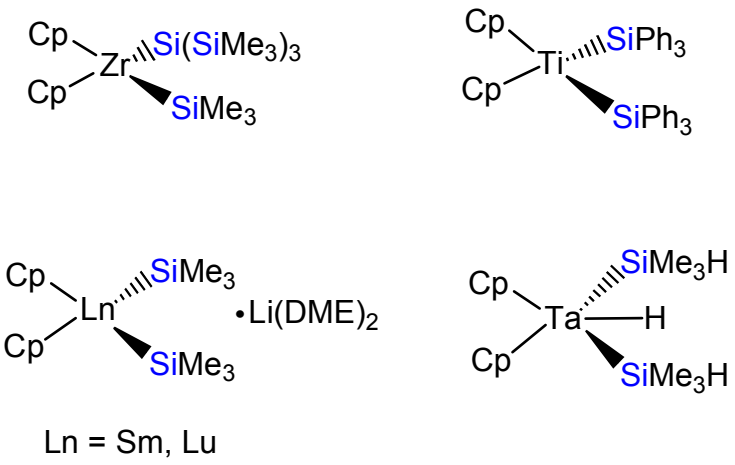

Scheme 3.1. Some reported disilyl complexes

reactions of MCl_4 (M = Zr, Hf) and $TaCl_5$ with $Li(THF)_2SiHMes_2$.[1a] We recently reported the preparation of the first Cp-free, d^0 disilyl complexes of zirconium and hafnium, $Li(THF)_4(Me_2N)_3M(SiPh_2Bu^t)_2$ (M = Zr, Hf).[39] The following d^0 disilyl complexes containing two silyl or one chelating disilyl ligand have been prepared: $K(18\text{-crown-6})_{3/2}\{(Me_2N)_3Hf[\eta^2\text{-}(Me_3Si)_2Si\text{-}(CH_2)_2\text{-}Si(SiMe_3)_2]\}$ (**10**), $(Me_2N)_3Ta[Si(SiMe_3)_3]_2$ (**11**),[39] $(Me_2N)_3Ta(SiBu^tPh_2)_2$ (**15**) and $(Me_2N)_3Ta(SiBu^tPh_2)[Si(SiMe_3)_3]$ (**16**, Scheme 3.2). **11**, **15** and **16** were reported earlier by our research group. Improved syntheses are used in the current work. In addition to study the reactivities of these disiyl complexes, their characterization by ^{29}Si NMR spectroscopy is provided.

3.2. Results and Discussion

3.2.1. *Preparation and characterization of Hf silyl amide complex $K(18\text{-crown-6})_{3/2}\{(Me_2N)_3Hf[\eta^2\text{-}(Me_3Si)_2Si\text{-}(CH_2)_2\text{-}Si(SiMe_3)_2]\}$ (10)*

The reaction of $(Me_2N)_3HfCl$ (**8**)[40a] with $[K(18\text{-crown-6})]_2[(Me_3Si)_2Si\text{-}(CH_2)_2\text{-}Si(SiMe_3)_2]$ (**9**)[41] in toluene was found to give chelating disilyl complexes $K(18\text{-crown-6})_{3/2}\{(Me_2N)_3Hf[\eta^2\text{-}(Me_3Si)_2Si\text{-}(CH_2)_2\text{-}Si(SiMe_3)_2]\}$ (**10**) (Scheme 3.3). The concentrations of both $(Me_2N)_3HfCl$ (**8**) and $[K(18\text{-crown-6})]_2[(Me_3Si)_2Si(CH_2)_2Si(SiMe_3)_2]$ (**9**) were found to be important to the success of the preparation. Solids of both reagents with 1:1 ratio were mixed in one Schlenk flask and dissolved in a small amount of toluene (ca. 15 mL) to start the reaction. The yellow-orange solid products were washed with hexanes leading to a bright

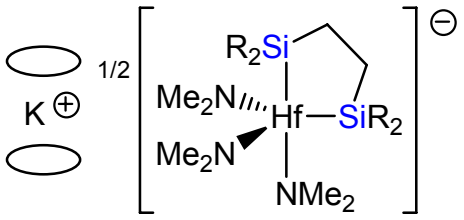

10

= 18-crown-6; R = $SiMe_3$

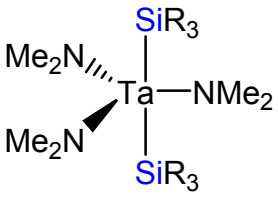

R_3 = $Si(SiMe_3)_3$, **11**; $SiBu^tPh_2$, **15**

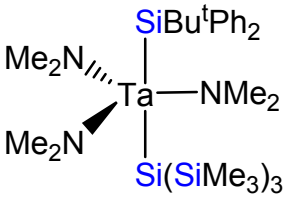

16

Scheme 3.2. New transition metal disilyl complexes

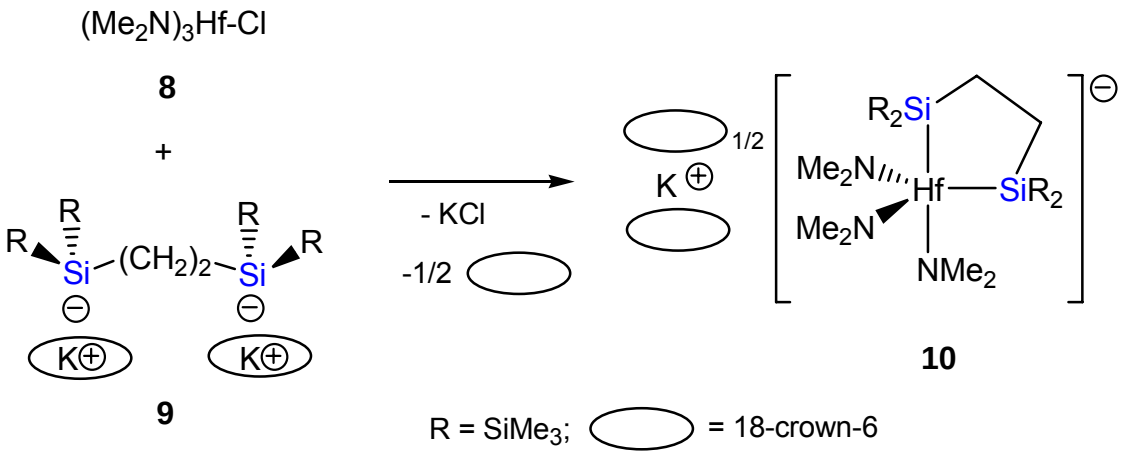

Scheme 3.3. Preparation of Hf disilyl complex **10**

yellow solid. The solid were crystallized from toluene at –30 °C to give crystals of **10·toluene**.

Four resonances were observed in the ^{1}H NMR spectra of **10**. In the ^{1}H NMR spectrum of **10**, the –Si*Me*$_3$ resonance (0.59 ppm) of the disilyl ligand and –O-C*H*$_2$ resonances (3.61 ppm) of 18-crown-6, respectively, are only slightly shifted from those in [K(18-crown-6)]$_2$[(Me$_3$Si)$_2$Si-(CH$_2$)$_2$-Si(SiMe$_3$)$_2$] (**9**)[41] and its Zr analog K(18-crown-6)$_{3/2}${(Me$_2$N)$_3$Zr[η^2-(Me$_3$Si)$_2$Si(CH$_2$)$_2$Si(SiMe$_3$)$_2$]} (**23**) (Table 3.1). The -C*H*$_2$- resonance in the Hf complex **10** is 0.02 ppm downfield shifted from that of its Zr analog **23**. Only one resonance attributed to the –NMe$_2$ ligands was observed at 23 °C in the ^{1}H NMR spectrum of **10** at 400 MHz. In the ^{13}C{^{1}H} NMR spectra of **10**, the –SiMe$_3$ resonance of **10** at 4.23 ppm is upfield-shifted from that (5.74 ppm) in [K(18-crown-6)]$_2$[(Me$_3$Si)$_2$Si(CH$_2$)$_2$Si(SiMe$_3$)$_2$] (**9**) and (4.23 ppm) K(18-crown-6)$_{3/2}${(Me$_2$N)$_3$Zr[η^2-(Me$_3$Si)$_2$Si(CH$_2$)$_2$Si(SiMe$_3$)$_2$]} (**23**). One –NMe$_2$ peak was observed for **10** at 44.31 ppm at 23 °C. In the ^{29}Si NMR spectra of **10**, the Hf-*Si*-SiMe$_3$ peak was observed at –48.8 ppm. The α-Si resonances of, e.g., (Me$_2$N)$_3$Hf-*Si*Bu^{t}Ph$_2$·0.5THF, CpCp*Hf(SiBu^{t}Ph$_2$)Cl,[42] and (Me$_2$N)$_3$Hf-Si(SiMe$_3$)$_3$[40b] were observed at 46.8, 51.48, and –103.5 ppm, respectively. In comparison, ^{29}Si{^{1}H} NMR spectrum of its Zr analog **14** at 23 °C, the Zr-*Si*-SiMe$_3$ peak at –73.11 ppm is consistent with those in other Zr-Si complexes such as (Me$_3$CCH$_2$)$_3$Zr-*Si*(SiMe$_3$)$_3$ (–85.5 ppm), (Me$_3$SiCH$_2$)$_3$Zr-*Si*(SiMe$_3$)$_3$ (–75.7 ppm)[4a,4b] and Cp$_2$Zr[*Si*(SiMe$_3$)$_3$]Cl (–85.5 ppm).[2a]

Table 3.1. NMR resonances of $[K(18\text{-crown-6})]_2[(Me_3Si)_2Si\text{-}(CH_2)_2\text{-}Si(SiMe_3)_2]$ (**9**), $K(18\text{-crown-6})_{3/2}\{(Me_2N)_3Hf[\eta^2\text{-}(Me_3Si)_2Si\text{-}(CH_2)_2\text{-}Si(SiMe_3)_2]\}$ (**10**) and $K(18\text{-crown-6})_{3/2}\{(Me_2N)_3Zr[\eta^2\text{-}(Me_3Si)_2Si(CH_2)_2Si(SiMe_3)_2]\}$ (**23**)

Complex	^{1}H NMR	^{13}C NMR	^{29}Si NMR
9 (Benzene–d_6)	3.32 (OCH_2) 1.33 (SiCH_2) 0.64 (SiMe_3)	70.20 (OCH_2) 17.09 (SiCH_2) 5.74 (SiMe_3)	-6.8 (SiMe$_3$) -111.8 (SiSiMe$_3$)
10 (THF–d_8)	3.61 (OCH_2) 3.01 (NMe_2) 1.19 (SiCH_2) 0.59 (SiMe_3)	71.37 (OCH_2) 44.31 (NMe_2) 15.73 (SiCH_2) 4.23 (SiMe_3)	-5.5 (SiMe$_3$) -48.8 (SiSiMe$_3$)
23 (THF–d_8)	3.63 (OCH_2) 2.99 (NMe_2) 1.07 (SiCH_2) 0.51(SiMe_3)	71.37 (OCH_2) 44.31 (NMe_2) 15.73 (SiCH_2) 4.23 (SiMe_3)	-8.01 (SiMe$_3$) -73.11 (SiSiMe$_3$)

3.2.2. *Crystal and molecular structure of 10·toluene*

A molecular drawing, crystallographic data, selected bond distances and angles and packing diagram of **10·toluene** are given in Figure 3.1, Figure 3.2, Table 3.2, Table 3.3 and Figure 3.3, respectively. Unlike the trigonal bipyramidal anion $[(Me_2N)_3Hf(SiBu^tPh_2)_2]^-$,[38] the $\{(Me_2N)_3Hf[\eta^2\text{-}(Me_3Si)_2Si\text{-}(CH_2)_2\text{-}Si(SiMe_3)_2]\}^-$ anion in **10** is severely distorted from either the trigonal bipyramidal or the square pyramidal geometry. In this case the two Si atoms in the chelating disilyl ligand are *cis* to each other in the pseudo-axial and pseudo-equatorial positions, respectively, with the Si-Hf-Si angle of 70.8º. The Hf-Si bond lengths [2.846(2)-2.863(2) Å] in **10** are slightly shorter than [2.896(7)-2.918(7) Å] in $[(Me_2N)_3Hf(SiBu^tPh_2)_2]^-$. In comparison, the Hf-Si bond [2.807(4) Å] in the monosilyl complex $(Me_2N)_3Hf\text{-}SiBu^tPh_2$ is shorter than in **10**.[40b] The Hf-N bond lengths [2.043(7)-2.063(7) Å] are also similar to 2.029(3)-2.063(5) Å in $[(Me_2N)_3Hf(SiBu^tPh_2)_2]^-$ and 2.019(9)-2.030(9) Å in $(Me_2N)_3HfSiBu^tPh_2$.[40b]

There are two types of cations in **10**: $K(18\text{-crown-6})^+$ or $K(18\text{-crown-6})_2^+$. The K^+ ion in the former was coordinated to one 18-crown-6 ligand. There is also weak interaction between K^+ and two toluene molecules. In the latter, the two 18-crown-6 ligands use six and two O atoms, respectively, to bond to the K^+ ion.

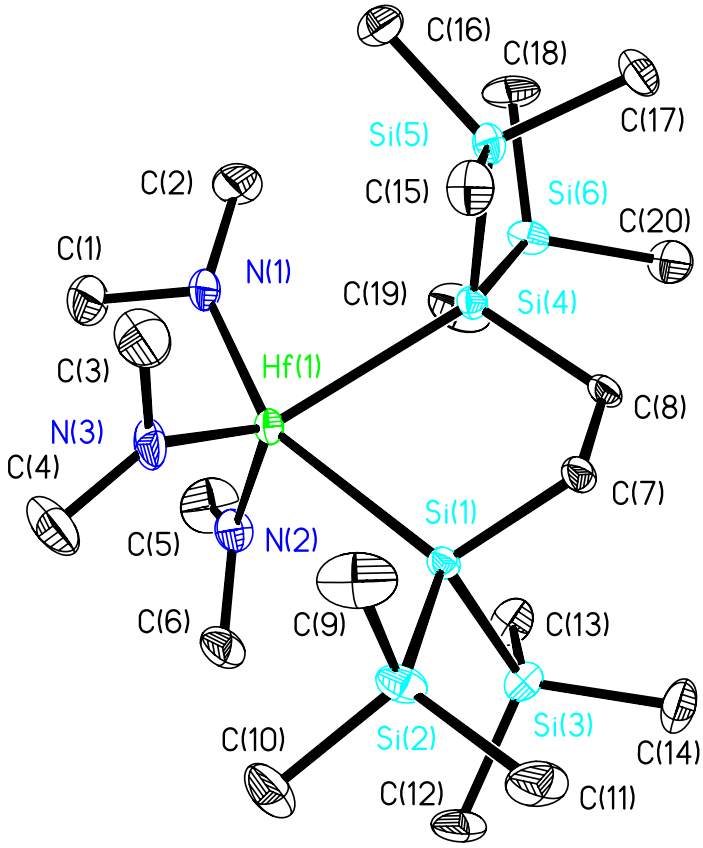

Figure 3.1. ORTEP diagram of the anion in Hf disilyl complex **10·toluene**, showing 30% thermal ellipsoids

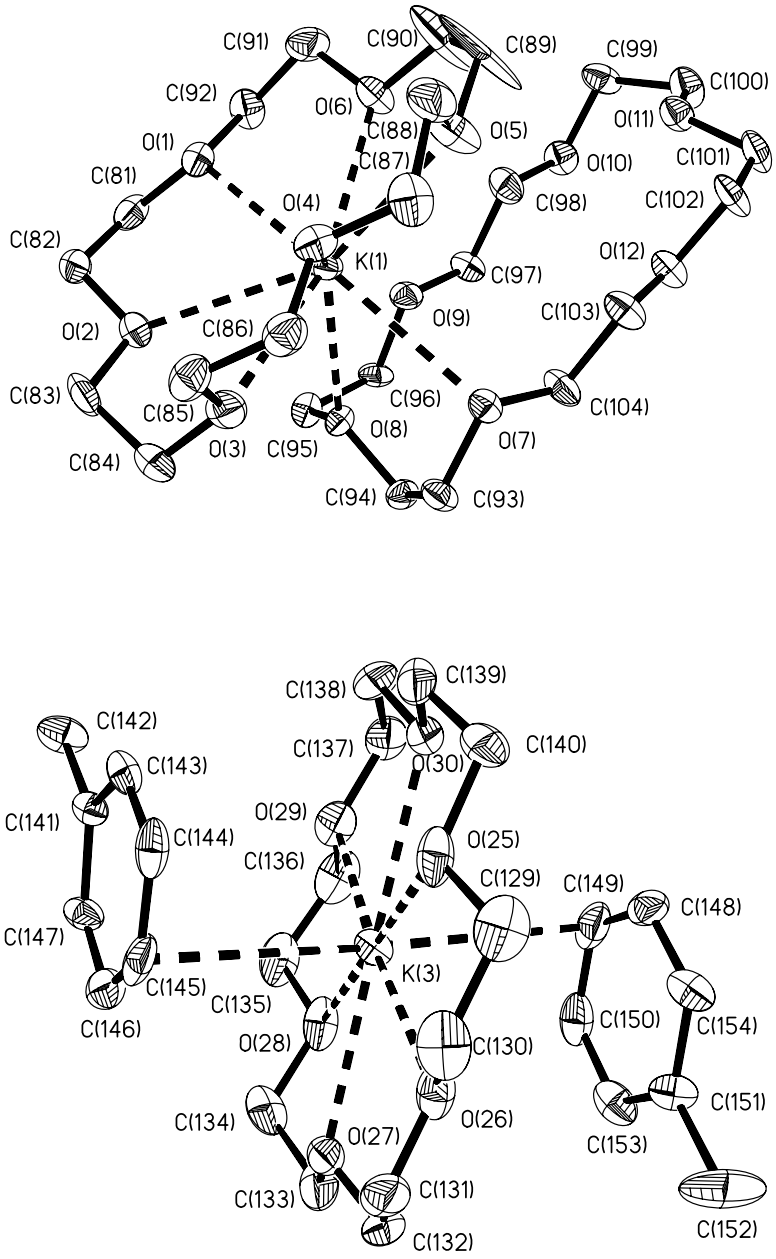

Figure 3.2. ORTEP diagram of the cations in two different molecules of **10·toluene**, showing 30% thermal ellipsoids

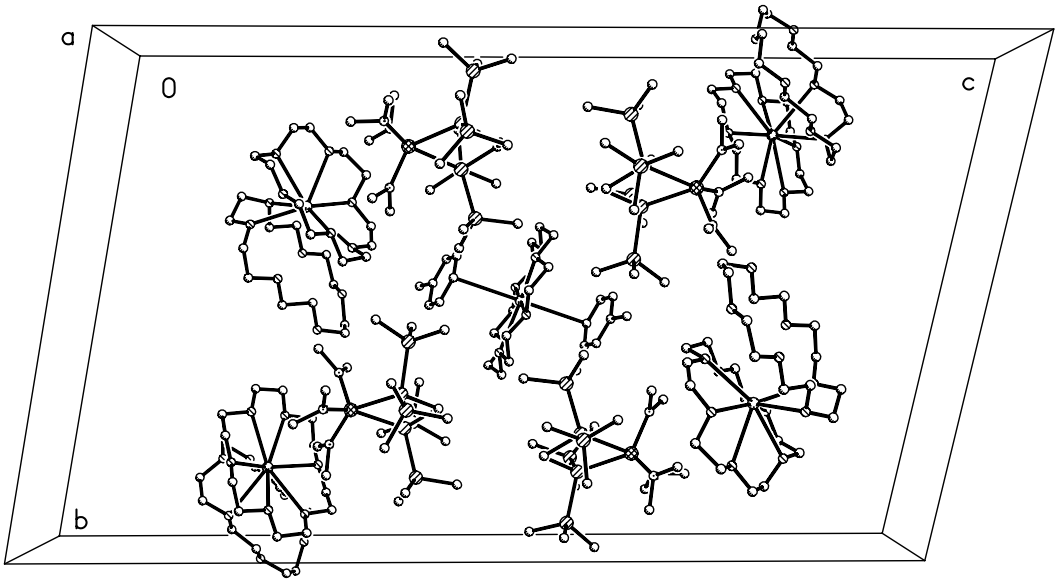

Figure 3.3. Packing diagram of **10** along the *a* axis

Table 3.2. Crystal data and structure refinement for **10·toluene**

Compound	**10·toluene**	
Empirical formula	C180 H420 Hf4 K4 N12 O36 Si24	
Formula weight	4873.80	
Temperature	293(2) K	
Wavelength	0.71073 Å	
Crystal system	Triclinic	
Space group	*P*-1	
Unit cell dimensions	*a* = 13.114(7) Å	α = 100.870(9)°
	b = 24.704(14) Å	β = 91.881(9)°
	c = 41.71(2) Å	γ = 101.425(10)°
Volume	12974(12) Å^3	
Z	2	
Density (calculated)	1.248 g/cm^3	
Absorption coefficient	1.828 mm^{-1}	
F(000)	5144	
Crystal size	0.30 x 0.25 x 0.23 mm^3	
θ range for data collection	1.00 to 28.99°	
Index ranges	$-17 \le h \le 17$, $-33 \le k \le 33$, $-55 \le l \le 55$	
Reflections collected	141993	
Independent reflections	61492 [*R*(int) = 0.0670]	

Table 3.2 Continued

Compound	**10·toluene**
Completeness to θ = 28.99°	89.2%
Max. and min. transmission	0.6785 and 0.6101
Refinement method	Full-matrix-block least-squares on F^2
Data / restraints / parameters	61492 / 0 / 2420
Goodness-of-fit on F^2	0.965
Final R indices [$I > 2\sigma(I)$]	$R1$ = 0.0621, w$R2$ = 0.1476
R indices (all data)	$R1$ = 0.1256, w$R2$ = 0.2000
Largest diff. peak and hole	3.759 and -1.707 e.Å^{-3}

[a] $wR2 = [\Sigma w(F_o^2 - F_c^2)^2/\Sigma w(F_o^2)^2]^{1/2}$; $R = \Sigma||F_o| - |F_c||/\Sigma|F_o|$;

$w = 1/[\sigma^2(F_o^2) + (aP)^2 + bP]$; $P = [2F_c^2 + \text{Max}(F_o^2, 0)]/3$

Table 3.3. Selected bond distances (Å) and angles (deg) in **10**

Distances			
Hf(1)-N(3)	2.043(7)	Hf(1)-N(2)	2.047(7)
Hf(1)-N(1)	2.063(7)	Hf(1)-Si(1)	2.846(2)
Hf(1)-Si(4)	2.863(2)	C(7)-C(8)	1.554(10)
C(7)-Si(1)	1.945(7)	C(8)-Si(4)	1.960(8)
Si(4)-Si(5)	2.357(3)	K(1)-O(8)	2.722(6)
C(1)-N(1)	1.463(12)	C(7)-Si(1)	1.945(7)
Angles			
N(3)-Hf(1)-N(2)	109.4(3)	N(3)-Hf(1)-N(1)	97.2(3)
N(2)-Hf(1)-N(1)	97.9(3)	N(3)-Hf(1)-Si(1)	96.8(2)
N(2)-Hf(1)-Si(1)	96.1(2)	N(1)-Hf(1)-Si(1)	155.7(2)
N(3)-Hf(1)-Si(4)	126.3(2)	N(2)-Hf(1)-Si(4)	123.5(2)
N(1)-Hf(1)-Si(4)	84.9(2)	Si(1)-Hf(1)-Si(4)	70.78(7)
C(8)-C(7)-Si(1)	108.4(5)	C(7)-C(8)-Si(4)	111.1(5)
C(7)-Si(1)-Si(2)	102.0(2)	C(14)-Si(3)-Si(1)	111.7(4)
C(6)-N(2)-Hf(1)	119.7(6)	C(8)-Si(4)-Hf(1)	112.8(2)

3.2.3. *Synthesis and spectroscopic properties of tantalum disilyl complexes $(Me_2N)_3Ta[Si(SiMe_3)_3]_2$ (11), $(Me_2N)_3Ta(SiBu^tPh_2)_2$ (15) and $(Me_2N)_3Ta(SiBu^tPh_2)[Si(SiMe_3)_3]$ (16)*

The tantalum disilyl complex $(Me_2N)_3Ta[Si(SiMe_3)_3]_2$ (**11**) was readily prepared either by the reaction of the silyl chloride complex $(Me_2N)_3Ta[Si(SiMe_3)_3]Cl$ (**12**) with one equiv of $Li(THF)_3Si(SiMe_3)_3$ (**13**) or by the reaction of $(Me_2N)_3TaCl_2$ (**14**) with two equiv of **13** (Scheme 3.4). $(Me_2N)_3Ta(SiBu^tPh_2)_2$ (**15**), an analog of **11**, was similarly prepared. The mixed bis(silyl) complex $(Me_2N)_3Ta(SiBu^tPh_2)[Si(SiMe_3)_3]$ (**16**) was prepared from the reaction of $(Me_2N)_3Ta(SiBu^tPh_2)Cl$ (**17**)[29] with one equiv of $Li(THF)_3Si(SiMe_3)_3$ (**13**, Scheme 3.4).

The NMR spectra of **11**, **15** and **16** are consistent with the structural assignment of the complexes. The ^1H NMR spectra of these disilyl complexes show only one resonance for $–NMe_2$ ligands at both low and room temperatures, suggesting that they may adopt a trigonal bipyramidal structure with two silyl ligands in the axial and three amide ligands in the equatorial positions. In the ^{29}Si NMR spectra of $(Me_2N)_3Ta[Si(SiMe_3)_3]_2$ (**11**) and $(Me_2N)_3Ta(SiBu^tPh_2)_2$ (**15**), the α-Si resonances appear at –6.25 (SiSiMe$_3$) and 48.9 (SiBu^{t}Ph$_2$) ppm, respectively. This follows the general trend of chemical shifts for the silyl ligands $–Si(SiMe_3)_3$ and $–SiBu^tPh_2$ in the complexes listed in Table 3.4 - The former usually is further upfield-shifted than the latter with the exception of $(Me_2N)_4Ta$-$SiBu^tPh_2$ (**1**) and $(Me_2N)_4Ta$-$Si(SiMe_3)_3$ (**20**). Based on this observation, the two α-Si resonances in $(Me_2N)_3Ta(SiBu^tPh_2)[Si(SiMe_3)_3]$ (**16**) at 40.9 and –19.8 ppm

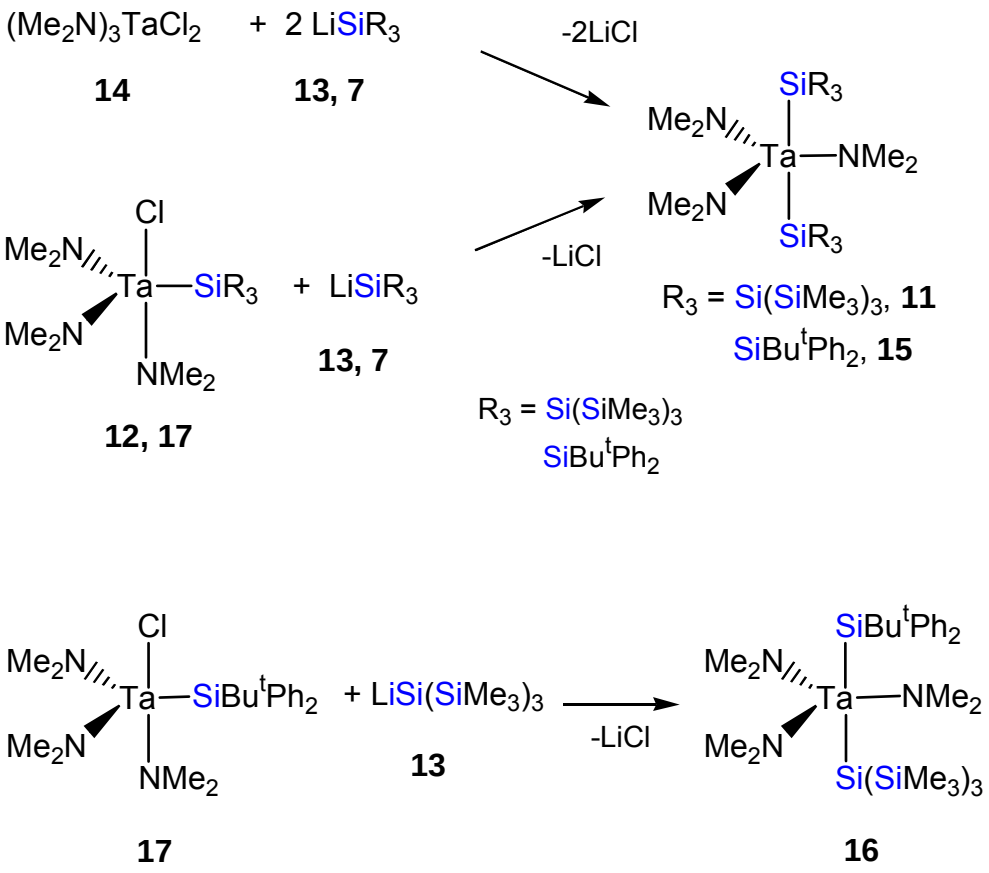

Scheme 3.4. Synthetic pathways to complexes **11**, **15** and **16**

Table 3.4. ^{29}Si NMR resonances of complexes containing the –SiBu^{t}Ph$_2$ or –Si(SiMe$_3$)$_3$ ligands

Compounds	^{29}Si NMR
[Li(THF)$_3$]SiBu^{t}Ph$_2$ (**7**) [a, 36a]	7.54 (*Si*Bu^{t}Ph$_2$)
[Li(THF)$_3$]Si(SiMe$_3$)$_3$ (**13**) [a, 36b]	–185.4 [*Si*(SiMe$_3$)$_3$]
	–5.3 (*Si*Me$_3$)
(Me$_2$N)$_3$Zr-SiBu^{t}Ph$_2$·0.5 THF [b,12b]	19.6 (*Si*Bu^{t}Ph$_2$)
(Me$_2$N)$_3$Zr-Si(SiMe$_3$)$_3$ [b,12b]	–4.4 (*Si*Me$_3$)
	–124.6 [*Si*(SiMe$_3$)$_3$]
(Me$_2$N)$_3$Hf-SiBu^{t}Ph$_2$·0.5 THF [b,40b]	46.8 (*Si*Bu^{t}Ph$_2$)
(Me$_2$N)$_3$Hf-Si(SiMe$_3$)$_3$ [b,40b]	–2.1 (*Si*Me$_3$)
	–103.5 [*Si*(SiMe$_3$)$_3$]
Cp$_2$Hf(SiBu^{t}Ph$_2$)Me [b, 42]	49.04 (*Si*Bu^{t}Ph$_2$)
Cp$_2$Hf[Si(SiMe$_3$)$_3$]Me [b, 42]	–84.12 [*Si*(SiMe$_3$)$_3$]
(Me$_2$N)$_3$Ta(SiBu^{t}Ph$_2$)Cl (**17**) [b,4i]	64.6 (*Si*Bu^{t}Ph$_2$)

Table 3.4. Continued

Compounds	^{29}Si NMR
$(Me_2N)_4Ta\text{-}SiBu^tPh_2$ (**1**) [b,4i]	–189.0 (SiBu^{t}Ph$_2$)
$(Me_2N)_4Ta\text{-}Si(SiMe_3)_3$ (**20**) [b,4i]	–4.0 (SiMe$_3$)
	–98.4 [Si(SiMe$_3$)$_3$]
$(Me_2N)_3Ta(SiBu^tPh_2)_2$ (**15**) [b]	48.94 (SiBu^{t}Ph$_2$)
$(Me_2N)_3Ta[Si(SiMe_3)_3]_2$ (**11**) [b]	0.95 (SiMe$_3$)
	–6.25 [Si(SiMe$_3$)$_3$]
$(Me_2N)_3Ta(SiBu^tPh_2)[Si(SiMe_3)_3]$ (**16**) [c]	40.9 (SiBu^{t}Ph$_2$)
	–11.1 (SiSiMe$_3$)
	–19.8 (SiSiMe$_3$)

[a] benzene-d_6

[b] room temperature, benzene-d_6

[c] 8 °C, benzene-d_6

are assigned to those of –*Si*Bu^{t}Ph$_2$ and –*Si*SiMe$_3$, respectively. Thermal decomposition of (Me$_2$N)$_3$Ta(SiBu^{t}Ph$_2$)[Si(SiMe$_3$)$_3$] (**16**), to be discussed in Chapter 5, prevented us from taking more scans during the NMR data acquisition to observe the $^1J_{Si\text{-}Si}$ couplings which would have helped the assignment.

3.2.4. *Attempted synthesis of chelating disilyl complexes from (NMe$_2$)$_3$TaCl$_2$ (14)*

Since we were able to prepare the Hf disilyl complex K(18-crown-6)$_{3/2}$ {(Me$_2$N)$_3$Hf[η^2-(Me$_3$Si)$_2$Si-(CH$_2$)$_2$-Si(SiMe$_3$)$_2$]} (**10**) as well as Ta complexes (Me$_2$N)$_3$Ta[Si(SiMe$_3$)$_3$]$_2$ (**11**), (Me$_2$N)$_3$Ta(SiBu^{t}Ph$_2$)$_2$ (**15**) and (Me$_2$N)$_3$Ta(SiBu^{t}Ph$_2$)[Si(SiMe$_3$)$_3$] (**16**) (Scheme 3.2), the synthesis of Ta chelating disilyl complexes was attempted using a similar method. Using the chelating silyl precursors [K(18-crown-6)]$_2$[(Me$_3$Si)$_2$Si-(CH$_2$)$_n$-Si(SiMe$_3$)$_2$] (n = 2, **10**; 3, **24**),[41] numerous tests were made to prepare Ta chelating disilyl metal complexes from the reactions with (NMe$_2$)$_3$TaCl$_2$ (**14**). Unfortunately, our attempts failed to yield an identifiable M-Si bonded species (Scheme 3.5). In both cases, once a disilyl precursor (**10** or **24**) was mixed with (NMe$_2$)$_3$TaCl$_2$ (**14**), the yellow solution turned purple quickly. But in the ^{1}H NMR spectrum of the products, the resonance of the -NMe$_2$ ligands was barely observable. Perhaps the Si-Ta bonds break to form the disilane and reduced Ta(III) species. Since Ta(III) species are likely paramagnetic, their NMR signals are broad and usually outside the regular NMR region.

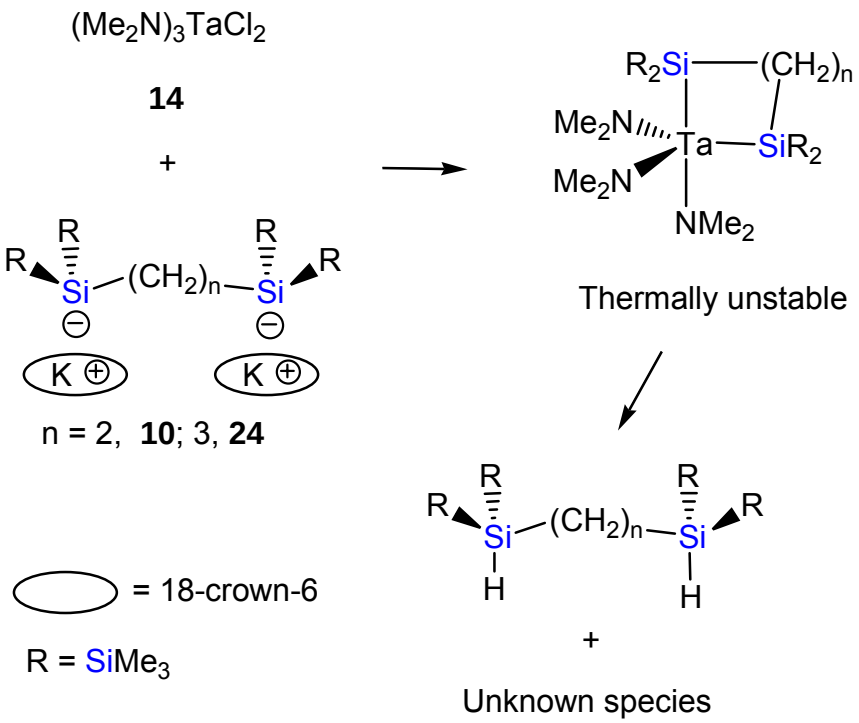

Scheme 3.5. Attempted synthesis of Ta disilyl complexes.

3.2.5. *Studies of a silyl amide exchange in K(18-crown-6)$_{3/2}${(Me$_2$N)$_3$Zr[η^2-(Me$_3$Si)$_2$Si(CH$_2$)$_2$Si(SiMe$_3$)$_2$]} (23)*

We recently reported substitutions of amide ligands in M(NMe$_2$)$_4$ (M = Zr, Hf) by silyl anions in Li(THF)$_2$SiBu^{t}Ph$_2$ (**7**) to give disilyl anions [(Me$_2$N)$_3$M(SiBu^{t}Ph$_2$)$_2$]$^-$ and [M(NMe$_2$)$_5$Li$_2$(THF)$_4$]$^+$ (Scheme 3.6).[43]

A similar exchange was observed in the reaction of Zr(NMe$_2$)$_4$ with 1 equiv of [K(18-crown-6)]$_2$[(Me$_3$Si)$_2$Si-(CH$_2$)$_2$-Si(SiMe$_3$)$_2$] (**9**) in benzene-d_6 (Scheme 3.7). A ^{1}H NMR spectrum of a mixture containing Zr(NMe$_2$)$_4$ and **9** is shown in Figure 3.4. K(18-crown-6)$_{3/2}${(Me$_2$N)$_3$Zr[η^2-(Me$_3$Si)$_2$Si(CH$_2$)$_2$Si(SiMe$_3$)$_2$]} (**23**) was

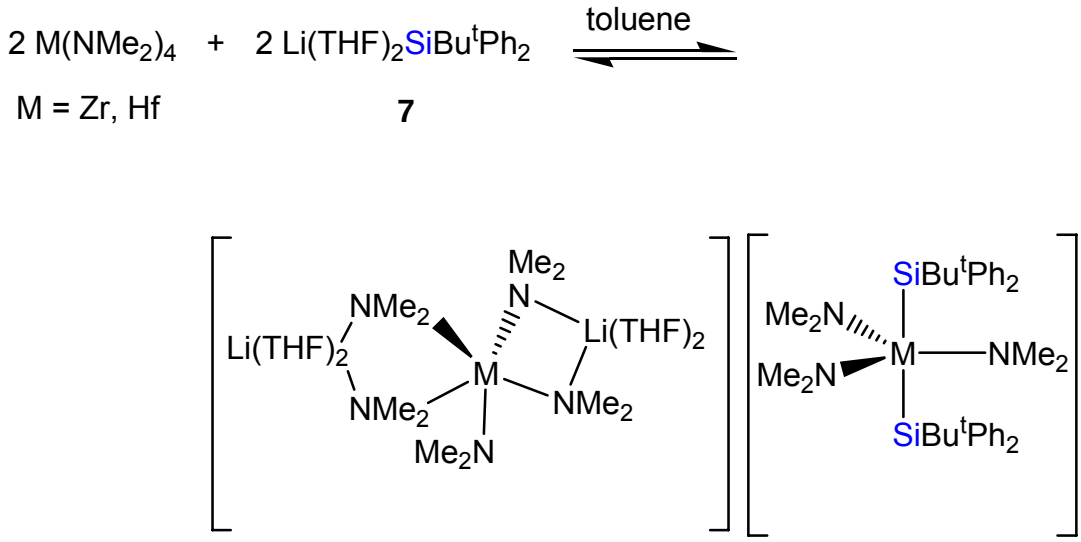

Scheme 3.6. The silyl amide exchanges involving $M(NMe_2)_4$ and $Li(THF)_2SiBu^tPh_2$ (**7**)[43]

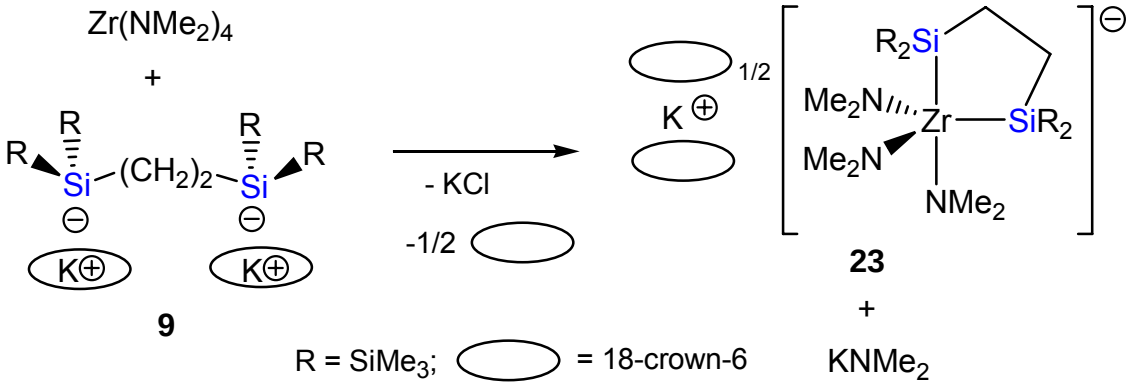

Scheme 3.7. Reaction of $Zr(NMe_2)_4$ and $[K(18\text{-crown-}6)]_2[(Me_3Si)_2Si\text{-}(CH_2)_2\text{-}Si(SiMe_3)_2]$ (**9**) to give $K(18\text{-crown-}6)_{3/2}\{(Me_2N)_3Zr[\eta^2\text{-}(Me_3Si)_2Si\text{-}(CH_2)_2\text{-}Si(SiMe_3)_2]\}$ (**23**). No reversed reaction was observed

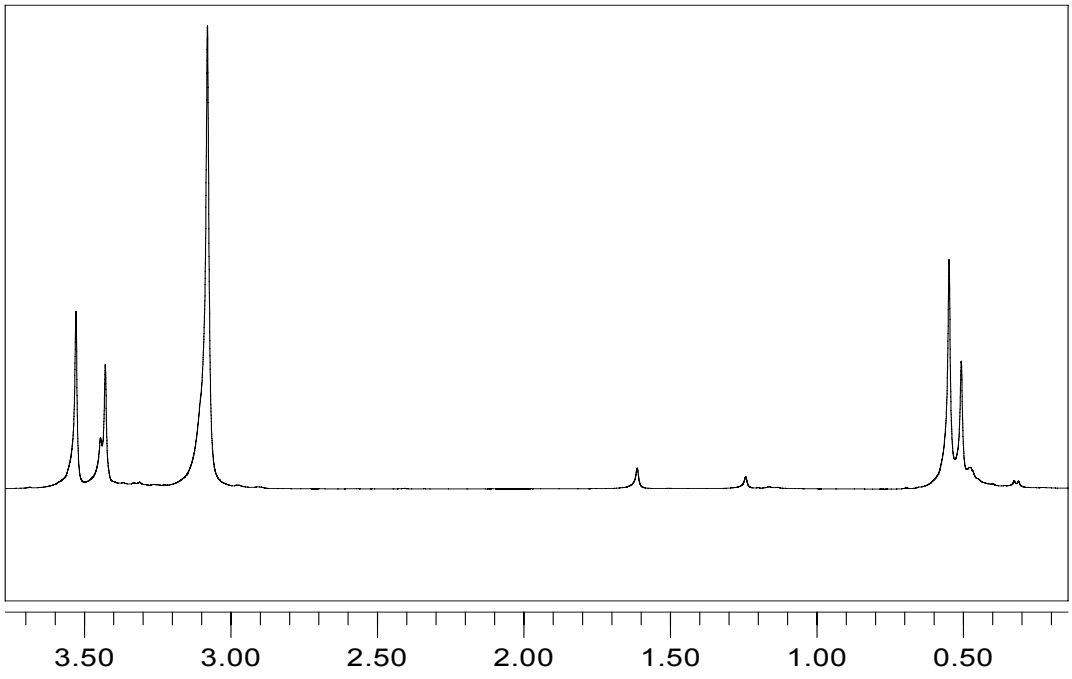

Figure 3.4. ^{1}H spectrum of a mixture of $Zr(NMe_2)_4$ and $[K(18\text{-crown-}6)]_2[(Me_3Si)_2Si\text{-}(CH_2)_2\text{-}Si(SiMe_3)_2]$ (**9**) after mixing the two compounds in benzene-d_6 for 10 min

observed in the ^{1}H NMR spectrum of the mixture after about 10 min (Figure 3.4). It is interesting to note that there is no sign of the starting material $Zr(NMe_2)_4$ in the mixture. This observation suggests that, unlike the equilibrium involving $Li(THF)_2SiBu^tPh_2$ (**7**) and the disilyl complexes $[(Me_2N)_3M(SiBu^tPh_2)_2]^-$ (Scheme 3.6), the substitution of amide ligands in $Zr(NMe_2)_4$ by chelating $[(Me_3Si)_2Si\text{-}(CH_2)_2\text{-}Si(SiMe_3)_2]^{2-}$ is irreversible. This is perhaps not surprising as the substitution of mono-dentate ligands by chelating ligands is driven in part thermodynamically by entropy increase.

A similar reaction between $Zr(NMe_2)_3[N(SiMe_3)_2]$ (**27**) and $[K(18\text{-crown-}6)]_2[(Me_3Si)_2Si\text{-}(CH_2)_2\text{-}Si(SiMe_3)_2]$ (**9**) in benzene-d_6 was investigated by using a 1:1 molar ratio of the reagents. The ^{1}H NMR spectrum of the reaction mixture showed that both **27** and **9** gradually disappeared with the formation of $K(18\text{-crown-}6)_{3/2}\{(Me_2N)_3Zr[\eta^2\text{-}(Me_3Si)_2Si(CH_2)_2Si(SiMe_3)_2]\}$ (**23**) in 21 h (Figure 3.5). Compared to the reaction of $Zr(NMe_2)_4$ with **9**, **27** and **9** were found to react much slower. The bulkiness of $Zr(NMe_2)_3[N(SiMe_3)_2]$ (**27**) in comparison to $Zr(NMe_2)_4$ probably contributes to the slow reaction of **27** with **9**.

3.2.6. *Preparation of $KNMe_2$*

$KNMe_2$ is expected to be a product in the reaction in Scheme 3.7. It was prepared in order to obtain its NMR spectra. Compound $KNMe_2$ was obtained by treating toluene first with a superbasic, 1:1 molar mixture of n-BuLi and $KOBu^t$, followed by the addition of 1 equiv of $HNMe_2$ (Eqs. 3.1-3.2). Such

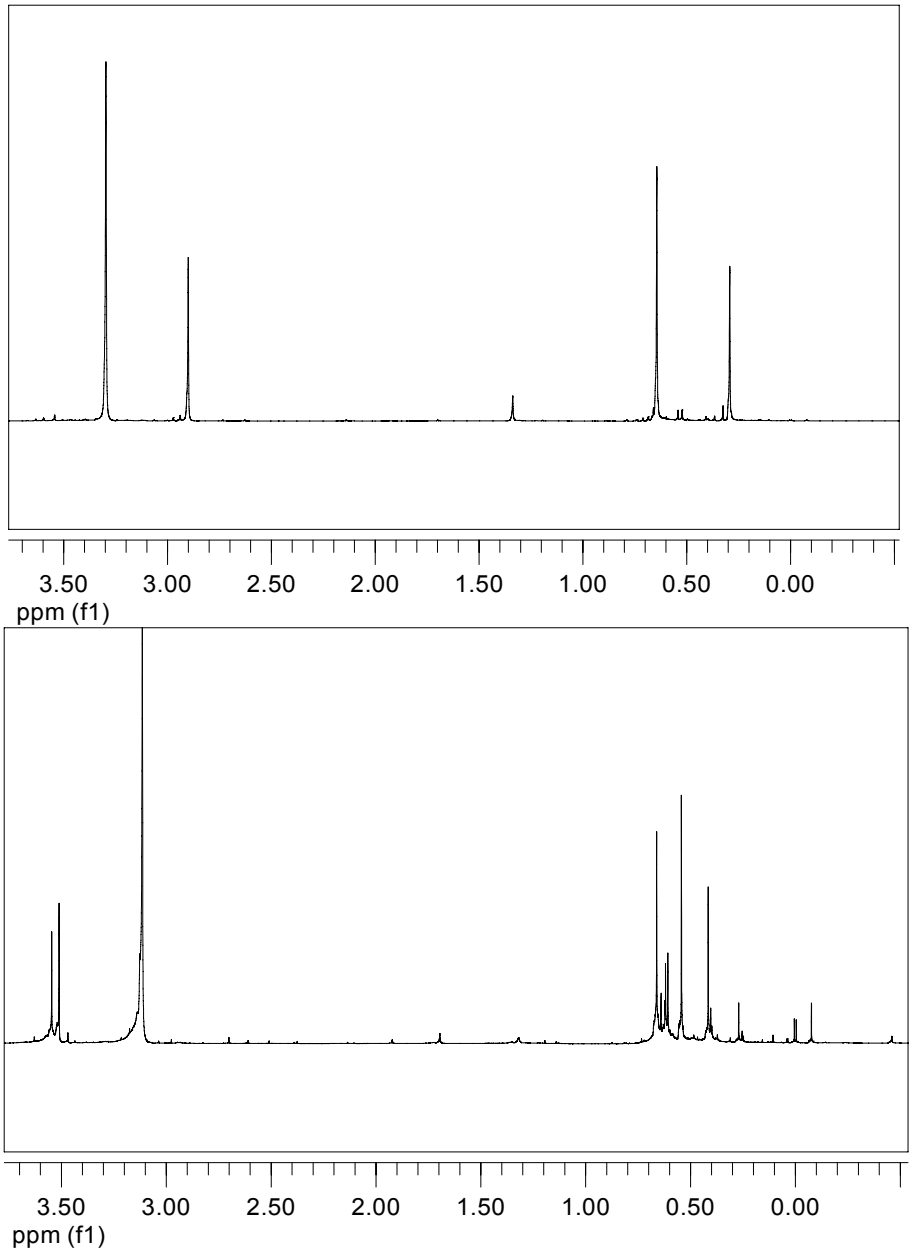

Figure 3.5. ^{1}H spectra of a mixture of $Zr(NMe_2)_3[N(SiMe_3)_2]$ (**27**) and $[K(18\text{-crown-6})]_2[(Me_3Si)_2Si\text{-}(CH_2)_2\text{-}Si(SiMe_3)_2]$ (**9**). Top: 0 h; Bottom: 21 h.

transmetallation is an exothermal reaction due to the formation of the strong Li-O bond.

$$PhCH_3 + \text{n-BuLi} + KOBu^t \longrightarrow PhCH_2K + \text{n-BuH} + LiOBu^t \quad \text{(Eq. 3.1)}$$

$$PhCH_2K + HNMe_2 \longrightarrow KNMe_2 + PhCH_3 \quad \text{(Eq. 3.2)}$$

3.3. Conclusions

Cyclopentadienyl-free, disilyl amide complexes of early-transition metals are readily prepared from either the substitution of chloride ligands [in, e.g., $(Me_2N)_3HfCl$ (**8**), $(Me_2N)_4TaCl$ (**5**)[33a] and $(Me_2N)_3TaCl_2$ (**14**)[33b]] or amide ligands in $Zr(NMe_2)_4$. Penta-coordination seems to be the favored mode of bonding in the amide disilyl complexes, probably because $-NMe_2$ ligands are relatively small. Chelating disilyl complexes $K(18\text{-crown-6})_{3/2}\{(Me_2N)_3Hf[\eta^2\text{-}(Me_3Si)_2Si(CH_2)_2Si(SiMe_3)_2]\}$ (**10**) and $K(18\text{-crown-6})_{3/2}\{(Me_2N)_3Zr[\eta^2\text{-}(Me_3Si)_2Si(CH_2)_2Si(SiMe_3)_2]\}$ (**23**) are much more stable, and the disilyl ligand $[(Me_3Si)_2Si\text{-}(CH_2)_2\text{-}Si(SiMe_3)_2]^{2-}$ apparently does not undergo exchange with amide anions.

3.4. Experimental Section

3.4.1. *General procedures*

All manipulations were performed under a dry nitrogen atmosphere with the use of either a dry box or standard Schlenk techniques. Solvents were

purified by distillation from potassium/benzophenone ketyl and stored under the nitrogen prior to use. $TaCl_5$ (Strem) was sublimed prior to use. $(Me_2N)_3HfCl$ (**8**),[40a] $(Me_2N)_3TaCl_2$ (**14**),[33b] $(Me_2N)_3Ta(SiBu^tPh_2)Cl$ (**17**),[29] $[K(18\text{-crown-}6)]_2[(Me_3Si)_2Si(CH_2)_2Si(SiMe_3)_2]$ (**9**),[41] $Li(THF)_3Si(SiMe_3)_3$ (**13**),[36b] and $Li(THF)_3SiBu^tPh_2$ (**7**)[36a] were prepared according to the literature procedures. Benzene-d_6, THF-d_8 and toluene-d_8 were dried over activated molecular sieves. ^1H and $^{13}C\{^1H\}$ NMR spectra were recorded on a Bruker AC-250 or AMX-400 spectrometer and referenced to solvent (residual protons in the ^1H spectra). $^{29}Si\{^1H\}$ data were obtained by a Bruker AMX-400 spectrometer and referenced to $SiMe_4$. Elemental analyses were performed by Complete Analysis Laboratories Inc., Parsippany, New Jersey.

3.4.2. *Preparation of $K(18\text{-crown-}6)_{3/2}\{(Me_2N)_3Hf[\eta^2\text{-}(Me_3Si)_2Si(CH_2)_2Si(SiMe_3)_2]\}$ (10)*

$(Me_2N)_3HfCl$ (**8**, 0.300 g, 0.867 mmol) and $[K(18\text{-crown-}6)]_2[(Me_3Si)_2Si(CH_2)_2Si(SiMe_3)_2]$ (**9**, 0.863 g, 0.878 mmol) were added to toluene (15 mL). All volatiles were removed *in vacuo* after the reaction mixture was stirred for 45 min. The resulting brown solid was washed with hexanes (3 × 15 mL) to give a bright yellow solid. This solid was dissolved in toluene, and the oil containing solution was cooled to –35 °C to give yellow crystals of **10·toluene** (0.494 g, 0.439 mmol, 51% yield). ^1H NMR (400.0 MHz, THF-d_8, 23 °C) δ 3.61 (s, 36H, O-CH_2), 3.01 (s, 18H, NMe_2), 1.19 (s, 4H, Si-CH_2), 0.59 (s, 36H, SiMe_3).

$^{13}C\{^1H\}$ NMR (100.60 MHz, THF-d_8, 23 ^oC) δ 71.37 (O-*C*H_2), 44.31 (N*Me*$_2$), 15.73 (Si-*C*H_2), 4.23 (Si*Me*$_3$). $^{29}Si\{^1H\}$ NMR (79.5 MHz, THF-d_8, 23 ^oC) δ -5.5 (*Si*Me_3), –48.8 (*Si*$SiMe_3$). The crystals of **10·toluene** were washed with pentane and the solid was then dried *in vacuo*. The ^1H NMR of the solid showed that there was one toluene molecule per three molecules of **10** in the solid. This sample was then submitted for elemental analysis. Anal. Calcd. for $C_{121}H_{290}K_3N_9O_{27}Si_{18}Hf_3$: C, 41.98; H, 8.44. Found: C, 41.67; H, 8.32.

3.4.3. *Preparation of $(Me_2N)_3Ta[Si(SiMe_3)_3]_2$ (11)*

To a yellow slurry of $(Me_2N)_3TaCl_2$ (**14**, 0.511 g, 1.33 mmol) in pentane (25 mL) was added 2 equiv of $Li(THF)_3Si(SiMe_3)_3$ (**13**, 1.25 g, 2.66 mmol) at room temperature. The solution immediately turned deep purple. After stirring for 3 h at room temperature, the volatiles were removed *in vacuo* yielding a purple solid. Extraction of the solid with pentane, followed by filtration and crystallization at -20 °C afforded purple crystals of **11** (0.31 g, 0.38 mmol, 29% yield). ^1H NMR (toluene-d_8, 400.1 MHz, -30 °C) δ 3.22 (s, 18H, N*Me*$_2$), 0.37 (s, 54H, Si*Me*$_3$). $^{13}C\{^1H\}$ NMR (toluene-d_8, 100.6 MHz, -30 °C) δ 44.9 (N*Me*$_2$), 6.5 (Si*Me*$_3$). $^{29}Si\{^1H\}$ NMR (DEPT, toluene-d_8, 79.5 MHz, -30 °C) δ 0.95 (Si*Si*Me_3), –6.25 (*Si*$SiMe_3$). Anal. Calcd for $C_{24}H_{72}N_3Si_8Ta$: C, 35.65; H, 8.98. Found: C, 35.42; H, 8.75.

3.4.4. *Preparation of $(Me_2N)_3Ta(SiBu^tPh_2)_2$ (15)*

$Li(THF)_2SiBu^tPh_2$ (**7**, 0.041 g, 0.11 mmol) was added to a mixture of $(Me_2N)_3TaCl_2$ (**14**, 0.020 g, 0.052 mmol) and 4,4'-dimethylbiphenyl (0.010 g, 0.055 mmol) in benzene-d_6 at room temperature. After 10 min, **15** was observed by NMR (0.041 mmol, 78% yield). Complex **15** was found to be thermally unstable, and it decomposed to $HSiBu^tPh_2$ and other unknown species. The structural assignment for **15** was thus based on its spectroscopic data. ^1H NMR (benzene-d_6, 250.1 MHz) δ 7.58-7.14 (m, 20H, C_6H_5), 2.99 (s, 18H, NMe_2), 1.07 (s, 18H, CMe_3). $^{13}C\{^1H\}$ NMR (benzene-d_6, 62.9 MHz) δ 148.7, 137.3, 127.1, 126.8 (C_6H_5), 44.5 (NMe_2), 31.1 (CMe_3), 24.2 (CMe$_3$). $^{29}Si\{^1H\}$ NMR (benzene-d_6, 79.5 MHz) δ 48.9 (SiBu^{t}Ph$_2$).

3.4.5. *Preparation of $(Me_2N)_3Ta(SiBu^tPh_2)[Si(SiMe_3)_3]$ (16)*

$(Me_2N)_3Ta(SiBu^tPh_2)Cl$ (**17**, 0.022 g, 0.037 mmol) in benzene-d_6 was treated with $Li(THF)_3Si(SiMe_3)_3$ (**13**, 0.017 g, 0.036 mmol) and 4,4'-dimethylbiphenyl (0.014 g, 0.077 mmol) at room temperature. The reaction solution immediately turned purple. **16** was observed by ^1H NMR (0.031 mmol, 86% yield). The complex was found to be unstable at room temperature, and it decomposed to $HSiBu^tPh_2$, $HSi(SiMe_3)_3$ and other unknown species. The structural assignment for **16** was thus based on its spectroscopic data. ^1H NMR (benzene-d_6, 250.1 MHz) δ 7.61-7.15 (m, 10H, C_6H_5), 3.14 (s, 18H, NMe_2), 1.08 (s, 9H, CMe_3), 0.32 (s, 27H, SiMe_3). $^{13}C\{^1H\}$ NMR (benzene-d_6, 62.9 MHz) δ

147.3, 137.2, 127.2, 127.1 (C_6H_5), 44.8 (NMe_2), 30.9 (CMe_3), 24.7 (CMe$_3$), 6.8 (SiMe_3). ^{29}Si{^{1}H} NMR (benzene-d_6, 79.5 MHz, 8 °C) δ 40.9 (SiBu^{t}Ph$_2$), -11.1 (SiSiMe$_3$), -19.8 (SiSiMe$_3$).

3.4.6. *Preparation of $KNMe_2$*

n-BuLi (5.5 mL, 1.6 M in hexane; 8.8 mmol) was added dropwise to a suspension of KOBu^t (1.0 g, 8.9 mmol) in toluene (30 mL) at –30 °C. A red solid was observed as a precipitate. After 2 h, the precipitate was filtered. Then the red solid was washed with pentane (20 mL) twice. At –30 °C, $HNMe_2$ (5.5 mL,1.6 M in THF, 8.8 mmol) was added to a suspension of the red solid in toluene (30 mL). The solution was stirred for another 2 h. The red solid disappeared, and a white solid gradually formed during this time. Extraction of the white solid with pentane, followed by filtration, gave a white solid of $KNMe_2$ (0.6553 g, 7.9 mmol, 89.7% yield).

3.4.7. *X-ray crystal structure determination of 10·toluene*

The crystal structure of **10·toluene** was determined on a Bruker AXS Smart 1000 X-ray diffractometer with Mo K_α radiation. Yellow crystals were selected in Paratone oil, and mounted a hairloop under a N_2 stream at –100 °C. The data of the crystals were collected on a Bruker AXS Smart 1000 X-ray diffractometer equipped with CCD area detector, and fitter with an upgraded Nicolet LT-2 low temperature device. The structure of **10·toluene** was solved by

direct methods. In SHELXTL, the normal L.S. 4 procedure was performed to refine non-hydrogen atoms isotropically. The L.S. 4 procedure could not be used in the anisotropic refinement because of the large size of the cell. The CGLS procedure is much faster and more suitable in most macromolecule refinements.[44] Hence the CGLS and, subsequently, the L.S./BLOC procedures were used in the next, anisotropic refinement. The CGLS procedure does not provide estimated standard deviations (esd), therefore, in the final refinement, L.S. 1 and BLOC 1 procedures were used to obtain estimated standard deviations of bond lengths and bond angles in **10·toluene**. All hydrogen atoms were included in the structure factor calculation at idealized positions and were allowed to ride on the neighboring atoms with relative isotropic displacement coefficients. The SHELXTL (Version 5.1) proprietary software package was used for all structure solution and refinement calculations.

CHAPTER 4

Kinetic and Mechanistic Studies of the Silyl Substitution Reaction in a Tantalum Disilyl Complex

4.1. Introduction

Substitution is a fundamental reaction of organometallic complexes,[45] and it has played an important role in the formation of metal silyl complexes.[2-7] Substitutions of ligands by silyl anions SiR_3^- are among the most widely used synthetic pathways to yield metal silyl complexes. There have been relatively few studies of the kinetics and mechanism in the substitution involving silyl ligands.[39] We recently found that the silyl ligand in $(Me_2N)_3ZrSi(SiMe_3)_3$ undergoes a reversible exchange with $SiBu^tPh_2^-$, probably through a disilyl intermediate $\{[(Me_2N)_3Zr(SiBu^tPh_2)[(SiMe_3)_3]\}^-$, to reach the following equilibrium (Eq. 4.1):[39]

$$(Me_2N)_3ZrSi(SiMe_3)_3 + SiBu^tPh_2^- \rightleftharpoons (Me_2N)_3ZrSiBu^tPh_2 + Si(SiMe_3)_3^- \quad \text{(Eq. 4.1)}$$

ΔH° = –4.6(0.5) kcal/mol and ΔS° = –7(2) eu

In comparison, the substitution of the silyl ligands $(Me_2N)_3Ta[Si(SiMe_3)_3]_2$ (**11**) by $SiBu^tPh_2^-$ anions at 23 °C (Scheme 4.1) was found to be irreversible.[39b] The two –$Si(SiMe_3)_3$ ligands in $(Me_2N)_3Ta[Si(SiMe_3)_3]_2$ (**11**) are replaced sequentially by

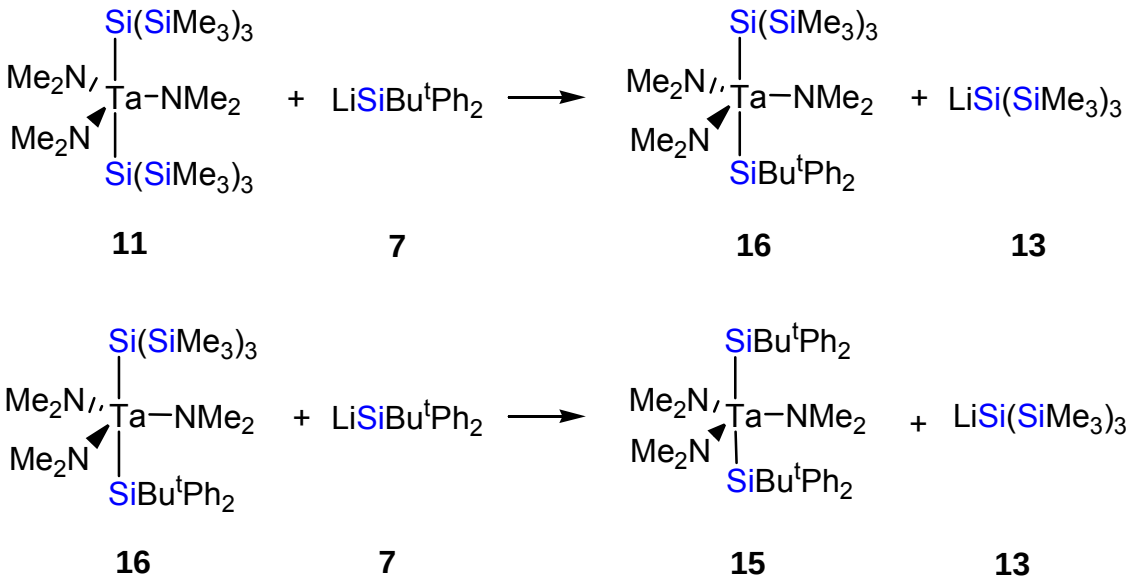

Scheme 4.1. Substitution of silyl ligands in **11** to give **15**

the $SiBu^tPh_2^-$ anions in benzene-d_6 or toluene-d_8 to give $(Me_2N)_3Ta(SiBu^tPh_2)[Si(SiMe_3)_3]$ (**16**) and $(Me_2N)_3Ta(SiBu^tPh_2)_2$ (**15**) (Scheme 4.1).[39b] **15** was found, however, to be inert to the exchange with the $Si(SiMe_3)_3^-$ anion.

The nature of the exchange among $(Me_2N)_3Ta[Si(SiMe_3)_3]_2$ (**11**), $(Me_2N)_3Ta(SiBu^tPh_2)[Si(SiMe_3)_3]$ (**16**) and $(Me_2N)_3Ta(SiBu^tPh_2)_2$ (**15**) is not clear. We have studied the kinetics and mechanistic pathways in the reaction of **11** with $SiBu^tPh_2^-$ to give **16**. The replacement of a silyl ligand in **11** to yield **16** was found to follow dissociative mechanism. Tetrahydrofuran (THF) in mixed THF-toluene-d_8 solvents promotes the substitution reactions, and the effect of THF on the kinetics of the reactions has been investigated. Our studies are reported here.

4.2. Results and Discussion

4.2.1. *Kinetic studies of the silyl ligand substitution reactions in $(Me_2N)_3Ta[Si(SiMe_3)_3]_2$ (11)*

Two possible reaction pathways in Scheme 4.2 were considered. The first pathway (**Path I**), a dissociative process, involves the dissociation of one $Si(SiMe_3)_3^-$ ligand in **11** to give a four coordination tantalum intermediate (**A**), followed by addition of a $SiBu^tPh_2^-$ anion. Second pathway (**Path II**), an associative process, involves the addition of a $SiBu^tPh_2^-$ anion to **11** to give a hexa-coordinated intermediate (**B**), followed by $Si(SiMe_3)_3^-$ dissociation. Excess

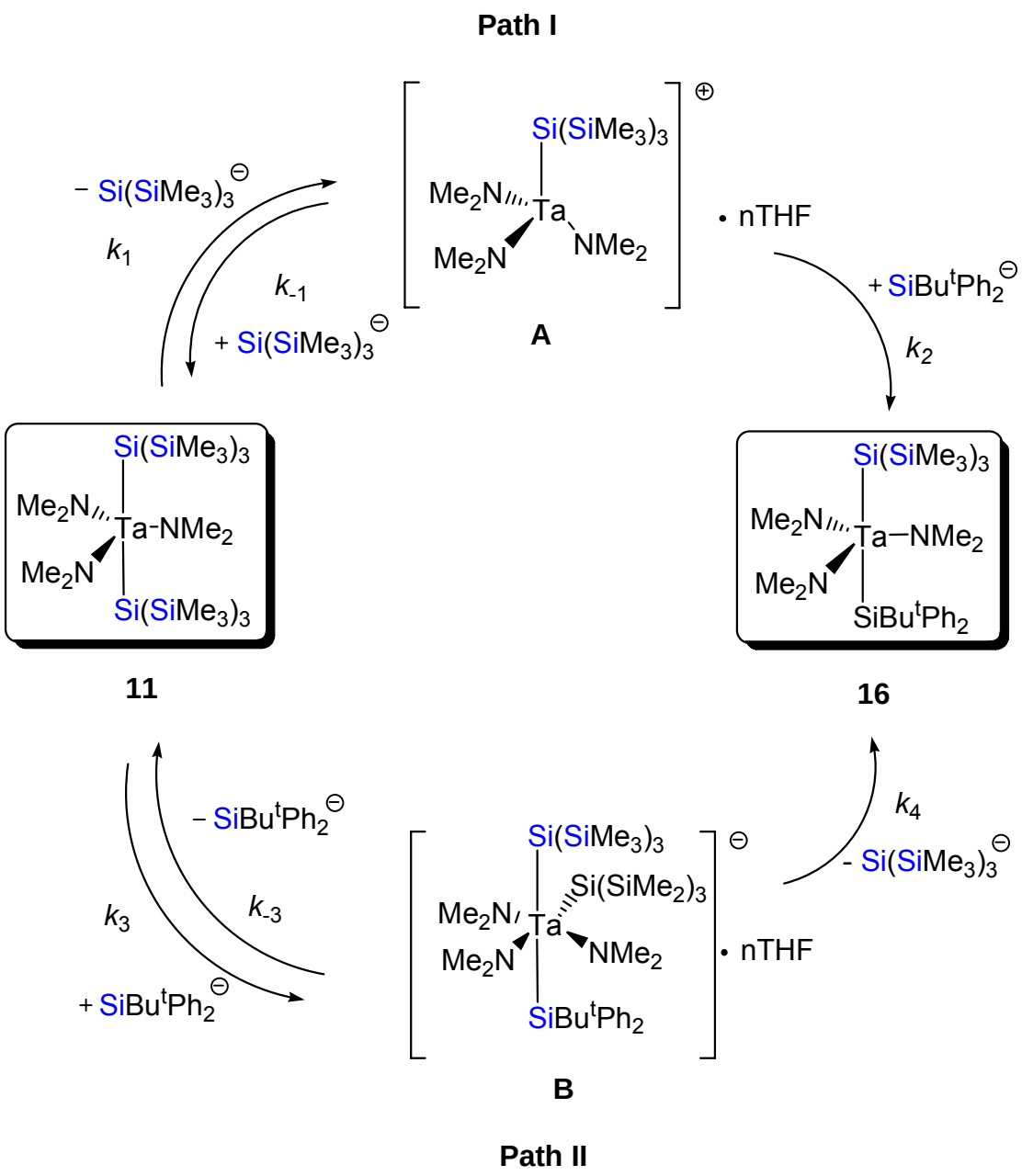

Scheme 4.2. Possible mechanic pathways in the conversion of **11** to **16**

$Li(THF)_3SiBu^tPh_2$ (**7**) was used in the kinetic studies so that the first reaction in Scheme 4.1, the **11** →**16** conversion, follows pseudo first-order kinetics . The substitution reactions with excess of $Li(THF)_3SiBu^tPh_2$ (**7**) in toluene-d_8 were found to be fast at room temperature. Kinetic studies of the conversion of **11** → **16** (Scheme 4.2) were thus performed at 233 K in toluene-d_8 with a ca. 15-fold excess of **7**. Since **7** is in much excess, the second reaction in Scheme 4.1, the **16** → **15** conversion, will have little effect on the kinetics of the first reaction (**11** → **16**). Even at 233 K, the reaction was found to be fast, and the control of both temperature and time of mixing **11** with $Li(THF)_3SiBu^tPh_2$ (**7**) was found to be important to obtaining accurate kinetic data. In addition, the THF concentration in mixed toluene-d_8-THF needs to be controlled, as it was found to affect the reaction rate. The effect of THF on the kinetics is discussed below. The kinetics of this ligand exchange reactions was monitored by the disappearance of **11** in ^{1}H NMR spectra (Figure 4.1).

If the dissociative mechanism in **Path I** (Scheme 4.2) was operative in this reaction, the kinetic law for the **11**→ **16** conversion through the steady-state approximation is given in Eq. 4.2.

$$-\frac{dC_1}{dt} = \frac{k_1 k_2 C_{LiSiBu^tPh_2} C_{THF}^{\ n}}{k_{-1} C_{LiSi(SiMe_3)_3} + k_2 C_{LiSiBu^tPh_2}} C_1 = k_{obs} C_1 \qquad \text{(Eq. 4.2a)}$$

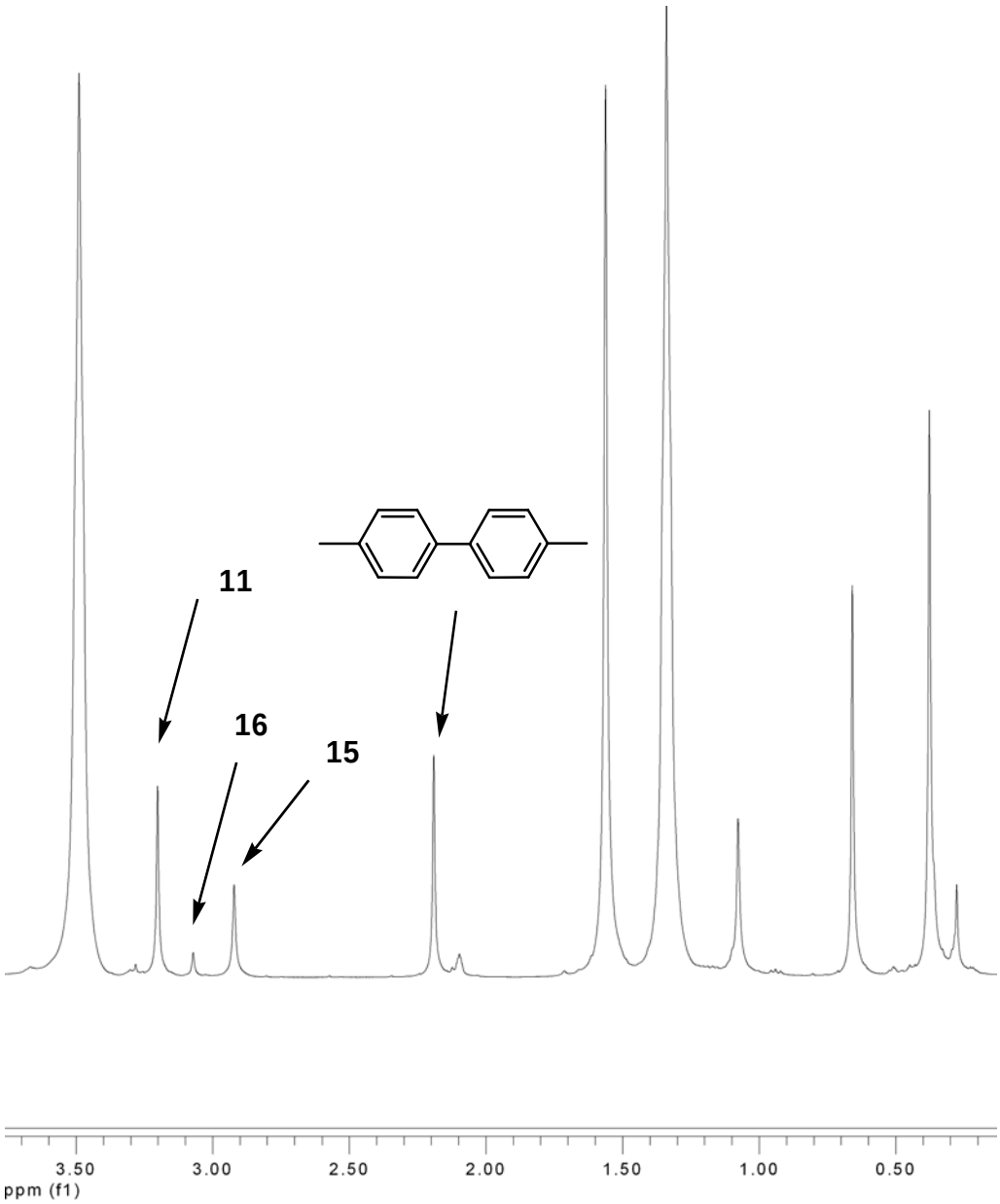

Figure 4.1. A ^{1}H NMR spectrum showing the conversion of **11** to **16**

$$k_{obs} = \frac{k_1 k_2 C_{LiSiBu^tPh_2} C_{THF}^{\ n}}{k_{-1} C_{LiSi(SiMe_3)_3} + k_2 C_{LiSiBu^tPh_2}} \qquad \text{(Eq. 4.2b)}$$

The order of THF (n = 1.7) will be discussed in Section 4.2.2.

Let $k_{obs}' = k_{obs}/C_{THF}^{\ 1.7}$, Eq. 4.2 gives

$$k_{obs}' = \frac{k_1 k_2 C_{LiSiBu^tPh_2}}{k_{-1} C_{LiSi(SiMe_3)_3} + k_2 C_{LiSiBu^tPh_2}} \qquad \text{(Eq. 4.3a)}$$

Which is expressed in the following linear form:

$$\frac{1}{k_{obs}'} = \frac{k_{-1} C_{LiSi(SiMe_3)_3}}{k_1 k_2 C_{LiSiBu^tPh_2}} + \frac{1}{k_1} \qquad \text{(Eq. 4.3b)}$$

In other words, a plot of $1/k_{obs}'$ *vs.* $C_{LiSi(SiMe_3)_3}/C_{LiSiBu^tPh_2}$ would be linear, showing values of k_1 and k_{-1}/k_2 in this dissociative pathway.

If the reaction proceeded by the associative pathway in **Path II** (Scheme 4.2), a much simpler rate law is obtained (Eq. 4.4) when $Li(THF)_3SiBu^tPh_2$ (**7**) is in excess. In such a case, the pseudo first-order rate constant k_{obs} is a function of the concentrations of $Li(THF)_3SiBu^tPh_2$ (**7**) ($C_{Li(THF)_3SiBu^tPh_2}$).

$$- dC_{\mathbf{1}}/dt = k_3 \, C_{THF}^{\,n} \, C_{Li(THF)_3SiBu^tPh_2} \, C_{\mathbf{1}} = k_{obs} \, C_{\mathbf{1}} \qquad \text{(Eq. 4.4a)}$$

$$k_{obs} = k_3 \, C_{THF}^{\,n} \, C_{Li(THF)_3SiBu^tPh_2} \qquad \text{(Eq. 4.4b)}$$

Kinetic studies were conducted with concentrations of $Li(THF)_3SiBu^tPh_2$ (**7**) ($C_{Li(THF)_3SiBu^tPh_2}$) ranging from 0.101 to 0.243 M and the THF concentration (C_{THF}) ranging from 0.607 to 0.738 M at 233 K. Under these conditions the disappearance of **11** was found to follow pseudo first-order kinetics. Values of k_{obs} and k_{obs}' are given in Table 4.1. A plot of k_{obs}' *vs.* $C_{LiSi(SiMe_3)_3}{}^{(AV)}/C_{LiSiBu^tPh_2}{}^{(AV)}$ in Figure 4.2 is linear, as expected for the dissociative process (**Path I**).

4.2.2. *THF dependence of the 11 → 16 conversion*

Both silyl reagents $Li(THF)_3Si(SiMe_3)_3$ (**13**) and $Li(THF)_3SiBu^tPh_2$ (**7**) contain THF. The former was used to prepare $(Me_2N)_3Ta[Si(SiMe_3)_3]_2$ (**11**) *in situ* which was then employed in the kinetic studies involving $Li(THF)_3SiBu^tPh_2$ (**7**). THF in the mixed THF-toluene-d_8 solution was found to promote the substitution reactions and to affect the kinetics. Studies were conducted at 233 K to establish the order of rate constants k_{obs} with respect to THF. A total of six THF concentrations (0.370, 0.465, 0.525, 0.616, 0.723 and 0.829 M) were used to conduct the studies with the initial concentration of **11** at 0.141 M. These kinetic studies give the kinetic plots in Figure 4.3 and rate constants k_{obs} in Table 4.2.

Table 4.1. Observed rate constants for the **11** → **16** conversion at 233 K

C_{THF} (M)	k_{obs} x 10^4 (s^{-1})	k_{obs}' x 10^4 (s^{-1})	$C_{LiSiBu^tPh_2}$ (M)	$C_{LiSi(SiMe_3)_3}{}^{(AV)}/C_{LiSiBu^tPh_2}{}^{(AV)}$
0.667	2.699	5.373	0.101	0.1834
0.681	2.743	5.271		
0.723	3.252	5.644	0.121	0.1497
0.724	3.401	5.889		
0.722	3.727	6.484	0.162	0.1087
0.738	3.930	6.587		
0.670	3.480	6.871	0.202	0.0858
0.702	3.791	6.918		
0.670	3.602	7.116	0.243	0.0706
0.607	3.193	7.452		

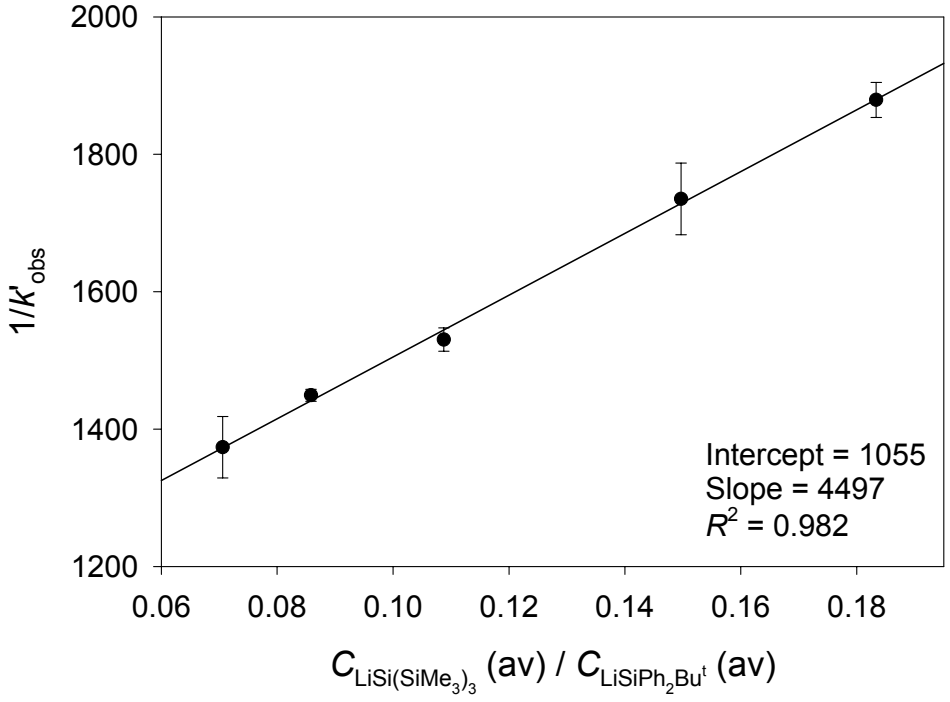

Figure 4.2. Kinetic plot of the **11** → **16** conversion

Table 4.2. Rate constant *k* at 233 K for the **11** $\rightarrow$ **16** conversion with different C_{THF}[a]

C_{THF} (M)	$[k_{obs} \pm \delta k_{(ran)}] \times 10^4$ (s^{-1})
0.370	1.07 $\pm$ 0.05
0.465	1.48 $\pm$ 0.11
0.525	1.88 $\pm$ 0.05
0.616	2.40 $\pm$ 0.08
0.723	3.33 $\pm$ 0.08

[a] The total uncertainty of $\delta k/k$ = 8.9% was calculated from $\delta k_{(ran)}/k$ = 7.4% and $\delta k_{(sys)}/k$ = 5%.

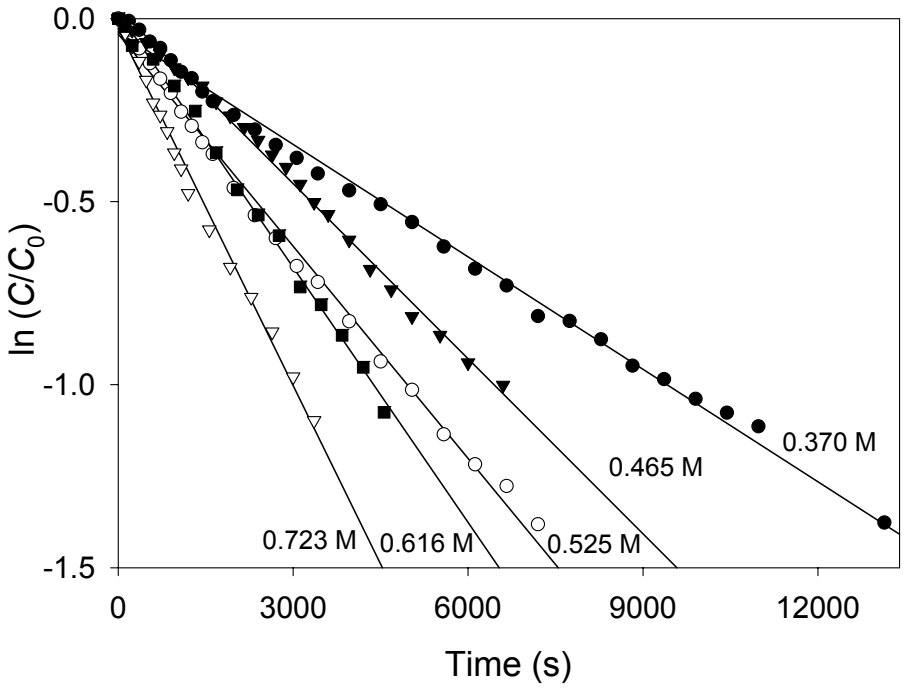

Figure 4.3. Kinetic plots of the **11** → **16** conversion with different C_{THF}

The rates of the **11** → **16** conversion with different THF concentrations are listed in Table 4.2. The plot of ln (k_{obs} x 10^4) vs. C_{THF} (Eq. 4.5) give a slope of 1.7(0.3) (Figure 4.4). The observation demonstrates that THF helps the dissociation of the $Si(SiMe_3)_3^-$ ligand in **11** to give intermediate **A** (Scheme 4.2). One interpretation is that, in the transition state leading to the formation of cationic **A** (from neutral **11**), there is a significant degree of charge separation. THF, a polar solvent, lowers the energy of the transition state and the activation energy of the Ta-Si bond cleavage process to give **A**. A highly solvent dependent alkylation was reported by Collum and coworker with seven orders on THF concentraion.[46]

$$\ln k_{obs} = n \ln C_{THF} + \ln k_1 \qquad \text{(Eq. 4.5)}$$

4.2.3. *Mechanistic studies of the conversion of $(Me_2N)_3Ta[Si(SiMe_3)_3]_2$ (11) to $(Me_2N)_3Ta(SiBu^tPh_2)_2$ (15)*

The proposed pathways for the **11** → $(Me_2N)_3Ta(SiBu^tPh_2)[Si(SiMe_3)_3]$ (**16**) conversion are shown in Scheme 4.2. From the kinetic studies of this reaction, at a large excess of $LiSiBu^tPh_2$, the observed rate constant k_{obs} was independent of the incoming silyl ligand, and this is consistent with the dissociative mechanism in **Path I** of Scheme 4.2. A similar process for the **16** → **15** conversion is expected, since the **16** → **15** conversion is also a silyl substitution reaction from $SiBu^tPh_2^-$ to $Si(SiMe_3)_3^-$. Therefore an overall

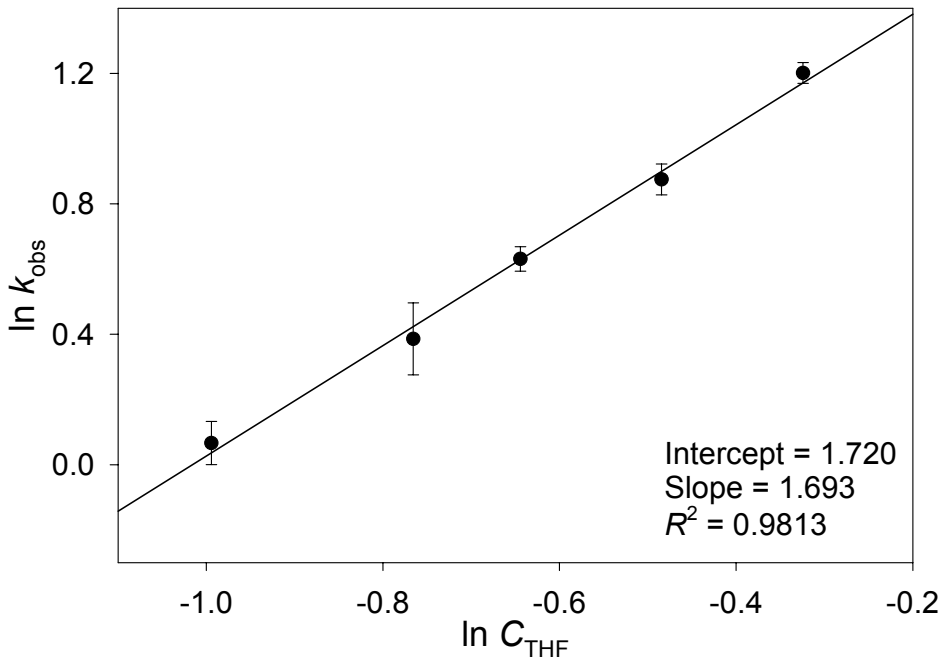

Figure 4.4. Plots of (k_{obs} x 10^4) vs. ln (C_{THF}) for the **11** → **16** conversion with different THF concentrations

mechanism similar to the **11** → **16** conversion is shown in Scheme 4.3, in which a -Si(SiMe$_3$)$_3$ ligand in **16** dissociates from **11** to give an intermediate complex **A** with an open coordination site to form a bond with the SiBu^{t}Ph$_2^-$ anion.

We reported earlier that in the silyl exchange equilibrium involving *monosilyl* complexes (Me$_2$N)$_3$ZrSi(SiMe$_3$)$_3$ and (Me$_2$N)$_3$ZrSiBu^{t}Ph$_2$ in Eq. 4.1.[39a] This exchange is likely an associative process through an anionic disilyl intermediate {(Me$_2$N)$_3$Zr(SiBu^{t}Ph$_2$)[Si(SiMe$_3$)$_3$]}$^-$ (Scheme 4.4).[39a] An analog of this intermediate, [(Me$_2$N)$_3$Zr(SiBu^{t}Ph$_2$)$_2$]$^-$, was directly observed in the silyl exchange involving (Me$_2$N)$_3$ZrSiBu^{t}Ph$_2$ and SiBu^{t}Ph$_2^-$.[39a] In the exchange in Eq. 4.1 (Scheme 4.4), (Me$_2$N)$_3$ZrSiBu^{t}Ph$_2$ is thermodynamically favored over (Me$_2$N)$_3$ZrSi(SiMe$_3$)$_3$ with, e.g., K_{eq} = 192.51(0.01) at 263(1) K. The -Si(SiMe$_3$)$_3$ ligand is bulkier than the SiBu^{t}Ph$_2$ ligand, although this alone may not be the deciding factor. The stability of complexes containing the -SiBu^{t}Ph$_2$ ligand(s) may also explain why [(Me$_2$N)$_3$Zr(SiBu^{t}Ph$_2$)$_2$]$^-$ was observed (and structurally characterized) but not its disilyl analogs containing either one or two -Si(SiMe$_3$)$_3$ ligands. The observations that complexes containing the -SiBu^{t}Ph$_2$ silyl ligand are more stable than their -Si(SiMe$_3$)$_3$ analogs may also explain why the substitution of the -Si(SiMe$_3$)$_3$ ligands by SiBu^{t}Ph$_2^-$ is irreversible.

Given the bulky structure of penta-coordinated, Zr disilyl complex [(Me$_2$N)$_3$Zr(SiBu^{t}Ph$_2$)$_2$]$^-$,[39a] it is perhaps not surprising that its Ta disilyl analog (Me$_2$N)$_3$Ta[Si(SiMe$_3$)$_3$]$_2$ (**11**) undergoes a dissociative pathway in the substitution of the silyl ligand by SiBu^{t}Ph$_2^-$ anion (Scheme 4.2, **Path I**). The first step in this

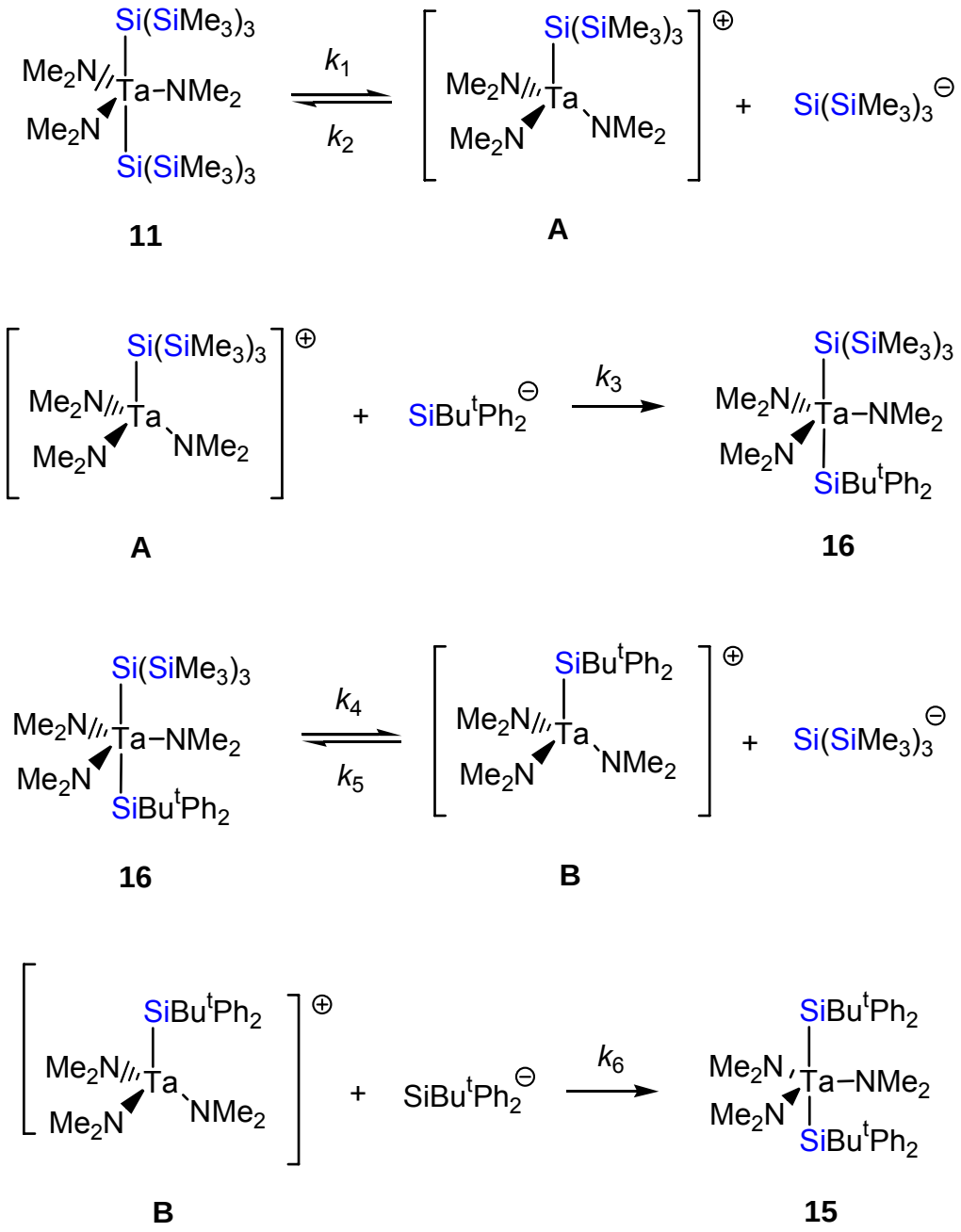

Scheme 4.3. Mechanic pathway in the conversion of **11** to **15**

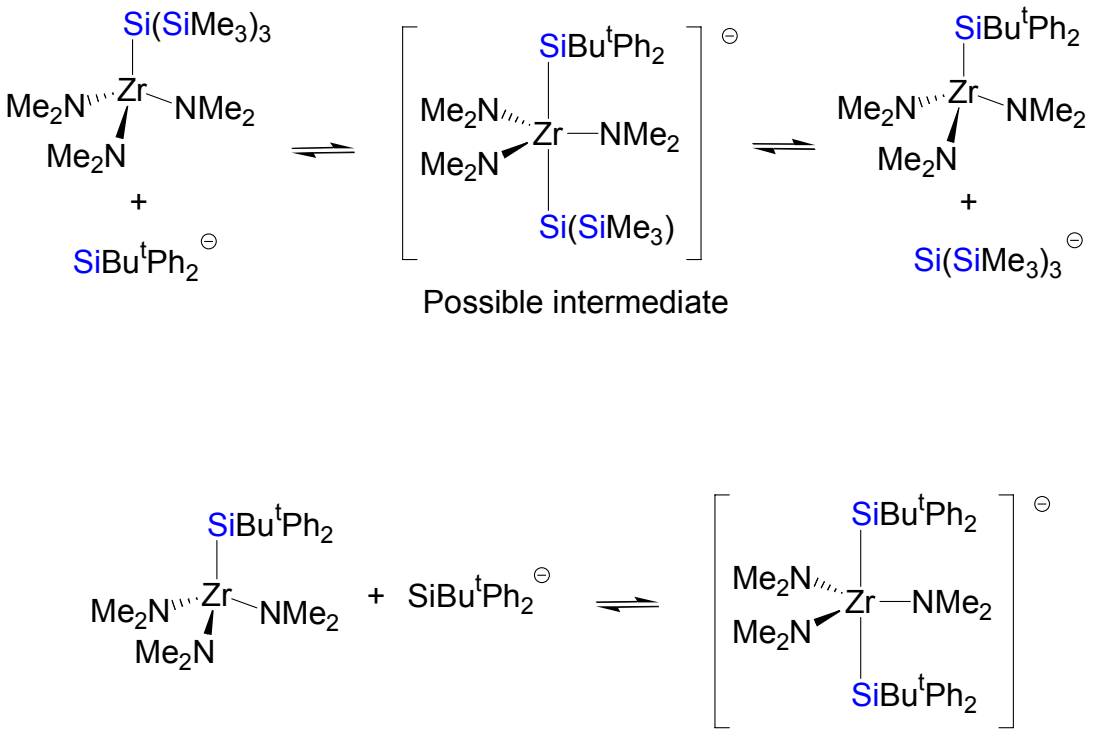

Scheme 4.4. Silyl exchanges involving $(Me_2N)_3ZrSi(SiMe_3)_3$ and $(Me_2N)_3ZrSiBu^tPh_2$

dissociative pathway is similar to the dissociation of one silyl group from the Zr disilyl intermediates $[(Me_2N)_3Zr(SiBu^tPh_2)(SiR_3)]^-$ [$R_3 = (SiMe_3)_3$, (Bu^tPh_2)] in Scheme 4.4, except that this step yields the cationic intermediate $[(Me_2N)_3TaSi(SiMe_3)_3]^+$ (**A**). Cationic **A** reacts with the anion $SiBu^tPh_2^-$ to give $(Me_2N)_3Ta(SiBu^tPh_2)[Si(SiMe_3)_3]$ (**16**).

4.2.4. *A test of silyl exchange in K(18-crown-6)$_{3/2}${(Me$_2$N)$_3$Hf[η^2-(Me$_3$Si)$_2$Si(CH$_2$)$_2$Si(SiMe$_3$)$_2$]} (10)*

Tantalum disilyl complexes undergo silyl exchanges and such exchange reactions convert **11** to **16** (Scheme 4.1). However, a mixture of chelating silyl complex **10** and excess $Li(THF)_3SiBu^tPh_2$ (**7**) in toluene-d_8 revealed no exchange between the two species in 24 h. This is perhaps not surprising, as the substitution of the chelating $[(Me_3Si)_2Si(CH_2)_2Si(SiMe_3)_2]^{2-}$ ligand in **10** by mono silyl $SiBu^tPh_2^-$ anion is thermodynamically unfavorable.

4.3. Conclusions

In summary, the current kinetic and mechanistic studies of the substitution reaction between $(Me_2N)_3Ta[Si(SiMe_3)_3]_2$ (**11**) and $Li(THF)_3SiBu^tPh_2$ (**7**) reveal that the first substitution in the reaction follows a dissociative pathway. In the presence of excess $Li(THF)_3SiBu^tPh_2$ (**7**), the disappearance of **11** follows pseudo first-order kinetics. THF, a polar solvent, was found to promote the substitution. It is likely that the second substitution converting

$(Me_2N)_3Ta(SiBu^tPh_2)[Si(SiMe_3)_3]$ (**16**) to $(Me_2N)_3Ta(SiBu^tPh_2)_2$ (**15**) also follows a dissociative pathway.

4.4. Experimental Section

4.4.1. *General procedures*

All manipulations were performed under a dry nitrogen atmosphere with the use of either a dry box or standard Schlenk techniques. Solvents were purified by distillation from potassium/benzophenone ketyl and stored under the nitrogen prior to use. $TaCl_5$ (Strem) was sublimed prior to use. $(Me_2N)_3TaCl_2$ (**14**),[33b] $Li(THF)_3Si(SiMe_3)_3$ (**13**),[36b] and $Li(THF)_3SiBu^tPh_2$ (**7**)[36a] were prepared according to the literature procedures. Toluene-d_8 was dried over activated molecular sieves. ^1H NMR spectra were recorded on a Bruker AMX-400 spectrometer and referenced to solvent (residual protons in the ^1H spectra).

For the kinetic studies of the **11** $\rightarrow$ **16** conversion and the effect of THF, the pseudo first-order rate constants k_{obs} were obtained from at least two separate experiments for a concentration of THF at 233 K, and their averages are listed. ^1H spectra were recorded directly on the NMR spectrometer. The estimated uncertainty in the temperature measurements for an NMR probe was 1 K. The order of THF (n) on rate constants was calculated from an unweighted nonlinear least-squares procedure contained in the SigmaPlot Scientific Graph System. The uncertainties in n was calculated from the following error propagation formulas (Eq. 4.5):[47]

$$(\sigma n)^2 = \frac{2(\Delta \ln k)^2}{(\Delta \ln C_{THF})^4}\left(\frac{\sigma C_{THF}}{C_{THF}}\right)^2 + \frac{2}{(\Delta \ln C_{THF})^2}\left(\frac{\sigma k}{k}\right)^2$$

$$\Delta \ln C_{THF} = (\ln C_{THF_{max}} - \ln C_{THF_{min}}) \qquad \text{(Eq. 4.5)}$$

4.4.2. *Kinetics studies of the reaction between $(Me_2N)_3Ta[Si(SiMe_3)_3]_2$ (11) and $Li(THF)_3SiBu^tPh_2$ (7) to give $(Me_2N)_3Ta(SiBu^tPh_2)[Si(SiMe_3)_3]$ (16) and $Li(THF)_3Si(SiMe_3)_3$ (13)*

Complex **11** was prepared *in situ* at 23 °C in a Young tube from a mixture of $(Me_2N)_3TaCl_2$ (**14**, 5.0 mg, 0.013 mmol) and $Li(THF)_3Si(SiMe_3)_3$ (**13**, 16.4 mg, 0.0349 mmol) in toluene-d_8, using 4,4'-dimethylbiphenyl (4.0 mg) as an internal standard. A small piece of filter paper was placed on the top of the Young's NMR tube in a glove box. $Li(THF)_3SiBu^tPh_2$ (**7**, 50.0, 60.0, 80.0, 100.0 or 120.0 mg; 0.108, 0.130, 0.173, 0.216 or 0.260 mmol) was then put on the paper and separated from the toluene-d_8 solution prior to the cooling of the solution. After the solution was cooled at 203 K for 10 min, the Young's tube was flipped over to mix the toluene solution and $Li(THF)_3SiBu^tPh_2$ (**7**). NMR spectrometer had been pre-cooled to 233 K, and the NMR tube was immediately inserted to the spectrometer. ^1H spectra were recorded directly on the NMR spectrometer. The concentrations of THF in toluene-d_8 (0.607-0.738 M) were measured through the integration of its ^1H NMR resonances. Rate constants derived from fitting of the

data by first-order kinetics (rate = $k_{obs}C_{11}$; $k_{obs}' = k_{obs}/C_{THF}^{1.7}$) are given in Table 4.1.

4.4.3. *Studies of the effect of THF on the rate of the reaction between $(Me_2N)_3Ta[Si(SiMe_3)_3]_2$ (11) and $Li(THF)_3SiBu^tPh_2$ (7) to give $(Me_2N)_3Ta(SiBu^tPh_2)[Si(SiMe_3)_3]$ (16) and $Li(THF)_3Si(SiMe_3)_3$ (13)*

Toluene-d_8 and THF were used to give mixed solvents with different THF concentrations (0.370, 0.465, 0.525, 0.616, 0.723 and 0.829 M). The THF concentrations (C_{THF}) of these solutions were calculated from ^{1}H NMR spectra. $(Me_2N)_3TaCl_2$ (**14**, 5.0 mg, 0.013 mmol), $Li(THF)_3Si(SiMe_3)_3$ (**13**, 16.4 mg, 0.0349 mmol), and 4,4'-dimethylbiphenyl (4.0 mg, internal standard) were dissolved in a toluene-d_8-THF mixture (1.07 mL). After the sample was cooled to 203 K for 10 min, $Li(THF)_3SiBu^tPh_2$ solid (**7**, 60.0 mg, 0.130 mmol) was mixed with the toluene solution. The NMR spectrometer was pre-cooled to 233 K before the NMR tube was inserted to the spectrometer. The first-order rate constants (rate = $k_{obs}C_{11}$; $k_{obs} = k_1 C_{THF}^n$) are listed in Table 4.2.

CHAPTER 5

Kinetic and Mechanistic Studies of the Decomposition of Tantalum Disilyl Complexes and the Formation of a Tungsten Alkyl Alkylidene Alkylidyne Complex

5.1. Introduction

We have recently found that both $(Me_2N)_3Ta(SiBu^tPh_2)_2$ (**15**) and $(Me_2N)_3Ta(SiBu^tPh_2)[Si(SiMe_3)_3]$ (**16**) are thermally unstable, and they decompose at 23 °C to give $HSiBu^tPh_2$ (from **15**), $HSiBu^tPh_2$ and $HSi(SiMe_3)_3$ (from **16**), and unknown Ta species. There are few reported Cp-free, early-transition-metal complexes containing silyl ligands, especially those containing two silyl ligands. Tantalum disilyl complexes were prepared earlier in our studies. The kinetics of their decomposition have not been investigated.

High-oxidation-state tungsten alkylidyne complexes have shown unique chemistry different from their alkyl analogues. For example, alkylidyne complexes are known to catalyze metathesis of acetylenes.[48] The tungsten alkylidyne complex $W(CH_2CMe_3)_3(\equiv CCMe_3)$ was prepared in ca. 50% yield by adding $W(OMe)_3Cl_3$ to 6 equiv of neopentylmagnesium chloride (Me_3CCH_2MgCl).[49a] $W(CH_2CMe_3)_3(\equiv CCMe_3)$ reacted rapidly with PMe_3 at 100 °C to yield $W(CH_2CMe_3)(=CHCMe_3)(\equiv CCMe_3)(PMe_3)_2$ (Scheme 5.1).[49b] The reaction of $W(CH_2CMe_3)_3(\equiv CCMe_3)$ with $Me_2PCH_2CH_2PMe_2$ (dmpe) in toluene gave an analogous compound $W(CH_2CMe_3)(=CHCMe_3)(\equiv CCMe_3)$(dmpe).[49b]

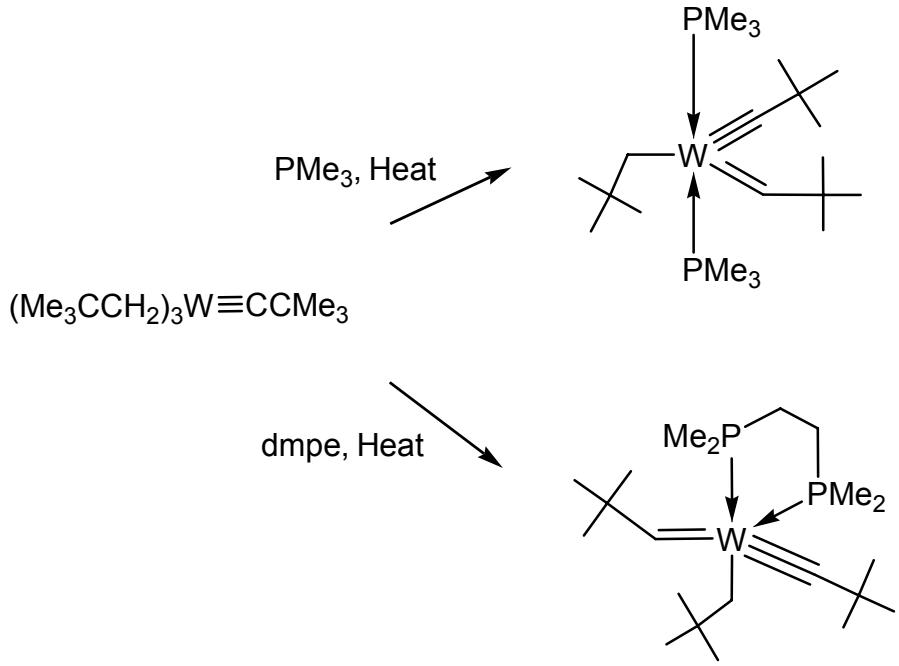

Scheme 5.1. Formation of tungsten alkyl alkylidene alkylidyne complexes[48]

We reported early that, when $W(CH_2SiMe_3)_3(\equiv CSiMe_3)$ was added PMe_3, an adduct $W(CH_2SiMe_3)_3(\equiv CSiMe_3)(PMe_3)$ (**25a**) was observed. It subsequently underwent a tautomerization process to give $W(CH_2SiMe_3)_2(=CHSiMe_3)_2(PMe_3)$ (**25b**). In the presence of excess PMe_3, **25a-b** were converted to alkyl alkylidene alkylidyne $W(CH_2SiMe_3)(=CHSiMe_3)(\equiv CSiMe_3)(PMe_3)_2$ (**26**) through an α-H abstraction process. Kinetic studies of the conversion were conducted.[51] The mixture of analogous alkyl alkylidyne $W(CH_2SiMe_3)_3(\equiv CSiMe_3)(PPhMe_2)$ (**18a**) and its bis(alkylidene) tautomer $W(CH_2SiMe_3)_2(=CHSiMe_3)_2(PPhMe_2)$ (**18b**) was prepared from $W(CH_2SiMe_3)_3(\equiv CSiMe_3)$ and $PPhMe_2$. The alkyl alkylidene alkylidyne $W(CH_2SiMe_3)(=CHSiMe_3)(\equiv CSiMe_3)(PPhMe_2)_2$ (**19**) was obtained by heating a mixture of **18a-b** with $PPhMe_2$ (Scheme 5.2). A kinetic study of the **18a/b** $\rightarrow$ **19** conversion by an earlier group member requires a comfirmation.[51b]

Our kinetic studies of the thermal decomposition of $(Me_2N)_3Ta(SiBu^tPh_2)_2$ (**15**) and $(Me_2N)_3Ta(SiBu^tPh_2)[Si(SiMe_3)_3]$ (**16**) as well as the formation of alkyl alkylidene alkylidyne $W(CH_2SiMe_3)(=CHSiMe_3)(\equiv CSiMe_3)(PPhMe_2)_2$ (**19**) are reported in this chapter.

5.2. Results and Discussion

5.2.1. *Kinetic studies of the thermal decomposition of $(Me_2N)_3Ta(SiBu^tPh_2)_2$ (15) and $(Me_2N)_3Ta(SiBu^tPh_2)[Si(SiMe_3)_3]$ (16)*

Both $(Me_2N)_3Ta(SiBu^tPh_2)_2$ (**15**) and $(Me_2N)_3Ta(SiBu^tPh_2)[Si(SiMe_3)_3]$ (**16**) are thermally unstable, decomposing at 23 °C to give $HSiBu^tPh_2$, $HSiBu^tPh_2$

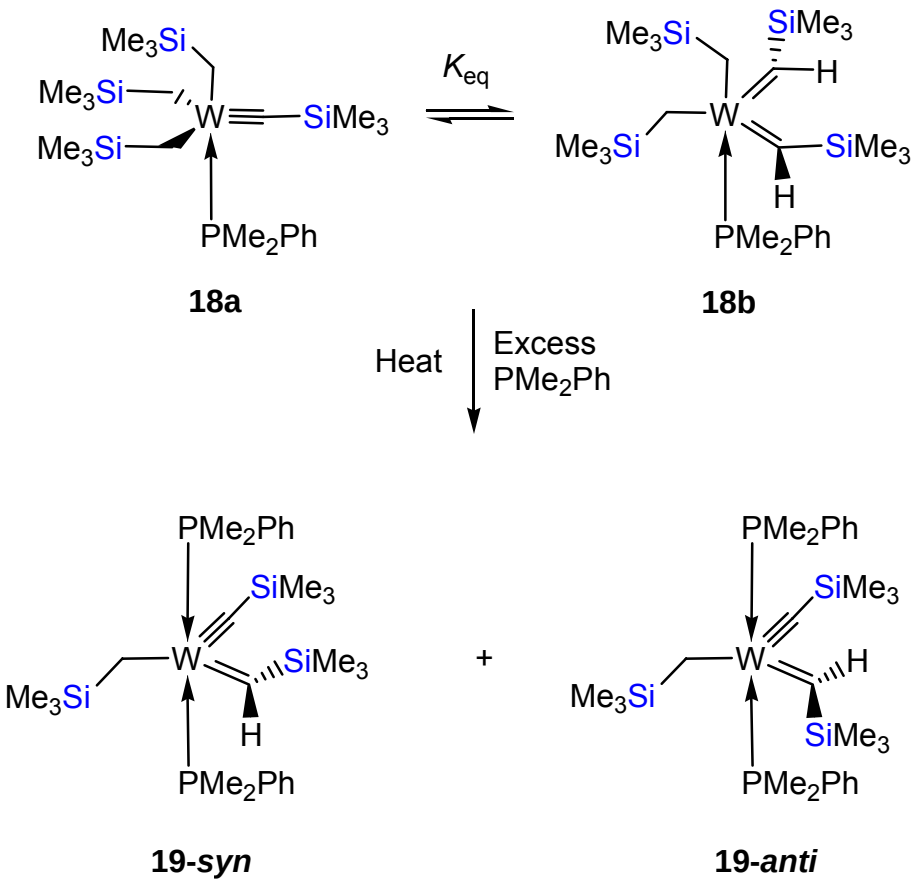

Scheme 5.2. The conversion from **18a-b** to **19-*syn*** and **19-*anti***

and $HSi(SiMe_3)_3$, respectively, and other unknown species (Scheme 5.3). $(Me_2N)_3Ta[(Si(SiMe_3)_3]_2$ (**11**) containing two $–Si(SiMe_3)_3$ ligands is thermally stable at room temperature under nitrogen. The decomposition reactions were not characterized, and not all products of the thermal decomposition are known. In order to compare the rates of the decomposition of the two complexes, the decomposition kinetics was studied. The decomposition was found to follow first-order (irreversible) kinetics. The sample of **16** used in the kinetic studies was prepared *in situ* from $(Me_2N)_3Ta[Si(SiMe_3)_3]Cl$ (**12**) and one equiv of $Li(THF)_3Si(SiMe_3)_3$ (**13**) in toluene-d_8. The kinetic studies were conducted between 298 and 323 K in toluene-d_8 to give plots of ln (C_0/C) (C = [**16**]) vs. time t (Figure 5.1) and the first-order rate constants k of the conversion (Table 5.1). An Eyring plot (Figure 5.2) gave activation parameters of the thermal decomposition: $\Delta H^{\neq}$ = 22.8(1.3) kcal/mol, $\Delta S^{\neq}$ = –3(5) eu and $\Delta G^{\neq}_{298\,K}$ = 24(3) kcal/mol.

The thermal decomposition of **15** was studied by NMR in toluene-d_8. The decomposition was found to follow first-order kinetics as well (Figure 5.3). The rate constant k for this decomposition at 303 K is $7.2(0.2) \times 10^{-5}$ s^{-1}, larger than that for the thermal decomposition of **16** [$4.33(0.16) \times 10^{-5}$ s^{-1}, Table 5.1] at this temperature, suggesting that **16** with one $–Si(SiMe_3)_3$ and one $–SiBu^tPh_2$ ligand decomposes faster than **15** containing two $–SiBu^tPh_2$ ligands.

Although the mechanism of the thermal decomposition is unknown, the formation of $HSiR_3$ suggests β-H abstraction involving a methyl group on a $-NMe_2$

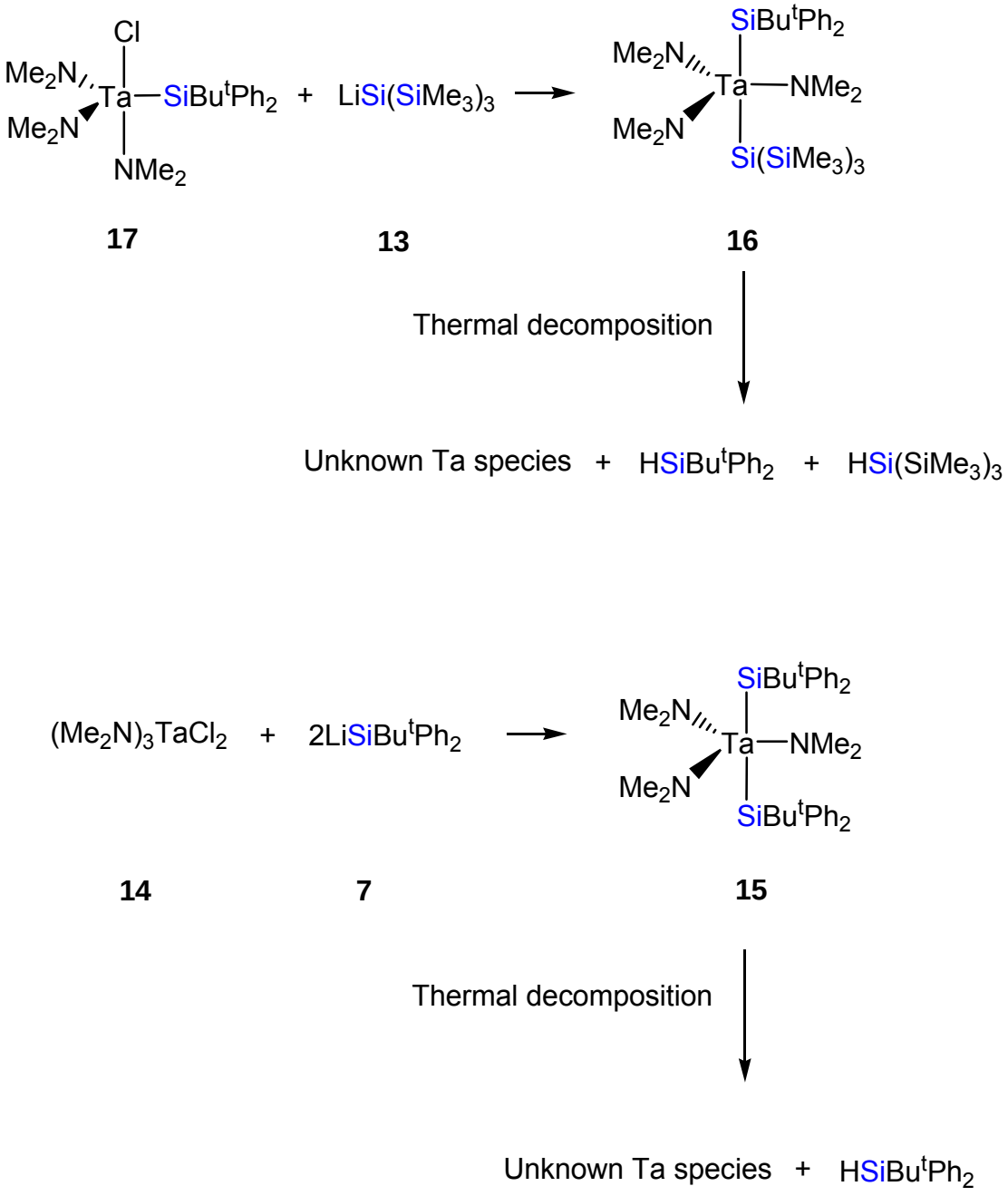

Scheme 5.3. The thermal decomposition of **15** and **16**

Table 5.1. Rate constants k for the decomposition of **16**[a]

T (K)	$[k \pm \delta k_{(ran)}] \times 10^5$ (s^{-1})
298(1)	2.48 ± 0.01
303(1)	4.33 ± 0.16
308(1)	8.7 ± 0.3
313(1)	16.9 ± 0.3
318(1)	31.9 ± 1.7
323(1)	47.1 ± 0.7

[a] The total uncertainty of $\delta k/k$ = 7.3% was calculated from $\delta k_{(ran)}/k$ = 5.3% and $\delta k_{(sys)}/k$ = 5%.

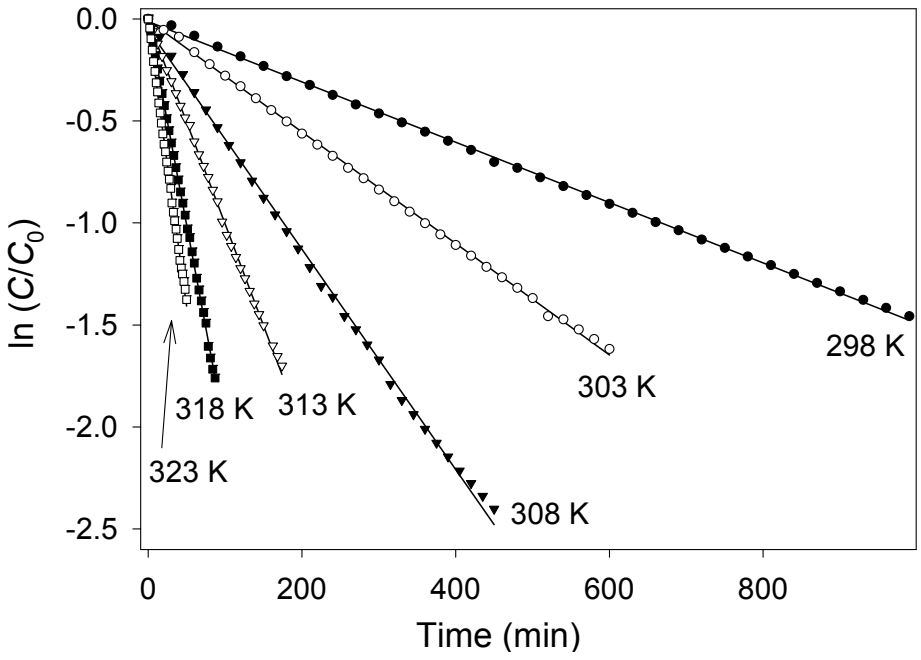

Figure 5.1. Kinetic plots of the thermal decomposition of **16**

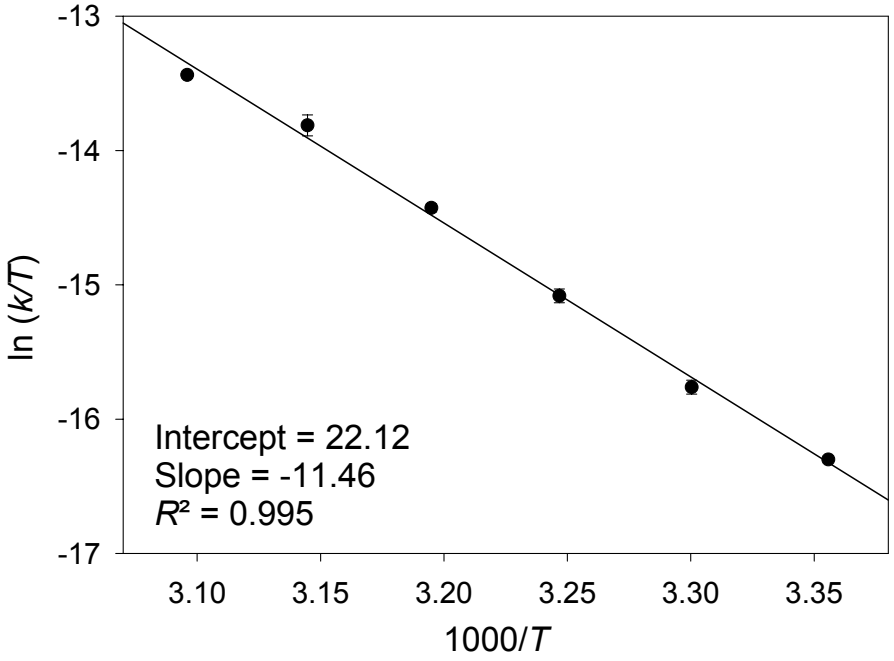

Figure 5.2. Eyring plot of the thermal decomposition of **16**

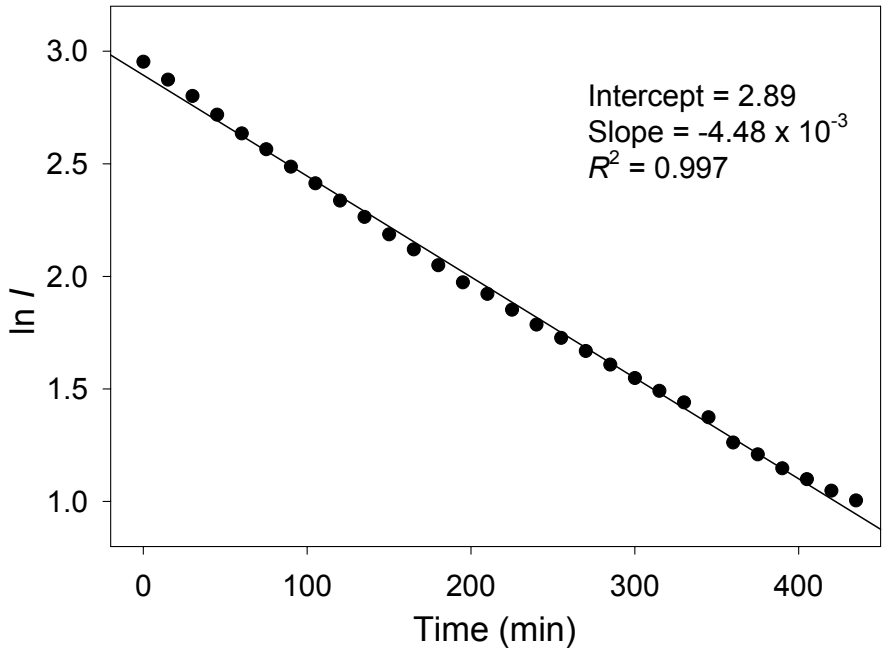

Figure 5.3. Kinetic plot of the thermal decomposition of **15** at 303 K

ligand. $Ta(NEt_2)_5$ has been found to undergo β-H abstraction between two $–NEt_2$ ligands, yielding ethylimino complex $Ta(\eta^2\text{-EtN=CHMe})(NEt_2)_3$.[50] Our own studies have shown that the $–NMe_2$ ligands in $Ta(NMe_2)_5$ are involved in such a β-H abstraction process in its reaction with H_2SiRPh (R = Me, Ph), yielding η^2-imine complex $(Me_2N)_3Ta(\mu\text{-H})_2(\mu\text{-}N\text{-}\eta^2\text{-}N,C\text{-}CH_2NMe)Ta(NMe_2)_3$. Monitoring the decomposition of $(Me_2N)_3Ta(SiBu^tPh_2)[Si(SiMe_3)_3]$ (**16**) reveals no new amide resonances in the ^1H NMR spectrum. One interpretation is that the metal center in **16** is reduced in the decomposition, yielding paramagnetic species that usually do not have resonances in the regular amide region. The first-order kinetics in the decomposition of both **15** and **16** suggests that the decomposition is an intramolecular process.

5.2.2. *Kinetic studies of the formation of $W(CH_2SiMe_3)(=CHSiMe_3)(\equiv CSiMe_3)(PMe_2Ph)_2$ (19)*

We have recently reported the equilibrium between alkyl alkylidynes $W(CH_2SiMe_3)_3(\equiv CSiMe_3)(PR_3)$ ($PR_3 = PMe_3$, **25a**; PMe_2Ph, **18a**) and their bis(alkylidene) tautomers $W(CH_2SiMe_3)_2(=CHSiMe_3)_2(PR_3)$ ($PR_3 = PMe_3$, **25b**; PMe_2Ph, **18b**).[51a] Laurel A. Morton, a former member of our research group, has found that, in the presence of phosphines, the equilibrium mixtures undergo an α-hydrogen abstraction reaction and give alkyl alkylidene alkylidynes $W(CH_2SiMe_3)(=CHSiMe_3)(\equiv CSiMe_3)(PR_3)_2$ ($PR_3 = PMe_3$, **26**; PMe_2Ph, **19**). Kinetic studies of the formation of **26** showed that the reaction follows pseudo

first-order reaction (Eq. 5.1) in the presence of excess phosphine PMe_3.

$$d\,[\mathbf{25a\text{-}b}] / dt = k_{obs}\,[\mathbf{25a\text{-}b}] \qquad \text{(Eq. 5.1)}$$

These kinetic studies also show that the k_{obs}'s at 65.0 °C (338.2 K) are independent of the phosphine concentrations. With the concentrations of PMe_3 and **25a-b** ranging from 1.5 to 3.1 M and 0.11 to 0.12 M, respectively, k = 1.40 (0.22) x 10^{-5} s^{-1} at 65.0 °C.

One kinetic test was done earlier for the formation of the PMe_2Ph analog $W(CH_2SiMe_3)(=CHSiMe_3)(\equiv CSiMe_3)(PMe_2Ph)_2$ (**19**).[51b] Additional studies have been conducted in the current work to complete the kinetic and mechanistic studies of the formation of the alkyl alkylidene alkylidyne complex **19** (as well as **26**). The two kinetic studies are summarized here with a discussion of the mechanistic pathways in the formation of **19** and **26**.

In the kinetic studies, a mixture of $W(CH_2SiMe_3)_3(\equiv CSiMe_3)(PMe_2Ph)$ (**18a**) and $W(CH_2SiMe_3)_2(=CHSiMe_3)_2(PMe_2Ph)$ (**18b**) was prepared by adding excess PMe_2Ph (13.5–30.8 equiv) to 1 equiv of $W(CH_2SiMe_3)_3(\equiv CSiMe_3)$ and keeping the mixture for two days to establish the equilibrium between **18a** and **18b**.[51b] The kinetics of the formation of alkyl alkylidene alkylidyne **19** was studied at 348.2 K. In the presence of excess PMe_2Ph, the formation was found to follow pseudo first-order kinetics (Eq. 5.2). Heating the mixture at 348.2 K gave a first-order kinetic plot (Figure 5.4).

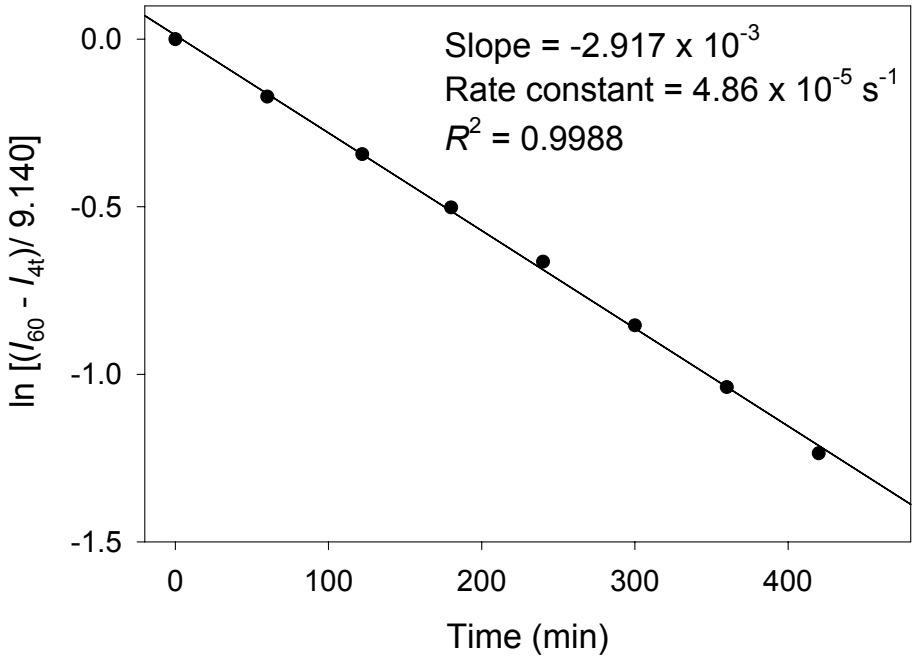

Figure 5.4. Kinetic plot for the formation of **19** at 348.2 K (Ratio = [PMe_2Ph]/[**18a-b**] = 13.5)

d[**18a-b**] / dt = k'_{obs} [**18a-b**] (Eq. 5.2)

Two kinetic studies with different [PMe_2Ph] / [$(Me_3SiCH_2)_3W{\equiv}CSiMe_3$] ratios (13.5 and 30.8) yielded the rate constant k'_{obs} = 5.1(0.2) $\times$ 10^{-5} s^{-1} at 348.2(0.1) K, suggesting that the formation of **19** is independent of the concentration of PMe_2Ph. In comparison, the rate constant (k_{obs}) for the formation of the PMe_3 analogue at the same temperature is 4.8(0.5) $\times$ 10^{-5} s^{-1}.[51b]

The observations that for the formation of $W(CH_2SiMe_3)(=CHSiMe_3)(\equiv CSiMe_3)(PMe_3)_2$ (**26**) and k'_{obs} for the formation of $W(CH_2SiMe_3)(=CHSiMe_3)(\equiv CSiMe_3)(PMe_2Ph)_2$ (**19**) are independent of phosphine concentrations suggest that the coordination of the second phosphine molecule is *not* the rate-determining step. Two pathways in Scheme 5.4 are consistent with the observation. In **Path I**, tautomeric alkyl alkylidyne-bis(alkylidene) mixtures **25a-b** and **18a-b** undergo a rate-determining, α-hydrogen abstraction to give mono-phosphine, alkyl alkylidene alkylidyne intermediates **A** which then binds with PR_3 to give the bisphosphine products **26** and **19**. In this pathway, the α-hydrogen abstraction is a spontaneous process in the penta-coordinated **25a-b** and **18a-b** to yield tetra-coordinated intermediates **A**. In the second step, phosphine coordinates to **A** to give **26** and **19**. The rates of the reactions are thus functions of the concentrations of **25a-b** and **18a-b**, and independence of C_{PR_3}.

In **Path II**, phosphine coordination to **25a-b** and **18a-b**, yielding hexa-

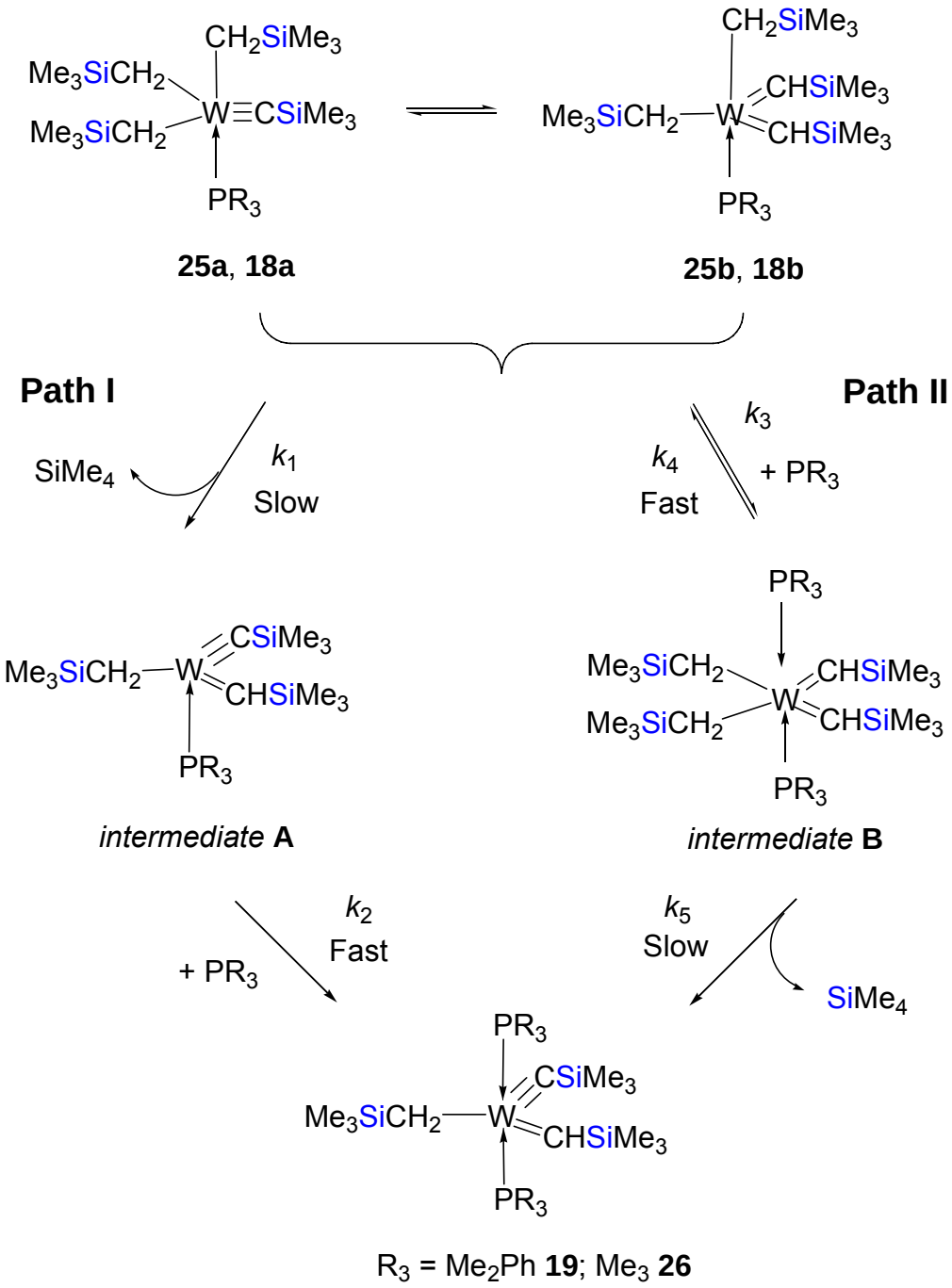

Scheme 5.4. Two proposed pathways in the formation of alkyl alkylidene alkylidyne complexes **19** and **26**

coordinated intermediates **B**, precedes the α-hydrogen abstraction. Kinetic analyses of **Path II** are given in the appendix. In **Path II**, both the steady-state or pre-equilibrium approaches show that the observed rates of the reactions are functions of concentrations of both **25a/b** (or **18a/b**) and PR_3. Two additional pathways in the formation of **26** were considered, and they both show the dependence of observed reaction rates on the concentration of PMe_3.

Thus the observations that the rates of the formation of alkyl alkylidene alkylidyne complexes **19** and **26** are independent of concentrations of PR_3 suggest that it follows **Path I** in Scheme 5.4. A review of the crystal structure of the bis(alkylidene) complex $W(CH_2SiMe_3)_2(=CHSiMe_3)_2(PMe_3)$ (**25b**) supports this view. A space-filling drawing of the molecular structure of penta-coordinated complex **25b** (Figure 5.5) suggests that there is little open space around the W atom in **25b** for the coordination of a second PMe_3 ligand, as would be required via **Path II**. In **Path I**, α-hydrogen abstraction eliminates a ligand as $SiMe_4$, converting *penta-coordinated* **25a-b** and **18a-b** to *tetra-coordinated* intermediates **A**. The *tetra-coordinated* **A** readily accepts the coordination of a second phosphine ligand, yielding the penta-coordinated products **19** and **26**.

5.3. Conclusions

Kinetic studies play an important role in the determination of mechanistic pathways in chemical reactions. In the current work, both $(Me_2N)_3Ta(SiBu^tPh_2)_2$ (**15**) and $(Me_2N)_3Ta(SiBu^tPh_2)[Si(SiMe_3)_3]$ (**16**) undergo thermal decomposition. Kinetic studies and the monitoring of the reaction by ^1H NMR spectroscopy

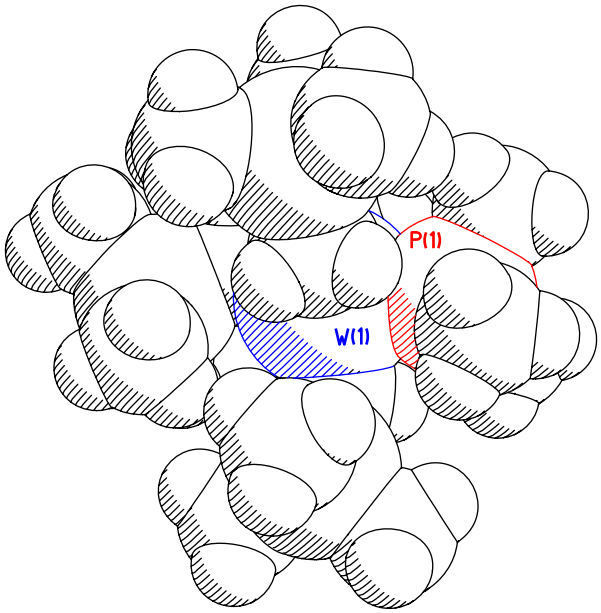

Figure 5.5. Space-filling drawing of the molecular structure of **25b**

suggest a β-hydrogen abstraction pathway with the following activation parameters for the decomposition of **16**: $\Delta H^{\neq}$ = 22.8(1.3) kcal/mol and $\Delta S^{\neq}$ = –3(5) eu.

The formation of alkyl alkylidene alkylidyne complexes $W(CH_2SiMe_3)(=CHSiMe_3)(\equiv CSiMe_3)(PR_3)_2$ (**26**, **19**) from $W(CH_2SiMe_3)_3(\equiv CSiMe_3)$ proceeds through PR_3 coordination. The adducts $W(CH_2SiMe_3)_3(\equiv CSiMe_3)(PR_3)$ undergo a hydrogen migration process to yield tautomers $W(CH_2SiMe_3)_2(=CHSiMe_3)_2(PR_3)$. A slow, α-hydrogen abstraction occurs in the tautomeric mixtures, followed by the coordination of second phosphine, produces the unusual alkyl alkylidene alkylidyne complexes **26** and **19** containing single, double and triple bonds in one single molecule.

5.4. Experimental Section

5.4.1. *General procedures*

All manipulations were performed under a dry nitrogen atmosphere with the use of either a dry box or standard Schlenk techniques. Solvents were purified by distillation from potassium/benzophenone ketyl and stored under the nitrogen prior to use. $TaCl_5$ (Strem) was sublimed prior to use. $(Me_2N)_3TaCl_2$ (**14**),[33b] $(Me_2N)_3Ta(SiBu^tPh_2)Cl$ (**17**),[29] $Li(THF)_3Si(SiMe_3)_3$ (**11**),[36b] $Li(THF)_3SiBu^tPh_2$ (**7**)[36a] and $W(CH_2SiMe_3)_3(\equiv CSiMe_3)$[51a] were prepared according to the literature procedures. Benzene-d_6 and toluene-d_8 were dried over activated molecular sieves. ^1H and $^{13}C\{^1H\}$ NMR spectra were recorded on a

Bruker AC-250 or AMX-400 spectrometer and referenced to solvent (residual protons in the ^{1}H spectra).

For the kinetic studies, the rate constants *k* was obtained from at least two separate experiments at a given temperature, and their averages are listed. The activation enthalpy ($\Delta H^{\neq}$) and entropy ($\Delta S^{\neq}$) were calculated from the Eyring equation using an unweighted nonlinear least-squares procedure contained in the SigmaPlot Scientific Graph System (Eq. 5.2). The estimated uncertainty in the temperature measurements for an NMR probe was 1 K. The *maximum* random uncertainty in the rate constants was combined with the estimated systematic uncertainty, ca. 5%. The uncertainties in $\Delta H^{\neq}$ and $\Delta S^{\neq}$ were computed from the following error propagation formulas (Eqs. 5.3 and 5.4),[52] which were derived from:

$$\ln\left(\frac{k}{T}\right) = -\frac{\Delta H^{\neq}}{RT} + \left[\frac{\Delta S^{\neq}}{R} - \ln\left(\frac{h}{k_b}\right)\right] \qquad \text{(Eq. 5.2)}$$

$$(\sigma\Delta H^{\neq})^2 = \frac{R^2 T_{\max}^2 T_{\min}^2}{\Delta T^2} \times \left\{\left(\frac{\sigma T}{T}\right)^2\left[\left(1 + T_{\min}\frac{\Delta L}{\Delta T}\right)^2 + \left(1 + T_{\max}\frac{\Delta L}{\Delta T}\right)^2\right] + 2\left(\frac{\sigma k}{k}\right)^2\right\} \qquad \text{(Eq. 5.3)}$$

$$(\sigma\Delta S^{\neq})^2 = \frac{R^2}{\Delta T^2} \times$$
$$\left\{\left(\frac{\sigma T}{T}\right)^2\left[T_{\max}^2\left(1+T_{\min}\frac{\Delta L}{\Delta T}\right)^2 + T_{\min}^2\left(1+T_{\max}\frac{\Delta L}{\Delta T}\right)^2\right] + \left(\frac{\sigma k}{k}\right)^2 (T_{\max}^2 + T_{\min}^2)\right\} \quad \text{(Eq. 5.4)}$$

$$\Delta L = \ln\left(\frac{k_{\max}}{T_{\max}}\right) - \ln\left(\frac{k_{\min}}{T_{\min}}\right)$$

5.4.2. *Kinetic study of the decomposition of $(Me_2N)_3Ta(SiBu^tPh_2)[Si(SiMe_3)_3]$ (16)*

Complex **16** was prepared *in situ* at 23 °C from a 1:1 mixture of $(Me_2N)_3Ta(SiBu^tPh_2)Cl$ (**17**) and $Li(THF)_3Si(SiMe_3)_3$ (**13**) in a toluene-d_8 solution containing 4,4'-dimethylbiphenyl as an internal standard. Once the starting materials were mixed, a deep purple solution appeared. The NMR spectrometer was preset to certain temperatures before the NMR tube was inserted to the spectrometer. The kinetic studies were conducted between 298 and 323 K. ^1H spectra were used to monitor the decomposition rate constant *k*. At least two separate experiments were conducted at a given temperature. At the end of the process the purple solution turned into light yellow. The first-order kinetic rate constants are listed in Table 5.1. The activation parameters of the decomposition of **16** are $\Delta H^{\neq}$ = 22.8(1.3) kcal/mol and $\Delta S^{\neq}$ = –3(5) eu.

5.4.3. *Kinetic study of the decomposition of $(Me_2N)_3Ta(SiBu^tPh_2)_2$ (15)*

Complex **15** was also prepared *in situ* from a mixture of 1 equiv of $(Me_2N)_3TaCl_2$ (**14**) and 2 equiv of $Li(THF)_3SiBu^tPh_2$ (**16**) in a toluene-d_8 solution containing 4,4'-dimethylbiphenyl as an internal standard. The NMR spectrometer was preset to 303 K before the NMR tube was inserted to the spectrometer. Two separate experiments were conducted at 303 K. The rate constants of the decomposition of **15** were found to be $k = 7.2(0.2) \times 10^{-5}$ s^{-1} at 303 K.

5.4.4. *Kinetic studies of the formation of $W(CH_2SiMe_3)(=CHSiMe_3)(\equiv CSiMe_3)(PMe_2Ph)_2$ (19)*

A mixture of $W(CH_2SiMe_3)_3(\equiv CSiMe_3)$, PMe_2Ph, and 4,4'-dimethylbiphenyl (an internal standard) in toluene-d_8 ($[W(CH_2SiMe_3)_3(\equiv CSiMe_3)]_0 = 0.123$ M, $[PMe_2Ph]_0 = 3.79$ M or $[W(CH_2SiMe_3)_3(\equiv CSiMe_3)]_0 = 0.107$ M, $[PMe_2Ph]_0 = 1.45$ M)[51b] in a Young NMR tube was kept for two days to yield $W(CH_2SiMe_3)_3(\equiv CSiMe_3)(PMe_2Ph)$ (**18a**) and $W(CH_2SiMe_3)_2(=CHSiMe_3)_2(PMe_2Ph)$ (**18b**) and to establish their equilibrium. The equilibrium mixture of **18a-b** and PMe_2Ph was heated in a circulation bath at 75.0 °C (348.2 K). The reaction was then quenched in dry ice/ethanol bath at −78 °C. ^1H NMR was acquired at room temperature, and the integration of the –P*Me*$_2$Ph resonances at 1.61-1.64 ppm in the ^1H spectra for **18a-b** versus an internal standard was used to give the pseudo first-order kinetic plot.

REFERENCES

1. (a) Tilley, T. D. In *The Silicon-Heteroatom Bond*; Patai, S., Rappoport, Z.; Eds.; Wiley: New York, 1991; Chapters 9 and 10. (b) Eisen, M. S. In *The Chemistry of Organic Silicon Compounds* Vol. 2, Rappoport, Z.; Apeloig, Y.; Eds.; Wiley: New York, 1998, Pt. 3, p. 2037. (c) Corey, J. Y. In *Advances in Silicon Chemistry*; Larson, G., Ed.; JAI Press: Greenwich, CT, 1991; Vol. 1, p 327. (d) Gauvin, F.; Harrod, J. F.; Woo, H. G. *Adv. Organomet. Chem.* **1998**, *42*, 363. (e) Sharma, H. K.; Pannell, K. H. *Chem. Rev.* **1995**, *95*, 1351. (f) Yu, X.-H.; Morton, L. A.; Xue, Z.-L. *Organometallics* **2004**, *23*, 2210. (g) Campion, B. K.; Falk, J.; Tilley, T. D. *J. Am. Chem. Soc.* **1987**, *109*, 2049. (h) Arnold, J.; Engeler, M. P.; Elsner, F. H.; Heyn, R. H.; Tilley, T. D. *Organometallics* **1989**, *8*, 2284. (i) Elsner, F. H.; Tilley, T. D.; Rheingold, A. L.; Geib, S. *J. Organomet. Chem*. **1988**, *358*, 169. (j) Heyn, R. H.; Tilley, T. D. *Inorg. Chem*. **1989**, *28*, 1768. (k) Campion, B. K.; Heyn, R. H.; Tilley, T. D. *J. Am. Chem. Soc.* **1990**, *112*, 2011. (l) Radu, N. S.; Engeler, M. P.; Gerlach, C. P.; Tilley, T. D.; Rheingold, A. L. *J. Am. Chem. Soc*. **1995**, *117*, 3621. (m) Imori, T.; Tilley, T. D. *Polyhedron* **1994**, *13*, 2231. (n) Dioumaev, V. K.; Harrod, J. F. *Organometallics* **1994**, *13*, 1548; **1997**, *16*, 2798. (o) Procopio, L. J.; Carroll, P. J.; Berry, D. H. *Polyhedron* **1995**, *14*, 45. (p) Huhmann, J. L.; Corey, J. Y.; Rath, N. P. *J. Organomet. Chem*. **1997**, *533*, 61. (q) Hengge, E.; Gspaltl, P.; Pinter, E. *J. Organomet. Chem*. **1996**, *521*, 145. (r) Banovetz, J. P.; Suzuki, H.; Waymouth, R. M. *Organometallics* **1993**, *12*, 4700. (s) Verdaguer, X.; Lange, U. E. W.; Reding, M. T.; Buchwald, S.

L. *J. Am. Chem. Soc*. **1996**, *118*, 6784. (t) Fu, P.-F.; Marks, T. J. *J. Am. Chem. Soc*. **1995**, *117*, 10747.

2 (a) Fu, P.-F.; Brard, L.; Li, Y.; Marks, T. J. *J. Am. Chem. Soc.* **1995**, *117*, 7157. (b) Gountchev, T. I.; Tilley, T. D. *Organometallics* **1999**, *18*, 5661. (c) Carter, M. B.; Schiott, B.; Butierrez, A.; Buchwald, S. L. *J. Am. Chem. Soc.* **1994**, *116*, 11667. (d) Molander, G. A.; Julius, M. *J. Org. Chem.* **1992**, *57*, 6347. (e) Molander, G. A.; Dowdy, D. E.; Noll, B. C. *Organometallics* **1998**, *17*, 37546. (f) Tilley, T. D. *Acc. Chem. Res.* **1993**, *26*, 22.

3. (a) Woo, H.-G.; Walzer, J. F.; Tilley, T. D. *J. Am. Chem. Soc.* **1992**, *114*, 7047. (b) Imori, T.; Tilley, T. D. *Polyhedron* **1994**, *13*, 2231. (c) Woo, H.-G.; Tilley, T. D. *J. Am. Chem. Soc.* **1989**, *111*, 3757. (d) Burckhardt, u.; Casty, G. L.; Gavenonis, J.; Tilley, T. D. *Organometallics* **2002**, *21*, 3108. (e) Casty, G. L.; Lugmair, C. G.; Radu, N. S.; Tilley, T. D.; Walzer, J. F.; Zargarian, D. *Organometallics* **1997**, *16*, 8. (f) Kreutzer, K. A.; Fisher, R. A.; Davis, W. M.; Spaltenstein, E.; Buchwald, S. L. *Organometallics* **1991**, *10*, 4301. (g) Spaltenstein, E.; Palma, P.; Kreutzer, K. A.; Willoughby, C. A.; Davis, W. M.; Buchwald, S. L. *J. Am. Chem. Soc.* **1994**, *116*, 10308. (h) Nikonov, G. I.; Mountford, P.; Green, J. C.; Cooke, P. A.; Leech, M. A.; Blake, A. J.; Howard, J. A. K.; Lemenovskii, D. A. *Eur. J. Inorg. Chem.* **2000**, 1917. (i) Nikonov, G. I. *J. Organomet. Chem.* **2001**, *635*, 24. (j). Nikonov, G. I.; Mountford, P.; Ignatov, S. K.; Green, J. C.; Leech, M. A.;

Kuzmina, L. G.; Razuvaev, A. G.; Rees, N. H.; Blake, A. J.; Howard, J. A. K.; Lemenovskii, D. A. *J. Chem. Soc., Dalton Trans.* **2001**, 2903.

4. (a) Xue, Z.; Li, L.; Hoyt, L. K.; Diminnie, J. B.; Pollitte, J. L. *J. Am. Chem. Soc.* **1994**, *116*, 2169. (b) McAlexander, L. H.; Hung, M.; Li, L.; Diminnie, J. B.; Xue, Z.; Yap, G. P. A.; Rheingold, A. L. *Organometallics* **1996**, *15*, 5231. (c) Diminnie, J. B.; Hall, H. D.; Xue, Z. *Chem. Commun*. **1996**, 2383. (d) Li, L.; Diminnie, J. B.; Liu, X.; Pollitte, J. L.; Xue, Z. *Organometallics* **1996**, *15*, 3520. (e) Diminnie, J. B.; Xue, Z. *J. Am. Chem. Soc.* **1997,** *119*, 12657. (f) Wu, Z.; Diminnie, J. B.; Xue, Z. *Organometallics* **1998**, *17*, 2917. (g) Wu, Z.; McAlexander, L. H.; Diminnie, J. B.; Xue, Z. *Organometallics* **1998**, *17*, 4853. (h) Fischer, R.; Zirngast, M.; Folck, M.; Baumgartner, J.; Marschner, C.; *J. Am. Chem. Soc.* **2005**, *127*, 70.

5. Casty, G. L.; Tilley, T. D.; Yap, G. P. A.; Rheingold, A. L. *Organometallics* **1997**, *16*, 4746.

6. (a) Hengge, E.; Zimmermann, H. *Angew. Chem., Int. Ed. Engl*. **1968**, *7*, 142. (b) Kingston, B. M.; Lappert, M. F. *J. Chem. Soc., Dalton Trans*. **1972**, 69.

7. $Ti(SiMe_3)_4$ was reported to exist at -78 °C, but no characterization was offered for this complex. Razuvaev, G. A.; Latyaeva, V. N.; Vyshinskaya, L. I.; Malysheva, A. V.; Vasileva, G. A. *Dokl. Akad. Nauk. SSSR* **1977**, *237*, 605.

8. Several zerovalent Zr-polytin complexes have been reported: (a) [K(15-crown-5)$_2$]$_2$[Zr(CO)$_5$(SnMe$_3$)$_2$], Ellis, J. E.; Yuen, P.; Jang, M. *J. Organomet. Chem*. **1996**, *507*, 283. (b) [*n*-Pr$_4$N]$_2$[(Ph$_3$Sn)$_4$M(CO)$_4$] (M = Zr, Hf), Ellis, J. E.; Chi, K. M.; DiMaio, A. J.; Frerichs, S. R.; Stenzel, J. R.; Rheingold, A. L.; Haggerty, B. S. *Angew. Chem., Int. Ed. Engl.* **1991**, *30*, 194.

9. For metallocene-based disilyl complexes of early transition and lanthanide metals, see, e.g., Cp$_2$Zr(SiMe$_3$)[Si(SiMe$_3$)$_3$];[2a] Cp$_2$Ti(SiPh$_3$)$_2$;[7] Cp$_2$Ti(SiPh$_2$)$_5$, Igonin, V. A.; Ovchinnikov, Yu. E.; Dementev, V. V.; Shklover, V. E.; Timofeeva, T. V.; Frunze, T. M.; Struchkov, Yu. T. *J. Organomet. Chem.* **1989**, *371*, 187; Cp$_2$Ti(SiPh$_2$)$_4$, Holtman, M. S.; Schram, E. P.; *J. Organomet. Chem*. **1980**, *187*, 147; Cp$_2$Ta(H)(SiMe$_2$H)$_2$, Jiang, Q.; Carroll, P. J.; Berry, D. H. *Organometallics* **1991**, *10*, 3648; [Cp$_2$Ln(SiMe$_3$)$_2$][Li(DME)$_2$] (Ln = Sm, Lu), Schumann, H.; Nickel, S.; Hahn, E.; Heeg, M. J. *Organometallics* **1985**, *4*, 800; Cp$_2$M[Si(SiMe$_3$)$_3$]$_2$ (M = Zr, Hf) Kayser, C.; Frank, D.; Baumgartner, J.; Marschner, C.; *J. Organomet. Chem*. **2003**, *667*, 149; Cp$_2$NbH(SiCl$_3$)$_2$, Dorogov, K. Yu.; Churakov, A. V.; Kuzmina, L. G.; Howard, J. A. K.; Nikonov, G. I. Euro. J. *Inorg. Chem.* **2004**, 771 and references therein.

10. (a) Wilk, G. D.; Wallace, R. M.; Anthony, J. M. *J. Appl. Phys*. **2001**, *89*, 5243. (b) Senzaki, Y.; Hochberg, A. K.; Norman, J. A. *Adv. Mater. Opt. Electron.* **2000**, *10*, 93. (c) Smith, R. C.; Ma, T.–Z.; Hoilien, N.; Tsung, L. Y.; Bevan, M. J.; Colombo, L.; Roberts, J.; Campbell, S. A.; Gladfelter, W.

L. *Adv. Mater. Opt. Electron.* **2000**, *10*, 105. (d) Huff, H. R.; Richter, C. A.; Green, M. L.; Lucovsky, G.; Hattori, T. Eds. *Mater. Res. Soc. Symp. Proc.* **1999**, 567. (e) Buchanan, D. A.; Edwards, A. H.; Von Bardeleben, H. J.; Hattori, T. Eds. *Mater. Res. Soc. Symp. Proc.* **2000**, 592. (f) Rayner, G. Jr.; Therrien, R.; Lucovsky, G. *Mater. Res. Soc. Symp. Proc.* **2001**, *611*, C1.3.1. (g) Senzaki, Y.; Hamilton, R. F.; Reid, K. G.; Hobbs, C. C.; Hedge, R. I.; Tiner, M. J. *Mater. Res. Soc. Symp. Proc.* **2000**, *606*, 13. (h) Son, K.–A.; Mao, A. Y.; Kim, B. Y.; Liu, F.; Pylant, E. D.; Hess, D. A.; White, J. M.; Kwong, D. L.; Roberts, D. A.; Vrtis, R. N. *J. Vac. Sci. Technol.* A. **1998**, *16*, 1670. (i) Niimi, H.; Johnson, R. S.; Lucovsky, G.; Massoud, H. Z. *Proc. Electrochem Soc.* **2000**, *2000*, 487. (j) Chiu, H.–T.; Wang, C.–N.; Chuang, S.–H. *Chem. Vap. Deposition* **2000**, *6*, 223. (k) Smith, R. C.; Taylor, C. J.; Roberts, J.; Campbell, S. A.; Tiner, M.; Hegde, R.; Hobbs, C.; Gladfelter, W. L. *Chem. Mater.* **2000**, *12*, 2822. (l) Taylor, C. J.; Gilmer, D. C.; Colombo, D. G.; Wilk, G. D.; Campbell. S. A.; Roberts, J.; Gladfelter, W. L. *J. Am. Chem. Soc*. **1999**, *121*, 5220. (m) Wilk, G. D.; Wallace, R. M.; Anthony, J. M. *J. Appl. Phys*. **2000**, *87*, 484. (n) Chambers, J. J.; Parsons, G. N. *Mater. Res. Soc. Symp. Proc.* **2001**, *611*, C1.6.1.

11. (a) Feig, A. L.; Lippard, S. J. *Chem. Rev.* **1994**, *94*, 759. (b) Klotz, I. M.; Kurtz, D. M. *Chem. Rev.* **1994**, *94*, 567. (c) Theopold, K. H.; Reinaud, O. M.; Blanchard, S.; Leelasubeharoen, S.; Hess, A.; Thyagarajan, S. *ACS Symp. Ser.* **2002**, *823*, 75. (d) Kopp, D. A.; Lippard, S. J. *Curr. Opin.*

Chem. Biol. **2002**, *6*, 568. (e) Que, L., Jr.; Tolman, W. B. *Angew. Chem. Inter. Ed.* **2002**, *41*, 1114. (f) Brown, S. N.; Mayer, J. M. *Inorg. Chem.* **1992**, *31*, 4091. (g) Balch, A. L.; Cornman, C. R.; Olmstead, M. M. *J. Am. Chem. Soc.* **1990**, *112*, 2963.

12. *Advances in Catalytic Activation of Dioxygen by Metal Complexes* Simándi, L. I. Ed., Kluwer: Boston: *Catal. Met. Complexes* **2003**, vol. 26: (a) Ezhova, M. B.; James, B. R. in pp. 1-77; (b) Zhang, C. Xin; Liang, H.-C.; Humphreys, K. J.; Karlin, K. D. in pp. 79-121; (c) Funabiki, T. in pp. 157-226; (d) Boring, E.; Geletii, Y. V.; Hill, C. L. in pp. 227-264; (e) Simandi, L. I. in pp. 265-328.

13. *The Activation of Dioxygen and Homogeneous Catalytic Oxidation*, Barton, D. H. R.; Martell, A. E.; Sawyer, D. T. Eds, Plenum: New York, 1993.

14. (a) Wallace, R. M.; Wilk, G. D. *Crit. Rev. Solid State Mater. Sci.* **2003**, *28*, 231. (b) Smith, R. C.; Ma, T.; Hoilien, N.; Tsung, L. Y.; Bevan, M. J.; Colombo, L.; Roberts, J.; Campbell, S. A.; Gladfelter, W. L. *Adv. Mater. Opt. Electron.* **2000**, *10*, 105. (c) Kelly, P. V.; et al. *Adv. Mater. Opt. Electron.* **2000**, *10*, 115. (d) Senzaki, Y.; Hochberg, A. K.; Norman, J. A. T. *Adv. Mater. Opt. Electron.* **2000**, *10*, 93. (e) Lucovsky, G.; Phillips, J. C. MRS Symp. Proc. **1999**, *567* (*Ultrathin SiO_2 and High-κ Materials for ULSI Gate Dielectrics*), 201.

15. (a) Bastianini, A.; Battiston, G. A.; Gerbasi, R.; Porchia, M.; Daolio, S. *J. Phys.* IV **1995**, *5*, C5-525. (b) Ohshita, Y.; Ogura, A.; Hoshino, A.; Hiiro,

S.; Machida, H. *J. Cryst. Growth* **2001**, *233*, 292. (c) Hendrix, B. C.; Borovik, A. S.; Xu, C.; Roeder, J. F.; Baum, T. H.; Bevan, M. J.; Visokay, M. R.; Chambers, J. J.; Rotondaro, A. L. P.; Bu, H.; Colombo, L. *Appl. Phys. Lett.* **2002**, *80*, 2362. (d) Vaartstra, B. A. U.S. Patent 2004040501, **2004**.

16. Son, K.-A.; Mao, A. Y.; Sun, Y.-M.; Kim, B. Y.; Liu, F.; Kamath, A.; White, J. M.; Kwong, D. L.; Roberts, D. A.; Vrtis, R. N. *Appl. Phys. Lett.* **1998**, *72*, 1187.

17 Miyazaki, S. *J. Vac. Sci. Technol.* **2001**, *B19*, 2212. (b) Yu, J. J.; Boyd, I. W. *Phys. Stat. Sol. (a)* **2006**, *203*, R9.

18 (a) Robertson, J.; Chen, C.W. *Appl. Phys. Lett.* **1999**, *74*, 1168. (b) Robertson, J. *J. Vac. Sci. Technol.* **2000**, *B18*, 1785. (c) Robertson, J. *Non-Cryst. Sol.* **2002**, *303*, 94.

19 (a) Labinger, J. A.; Hart, D. W.; Seibert, W. E.; Schwartz, J. *J. Am. Chem. Soc.* **1975**, *97*, 3851. (b) Blackburn, T. F.; Labinger, J. A.; Schwartz, J. *Tetrahedron Lett.* **1975**, *16*, 3041.

20 (a) Lubben, T. V.; Wolczanski, P. T. *J. Am. Chem. Soc.* **1985**, *107*, 701. (b) Lubben, T. V.; Wolczanski, P. T. *J. Am. Chem. Soc.* **1987**, *109*, 424.

21 Brindley, P. B.; Scotton, M. J. *J. Chem. Soc., Perkin Trans.* **1981**, 419.

22 Tilley, T. D. *Organometallics* **1985**, *4*, 1452.

23 Wang, R.; Folting, K.; Huffman, J. C.; Chamberlain, L. R.; Rothwell, I. P. *Inorg. Chem. Acta* **1986**, *120*, 81.

24 Gibson, V. C.; Redshaw, C.; Walker, G. L. P.; Howard, J. A. K.; Hoy, V. J.; Cole, J. M.; Kuzmina, L. G.; De Silva, D. S. *J. Chem. Soc., Dalton Trans.* **1999**, 161.

25. Brindley, P. B.; Hodgson, J. C. *J. Organomet. Chem.* **1974**, *65*, 57.

26. (a) Van Asselt, A.; Trimmer, M. S.; Healing, L. M.; Bercaw, J. E. *J. Am. Chem. Soc.* **1988**, *110*, 8254. (b) Coughlin, E. B.; Bercaw, J. E. *Organometallics* **1992**, *11*, 465.

27. Gibson, T. *Organometallics* **1987**, *6*, 918.

28. Kim, S.-J.; Jung, I. N.; Yoo, B. R.; Cho, S.; Ko, J.; Kim, S. H.; Kang, S. O. *Organometallics* **2001**, *20*, 1501.

29. Wu, Z.-Z.; Cai, H.; Yu, X.-H.; Blanton, J. R.; Diminnie, J. B.; Pan, H.-J.; Xue, Z.-L. *Organometallics* **2002**, *21*, 3973.

30. Chen, T.-N.; Wu, Z.-Z.; Li, L.-T.; Sorasaenee, K. R.; Diminnie, J. B.; Pan, H.-J.; Guzei, I. A.; Rheingold, A. L.; Xue, Z.-L. *J. Am. Chem. Soc*. **1998**, *120*, 13519.

31. Wang, R.; Zhang, X.-H.; Chen, S.-J.; Yu, X.; Wang, C.-S.; Beach, D.B.; Wu, Y.-D.; Xue, Z.-L. *J. Am. Chem. Soc.* **2005**, *127*, 5204.

32. Jones, T. C.; Nielson, A. J.; Rickard, E. F. *Chem. Commun*. **1984**, 205.

33. (a) Chisholm, M. H.; Tan, L.-S.; Huffman, J. C. *J. Am. Chem. Soc.* **1982**, *104*, 4879. (b) Chisholm, M.H.; Huffman, J. C.; Tan, L.-S. *Inorg. Chem.* **1981**, *20*, 1859.

34. Carballeira , L.; Pérez-Juste, L. *J. Comput. Chem.* **2001**, *22*,135.

35. Cai, H.; Chen, S. J.; Yu, X. Y.; Xue, Z.–L. Unpublished work.

36. (a) Campion, B. K.; Heyn, R. H.; Tilley, T. D. *Organometallics* **1993**, *12*, 2584. (b) Gutekunst, G.; Brook, A. G. *J. Organomet. Chem*. **1982**, *225*, 1.

37. (a) Sheldrick, G. M. *SADABS, A Program for Empirical Absorption Correction of Area Detector Data*; University of Göttingen, Göttingen, Germany, 2000. (b) Sheldrick, G. M. *SHELXL-97, A Program for the Refinement of Crystal Structures*, University of Göttingen, Göttingen, Germany, 1997.

38 (a) Li, L.; Hung, M.; Xue, Z.-L. *J. Am. Chem. Soc.* **1995**, *117*, 12746. (b) Davidson, P. J.; Lappert, M. F.; Pearce, R. *Chem. Rev.* **1976**, *76*, 219. (c) Schrock, R. R.; Parshall, G. W. *Chem. Rev.* **1976**, *76*, 243. (d) Wu, Y.-D.; Chan, K. W. K.; Xue, Z.-L. *J. Am. Chem. Soc.* **1995**, *117*, 9259. (e) Wu, Y.-D.; Peng, Z.-H.; Xue, Z.-L. *J. Am. Chem. Soc.* **1996**, *118*, 9772.

39 (a) Wu, Z.; Diminnie, J. B.; Xue, Z.-L. *J. Am. Chem. Soc*. **1999**, *121*, 4300. (b) Qiu, H.; Cai, H.; Woods, J. B.; Chen, T.; Yu, X.; Xue, Z.-L. *Organometallics* **2005**, *24*, 4190.

40 (a) Wu, Z.; Diminnie, J. B.; Xue, Z.-L. *Inorg. Chem*. **1998**, *37*, 2570. (b) Wu, Z.; Diminnie, J. B.; Xue, Z.-L. *Inorg. Chem*. **1998**, *43*, 6366.

41. Blanton, J. R.; Diminnie, J. B.; Chen, T.; Wiltz, A. M.; Xue, Z.-L. *Organometallics* **2001**, *20*, 5542. For related potassium silyl complexes, see, e.g., (a) Marschner, C. *Eur. J. Inorg. Chem.* **1998**, 221. (b) Jenkins, D. M.; Teng, W.; Englich, U.; Stone, D.; Ruhlandt-Senge, K. *Organometallics*, **2001**, *20*, 4600. (c) Teng, W.; Ruhlandt-Senge, K.

Organometallics, **2004**, *23*, 2694. (d) Fischer, R.; Konopa, T.; Ully, S.; Baumgartner, J.; Marschner, C; *J. Organomet. Chem*. **2003**, *685*, 79.

42. Sadow, A. D.; Tilley, T. D. *J. Am. Chem. Soc.* **2003**, *125*, 9462.

43. Yu, X.; Cai, H., Xue, Z.-L. *J. Am. Chem. Soc.* **2004**, *126*, 4472.

44. (a) Sheldrick, G. M. *A Program for Empirical Absorption Correction of Area Detector Data*; University of Gottingen: Gottingen, Germany, 1996. (b) Sheldrick, G. M. *A Program for the Refinement of Crystal Structures*; University of Gottingen: Gottingen, Germany, 1997.

45. (a) Langford, C. H.; Gray, H. B. *Ligand Substitution Processes*; Benjamin: New York, 1965. (b) Basolo, F.; Pearson R. G. *Mechanisms of Inorganic Reaction*; 2nd Ed., Wiley: New York, 1967. (c) Purcell, K. F.; Kotz, J. C. *Inorganic Chemistry*, W. B. Saunders Co.: Philadelphia, 1977, Ch. 13. (d) Wilkins, R. G. *Kinetics and Mechanism of Reactions of Transition Metal Complexes*, VCH: New York, 1991, Ch. 4. (e) Atwood, J. D. *Inorganic and Organometallic Reaction Mechanisms*, 2nd Ed., Wiley: New York, 1997, Chs. 2-4. (f) Jordan, R. B. *Reaction Mechanisms of Inorganic and Organometallic Systems;* 2nd Ed., Oxford University Press: Oxford, UK, 1998, Chs. 3 and 5.

46. DePue, J. S.; Collum, D. B. *J. Am. Chem. Soc.* **1988**, *110*, 5524.

47. Yu, X.; Xue, Z.-L. *Inorg. Chem.* **2005**, *44*, 1505.

48. (a) Casey, C. P.; Burkhardt, T. J. *J. Am. Chem. Soc.* **1973**, *95*, 5833. (b) Casey, C. P.; Burkhardt, T. J. *J. Am. Chem. Soc.* **1974**, *96*, 7808. (c)

Katz, T. J.; Lee, S. J.; Acton, N. *Tetrahedron Lett.* **1976**, *17*, 4247. (d) Katz, T. J.; Rothchild, R. *J. Am. Chem. Soc.* **1976**, *98*, 2519.

49. (a) Schrock R. R.; Clark, D. N.; Sancho, J. C.; Wengrovius, J. H.; Rocklage, S. M.; Pedersen, S. F. *Organometallics* **1982**, *1*, 1645. (b) Clark, D. N.; Schrock R. R. *J. Am. Chem. Soc*. **1978**, *100*, 6774.

50. Takahashi, Y.; Onoyama, N.; Ishikawa, S.; Motojima, S.; Sugiyama, K. *Chem. Lett.* **1978**, 525.

51. (a) Morton, L. A.; Zhang, X-H.; Wang, R.; Lin, Z.; Wu, Y-D.; Xue, Z-L. *J. Am. Chem. Soc.* **2004**, *126*, 10208. (b) Morton, L. A. Ph.D. Dissertation, University of Tennessee, 2005.

52. Scoles, L.; Ruppa, K. B. P.; Gambarotta, S. *J. Am. Chem. Soc.* **1996**, *118*, 2529.

APPENDIX

Table A1 Atomic coordinates (x 10^4) and equivalent isotropic displacement parameters (Å^2 x 10^3) in **4·CH_2Cl_2**. U(eq) is defined as one third of the trace of the orthogonalized U^{ij} tensor.

	x	y	z	U(eq)
Ta(1)	5639(1)	-913(1)	2861(1)	23(1)
Ta(2)	4563(1)	792(1)	2149(1)	23(1)
Si(1)	8229(1)	-2243(1)	2010(1)	25(1)
Si(2)	2019(1)	2167(1)	2996(1)	25(1)
Cl(1)	2007(2)	6025(1)	734(1)	72(1)
Cl(2)	4418(2)	5434(1)	1003(1)	67(1)
Cl(3)	8797(2)	4127(1)	4292(1)	85(1)
Cl(4)	6265(2)	4425(2)	4104(1)	87(1)
O(1)	6916(2)	-1804(2)	2438(2)	25(1)
O(2)	4118(2)	-201(2)	3047(1)	23(1)
O(3)	6085(2)	78(2)	1960(1)	22(1)
O(4)	3308(3)	1689(2)	2571(2)	27(1)
N(1)	4874(3)	-1878(3)	3790(2)	34(1)
N(2)	6600(3)	-84(3)	3342(2)	31(1)
N(3)	5774(3)	1476(2)	2950(2)	30(1)
N(4)	4419(3)	-1595(2)	2060(2)	30(1)

Table A1 (continued)

	x	y	z	U(eq)
N(5)	3587(3)	-31(2)	1677(2)	31(1)
N(6)	5340(3)	1757(3)	1219(2)	34(1)
C(1)	9209(4)	-1315(3)	1250(2)	29(1)
C(2)	9452(5)	-470(3)	1630(3)	41(1)
C(3)	8487(4)	-960(3)	644(3)	37(1)
C(4)	10502(4)	-1691(3)	865(3)	36(1)
C(5)	7857(4)	-3350(3)	1638(2)	29(1)
C(6)	8370(5)	-3570(3)	910(3)	39(1)
C(7)	8105(5)	-4431(4)	702(3)	48(1)
C(8)	7299(5)	-5093(3)	1211(3)	45(1)
C(9)	6765(4)	-4891(3)	1944(3)	40(1)
C(10)	7049(4)	-4037(3)	2148(3)	34(1)
C(11)	9154(4)	-2651(3)	2725(2)	29(1)
C(12)	9901(4)	-3455(3)	2669(3)	40(1)
C(13)	10633(5)	-3722(4)	3163(3)	53(1)
C(14)	10626(5)	-3196(4)	3745(3)	55(2)
C(15)	9936(5)	-2391(4)	3805(3)	53(1)
C(16)	9190(5)	-2128(4)	3304(3)	42(1)
C(17)	5475(5)	-2742(4)	4037(3)	50(1)

Table A1 (continued)

	x	y	z	U(eq)
C(18)	3636(5)	-1814(4)	4316(3)	48(1)
C(20)	6914(4)	897(3)	2999(3)	33(1)
C(19)	6806(5)	-323(4)	4110(3)	45(1)
C(21)	4982(4)	1516(3)	3727(3)	39(1)
C(22)	6245(5)	2439(3)	2598(3)	45(1)
C(23)	3964(5)	-2566(3)	2419(3)	45(1)
C(24)	5199(4)	-1641(3)	1283(2)	35(1)
C(25)	3282(4)	-1011(3)	2013(3)	35(1)
C(26)	3340(5)	221(4)	917(3)	46(1)
C(27)	4771(5)	2657(4)	991(3)	54(2)
C(28)	6557(5)	1680(4)	683(3)	51(1)
C(29)	958(4)	1236(3)	3709(2)	31(1)
C(30)	653(5)	451(3)	3292(3)	45(1)
C(31)	1623(4)	782(3)	4309(3)	41(1)
C(32)	-294(4)	1667(3)	4094(3)	37(1)
C(33)	2431(4)	3204(3)	3425(2)	29(1)
C(34)	2089(5)	3295(4)	4195(3)	47(1)
C(35)	2416(6)	4088(4)	4475(3)	64(2)
C(36)	3122(5)	4818(4)	3980(4)	57(2)

Table A1 (continued)

	x	y	z	U(eq)
C(37)	3492(5)	4754(3)	3211(3)	46(1)
C(38)	3156(4)	3960(3)	2943(3)	38(1)
C(39)	1178(4)	2651(3)	2258(2)	30(1)
C(41)	-130(5)	3823(4)	1757(3)	43(1)
C(42)	-204(5)	3286(4)	1201(3)	48(1)
C(43)	389(5)	2431(4)	1169(3)	53(2)
C(44)	1081(5)	2126(4)	1690(3)	43(1)
C(45)	3041(6)	5106(5)	817(4)	76(2)
C(46)	7876(7)	4543(7)	3717(4)	116(3)

Table A2 Bond distances (Å) in **4·CH_2Cl_2**

Distances			
Ta(1)-O(2)	1.925(3)	Ta(2)-O(4)	1.955(3)
Ta(1)-O(1)	1.965(3)	Ta(2)-O(2)	1.977(3)
Ta(1)-O(3)	1.978(3)	Ta(2)-N(5)	2.008(3)
Ta(1)-N(2)	2.014(3)	Ta(2)-N(6)	2.037(4)
Ta(1)-N(1)	2.034(4)	Ta(2)-N(3)	2.505(3)
Ta(1)-N(4)	2.511(3)	Si(1)-O(1)	1.621(3)
Ta(1)-Ta(2)	2.9726(5)	Si(1)-C(11)	1.883(4)
Ta(2)-O(3)	1.928(3)	Si(1)-C(5)	1.885(4)
Si(1)-C(1)	1.895(4)	Cl(4)-C(46)	1.730(7)
Si(2)-O(4)	1.626(3)	N(1)-C(17)	1.459(6)
Si(2)-C(33)	1.874(4)	N(1)-C(18)	1.464(6)
Si(2)-C(39)	1.877(4)	N(2)-C(20)	1.454(6)
Si(2)-C(29)	1.894(4)	N(2)-C(19)	1.476(5)
Cl(1)-C(45)	1.739(6)	N(3)-C(22)	1.467(6)
Cl(2)-C(45)	1.711(6)	N(3)-C(21)	1.478(5)
Cl(3)-C(46)	1.686(7)	N(3)-C(20)	1.506(5)
N(4)-C(24)	1.474(5)	N(4)-C(25)	1.507(5)
N(4)-C(23)	1.476(6)	N(5)-C(25)	1.447(6)
N(5)-C(26)	1.482(5)	N(6)-C(28)	1.457(6)

Table A2 (continued)

Distances			
N(6)-C(27)	1.473(6)	C(3)-H(3C)	0.9800
C(1)-C(2)	1.526(6)	C(4)-H(4A)	0.9800
C(1)-C(4)	1.543(5)	C(4)-H(4B)	0.9800
C(1)-C(3)	1.551(6)	C(4)-H(4C)	0.9800
C(2)-H(2A)	0.9800	C(5)-C(6)	1.391(6)
C(2)-H(2B)	0.9800	C(5)-C(10)	1.397(6)
C(2)-H(2C)	0.9800	C(6)-C(7)	1.385(6)
C(3)-H(3A)	0.9800	C(6)-H(6)	0.9500
C(3)-H(3B)	0.9800	C(7)-C(8)	1.375(7)
C(7)-H(7)	0.9500	C(11)-C(16)	1.388(6)
C(8)-C(9)	1.393(7)	C(11)-C(12)	1.400(6)
C(8)-H(8)	0.9500	C(12)-C(13)	1.371(6)
C(9)-C(10)	1.379(6)	C(12)-H(12)	0.9500
C(9)-H(9)	0.9500	C(13)-C(14)	1.384(8)
C(10)-H(10)	0.9500	C(13)-H(13)	0.9500
C(14)-C(15)	1.368(8)	C(15)-H(15)	0.9500
C(14)-H(14)	0.9500	C(16)-H(16)	0.9500
C(15)-C(16)	1.391(7)	C(17)-H(17A)	0.9800
C(17)-H(17B)	0.9800	C(17)-H(17C)	0.9800

Table A2 (continued)

Distances			
C(18)-H(18A)	0.9800	C(20)-H(20B)	0.9900
C(18)-H(18B)	0.9800	C(21)-H(21A)	0.9800
C(18)-H(18C)	0.9800	C(21)-H(21B)	0.9800
C(19)-H(19A)	0.9800	C(21)-H(21C)	0.9800
C(19)-H(19B)	0.9800	C(22)-H(22A)	0.9800
C(19)-H(19C)	0.9800	C(22)-H(22B)	0.9800
C(20)-H(20A)	0.9900	C(22)-H(22C)	0.9800
C(23)-H(23A)	0.9800	C(25)-H(25B)	0.9900
C(23)-H(23B)	0.9800	C(26)-H(26A)	0.9800
C(23)-H(23C)	0.9800	C(26)-H(26B)	0.9800
C(24)-H(24A)	0.9800	C(26)-H(26C)	0.9800
C(24)-H(24B)	0.9800	C(27)-H(27A)	0.9800
C(24)-H(24C)	0.9800	C(27)-H(27B)	0.9800
C(25)-H(25A)	0.9900	C(27)-H(27C)	0.9800
C(28)-H(28A)	0.9800	C(29)-C(30)	1.521(6)
C(28)-H(28B)	0.9800	C(29)-C(31)	1.538(6)
C(28)-H(28C)	0.9800	C(29)-C(32)	1.541(6)
C(30)-H(30A)	0.9800	C(30)-H(30B)	0.9800
C(30)-H(30C)	0.9800	C(31)-H(31A)	0.9800

Table A2 (continued)

Distances			
C(31)-H(31B)	0.9800	C(35)-C(36)	1.377(8)
C(31)-H(31C)	0.9800	C(35)-H(35)	0.9500
C(32)-H(32A)	0.9800	C(36)-C(37)	1.382(7)
C(32)-H(32B)	0.9800	C(36)-H(36)	0.9500
C(32)-H(32C)	0.9800	C(37)-C(38)	1.380(6)
C(33)-C(34)	1.392(6)	C(37)-H(37)	0.9500
C(33)-C(38)	1.400(6)	C(38)-H(38)	0.9500
C(34)-C(35)	1.385(7)	C(39)-C(44)	1.389(6)
C(34)-H(34)	0.9500	C(39)-C(40)	1.397(6)
C(40)-C(41)	1.377(6)	C(43)-C(44)	1.388(6)
C(40)-H(40)	0.9500	C(43)-H(43)	0.9500
C(41)-C(42)	1.373(7)	C(44)-H(44)	0.9500
C(41)-H(41)	0.9500	C(45)-H(45A)	0.9900
C(42)-C(43)	1.375(7)	C(45)-H(45B)	0.9900
C(42)-H(42)	0.9500	C(46)-H(46A)	0.9900
C(46)-H(46B)	0.9900		

Symmetry transformations used to generate equivalent atoms:

#1 -x+1, -y+2, -z+1

Table A3 Bond angles (deg) in **4·CH_2Cl_2**

Angles			
O(2)-Ta(1)-O(1)	160.95(11)	O(1)-Ta(1)-N(4)	82.99(11)
O(2)-Ta(1)-O(3)	80.84(11)	O(3)-Ta(1)-N(4)	81.75(11)
O(1)-Ta(1)-O(3)	95.13(11)	N(2)-Ta(1)-N(4)	166.64(13)
O(2)-Ta(1)-N(2)	95.52(12)	N(1)-Ta(1)-N(4)	92.84(13)
O(1)-Ta(1)-N(2)	102.78(12)	O(2)-Ta(1)-Ta(2)	41.02(8)
O(3)-Ta(1)-N(2)	85.71(13)	O(1)-Ta(1)-Ta(2)	132.32(8)
O(2)-Ta(1)-N(1)	90.18(13)	O(3)-Ta(1)-Ta(2)	39.82(7)
O(1)-Ta(1)-N(1)	92.18(13)	N(2)-Ta(1)-Ta(2)	90.61(10)
O(3)-Ta(1)-N(1)	170.30(12)	N(1)-Ta(1)-Ta(2)	131.11(10)
N(2)-Ta(1)-N(1)	98.90(15)	N(4)-Ta(1)-Ta(2)	76.81(8)
O(2)-Ta(1)-N(4)	78.01(11)	O(3)-Ta(2)-O(4)	160.57(11)
O(3)-Ta(2)-O(2)	80.80(11)	O(3)-Ta(2)-N(6)	89.83(12)
O(4)-Ta(2)-O(2)	95.50(11)	O(4)-Ta(2)-N(6)	92.13(13)
O(3)-Ta(2)-N(5)	95.88(12)	O(2)-Ta(2)-N(6)	169.94(12)
O(4)-Ta(2)-N(5)	102.86(13)	N(5)-Ta(2)-N(6)	99.36(15)
O(2)-Ta(2)-N(5)	85.35(13)	O(3)-Ta(2)-N(3)	78.39(11)
O(4)-Ta(2)-N(3)	82.20(11)	N(5)-Ta(2)-N(3)	166.72(13)
O(2)-Ta(2)-N(3)	81.92(11)	N(6)-Ta(2)-N(3)	92.65(14)
O(3)-Ta(2)-Ta(1)	41.06(8)	O(4)-Ta(2)-Ta(1)	132.36(8)

Table A3 (continued)

Angles			
O(2)-Ta(2)-Ta(1)	39.74(7)	C(39)-Si(2)-C(29)	108.7(2)
N(5)-Ta(2)-Ta(1)	90.82(10)	Si(1)-O(1)-Ta(1)	162.53(18)
N(6)-Ta(2)-Ta(1)	130.78(10)	Ta(1)-O(2)-Ta(2)	99.24(12)
N(3)-Ta(2)-Ta(1)	76.95(8)	Ta(2)-O(3)-Ta(1)	99.11(12)
O(1)-Si(1)-C(11)	109.23(17)	Si(2)-O(4)-Ta(2)	164.04(18)
O(1)-Si(1)-C(5)	108.70(17)	C(17)-N(1)-C(18)	109.4(4)
C(11)-Si(1)-C(5)	105.54(19)	C(17)-N(1)-Ta(1)	125.3(3)
O(1)-Si(1)-C(1)	110.65(17)	C(18)-N(1)-Ta(1)	125.3(3)
C(11)-Si(1)-C(1)	108.75(19)	C(20)-N(2)-C(19)	114.6(4)
C(5)-Si(1)-C(1)	113.77(19)	C(20)-N(2)-Ta(1)	119.5(3)
O(4)-Si(2)-C(33)	109.25(17)	C(19)-N(2)-Ta(1)	124.8(3)
O(4)-Si(2)-C(39)	108.15(17)	C(22)-N(3)-C(21)	109.0(4)
C(33)-Si(2)-C(39)	106.85(19)	C(22)-N(3)-C(20)	106.5(3)
O(4)-Si(2)-C(29)	110.06(17)	C(21)-N(3)-C(20)	109.1(3)
C(33)-Si(2)-C(29)	113.6(2)	C(22)-N(3)-Ta(2)	109.9(3)
C(21)-N(3)-Ta(2)	111.4(3)	C(24)-N(4)-C(25)	109.1(3)
C(20)-N(3)-Ta(2)	110.7(2)	C(23)-N(4)-C(25)	107.7(3)
C(24)-N(4)-C(23)	108.6(3)	C(24)-N(4)-Ta(1)	111.9(2)
C(23)-N(4)-Ta(1)	109.0(3)	C(25)-N(4)-Ta(1)	110.5(2)

Table A3 (continued)

Angles			
C(25)-N(5)-C(26)	114.5(4)	H(2A)-C(2)-H(2C)	109.5
C(25)-N(5)-Ta(2)	119.7(3)	C(1)-C(2)-H(2C)	109.5
C(26)-N(5)-Ta(2)	124.8(3)	H(2B)-C(2)-H(2C)	109.5
C(28)-N(6)-C(27)	109.1(4)	C(1)-C(3)-H(3A)	109.5
C(28)-N(6)-Ta(2)	125.6(3)	C(1)-C(3)-H(3B)	109.5
C(27)-N(6)-Ta(2)	125.2(3)	H(3A)-C(3)-H(3B)	109.5
C(2)-C(1)-C(4)	107.6(3)	C(1)-C(3)-H(3C)	109.5
C(2)-C(1)-C(3)	108.2(4)	H(3A)-C(3)-H(3C)	109.5
C(4)-C(1)-C(3)	110.0(4)	H(3B)-C(3)-H(3C)	109.5
C(2)-C(1)-Si(1)	108.2(3)	C(1)-C(4)-H(4A)	109.5
C(4)-C(1)-Si(1)	112.0(3)	C(1)-C(4)-H(4B)	109.5
C(3)-C(1)-Si(1)	110.7(3)	H(4A)-C(4)-H(4B)	109.5
C(1)-C(2)-H(2A)	109.5	C(1)-C(4)-H(4C)	109.5
C(1)-C(2)-H(2B)	109.5	H(4A)-C(4)-H(4C)	109.5
H(2A)-C(2)-H(2B)	109.5	H(4B)-C(4)-H(4C)	109.5
C(6)-C(5)-C(10)	116.6(4)	C(7)-C(6)-C(5)	121.8(5)
C(6)-C(5)-Si(1)	125.8(3)	C(7)-C(6)-H(6)	119.1
C(10)-C(5)-Si(1)	117.5(3)	C(5)-C(6)-H(6)	119.1
C(8)-C(7)-C(6)	120.5(5)	C(8)-C(7)-H(7)	119.7

Table A3 (continued)

Angles			
C(6)-C(7)-H(7)	119.7	C(12)-C(13)-C(14)	119.6(5)
C(7)-C(8)-C(9)	119.1(4)	C(12)-C(13)-H(13)	120.2
C(7)-C(8)-H(8)	120.5	C(14)-C(13)-H(13)	120.2
C(9)-C(8)-H(8)	120.5	C(15)-C(14)-C(13)	120.2(5)
C(10)-C(9)-C(8)	119.9(5)	C(15)-C(14)-H(14)	119.9
C(10)-C(9)-H(9)	120.1	C(13)-C(14)-H(14)	119.9
C(8)-C(9)-H(9)	120.1	C(14)-C(15)-C(16)	119.9(5)
C(9)-C(10)-C(5)	122.2(4)	C(14)-C(15)-H(15)	120.0
C(9)-C(10)-H(10)	118.9	C(16)-C(15)-H(15)	120.0
C(5)-C(10)-H(10)	118.9	C(11)-C(16)-C(15)	121.3(5)
C(16)-C(11)-C(12)	117.1(4)	C(11)-C(16)-H(16)	119.3
C(16)-C(11)-Si(1)	121.0(3)	C(15)-C(16)-H(16)	119.3
C(12)-C(11)-Si(1)	121.8(3)	N(1)-C(17)-H(17A)	109.5
C(13)-C(12)-C(11)	121.9(5)	N(1)-C(17)-H(17B)	109.5
C(13)-C(12)-H(12)	119.0	H(17A)-C(17)-H(17B)	109.5
C(11)-C(12)-H(12)	119.0	N(1)-C(17)-H(17C)	109.5
H(17A)-C(17)-H(17C)	109.5	N(1)-C(18)-H(18A)	109.5
H(17B)-C(17)-H(17C)	109.5	N(1)-C(18)-H(18B)	109.5
H(18A)-C(18)-H(18B)	109.5	N(1)-C(18)-H(18C)	109.5

Table A3 (continued)

Angles			
H(18A)-C(18)-H(18C)	109.5	N(3)-C(21)-H(21B)	109.5
H(18B)-C(18)-H(18C)	109.5	H(21A)-C(21)-H(21B)	109.5
N(2)-C(19)-H(19A)	109.5	N(3)-C(21)-H(21C)	109.5
N(2)-C(19)-H(19B)	109.5	H(21A)-C(21)-H(21C)	109.5
H(19A)-C(19)-H(19B)	109.5	H(21B)-C(21)-H(21C)	109.5
N(2)-C(19)-H(19C)	109.5	N(3)-C(22)-H(22A)	109.5
H(19A)-C(19)-H(19C)	109.5	N(3)-C(22)-H(22B)	109.5
H(19B)-C(19)-H(19C)	109.5	H(22A)-C(22)-H(22B)	109.5
N(2)-C(20)-N(3)	13.3(3)	N(3)-C(22)-H(22C)	109.5
N(2)-C(20)-H(20A)	108.9	H(22A)-C(22)-H(22C)	109.5
N(3)-C(20)-H(20A)	108.9	H(22B)-C(22)-H(22C)	109.5
N(2)-C(20)-H(20B)	108.9	N(4)-C(23)-H(23A)	109.5
N(3)-C(20)-H(20B)	108.9	N(4)-C(23)-H(23B)	109.5
H(20A)-C(20)-H(20B)	107.7	H(23A)-C(23)-H(23B)	109.5
N(3)-C(21)-H(21A)	109.5	N(4)-C(23)-H(23C)	109.5
H(23A)-C(23)-H(23C)	109.5	N(4)-C(24)-H(24A)	109.5
H(23B)-C(23)-H(23C)	109.5	N(4)-C(24)-H(24B)	109.5
H(24A)-C(24)-H(24B)	109.5	N(4)-C(24)-H(24C)	109.5

Table A3 (continued)

Angles			
H(24A)-C(24)-H(24C)	109.5	H(27A)-C(27)-H(27B)	109.5
H(24B)-C(24)-H(24C)	109.5	N(6)-C(27)-H(27C)	109.5
N(5)-C(25)-N(4)	113.8(3)	H(27A)-C(27)-H(27C)	109.5
N(5)-C(25)-H(25A)	108.8	H(27B)-C(27)-H(27C)	109.5
N(4)-C(25)-H(25A)	108.8	N(6)-C(28)-H(28A)	109.5
N(5)-C(25)-H(25B)	108.8	N(6)-C(28)-H(28B)	109.5
N(4)-C(25)-H(25B)	108.8	H(28A)-C(28)-H(28B)	109.5
H(25A)-C(25)-H(25B)	107.7	N(6)-C(28)-H(28C)	109.5
N(5)-C(26)-H(26A)	109.5	H(28A)-C(28)-H(28C)	109.5
N(5)-C(26)-H(26B)	109.5	H(28B)-C(28)-H(28C)	109.5
H(26A)-C(26)-H(26B)	109.5	C(30)-C(29)-C(31)	107.7(4)
N(5)-C(26)-H(26C)	109.5	C(30)-C(29)-C(32)	108.0(4)
H(26A)-C(26)-H(26C)	109.5	C(31)-C(29)-C(32)	110.5(4)
H(26B)-C(26)-H(26C)	109.5	C(30)-C(29)-Si(2)	108.8(3)
N(6)-C(27)-H(27A)	109.5	C(31)-C(29)-Si(2)	111.0(3)
N(6)-C(27)-H(27B)	109.5	C(32)-C(29)-Si(2)	110.8(3)
C(29)-C(30)-H(30A)	109.5	H(30A)-C(30)-H(30B)	109.5
C(29)-C(30)-H(30B)	109.5	C(29)-C(30)-H(30C)	109.5
H(30A)-C(30)-H(30C)	109.5	H(30B)-C(30)-H(30C)	109.5

Table A3 (continued)

Angles			
C(29)-C(31)-H(31A)	109.5	C(35)-C(34)-H(34)	118.6
C(29)-C(31)-H(31B)	109.5	C(33)-C(34)-H(34)	118.6
H(31A)-C(31)-H(31B)	109.5	C(36)-C(35)-C(34)	119.5(5)
C(29)-C(31)-H(31C)	109.5	C(36)-C(35)-H(35)	120.3
H(31A)-C(31)-H(31C)	109.5	C(34)-C(35)-H(35)	120.3
H(31B)-C(31)-H(31C)	109.5	C(35)-C(36)-C(37)	119.7(5)
C(29)-C(32)-H(32A)	109.5	C(35)-C(36)-H(36)	120.2
C(29)-C(32)-H(32B)	109.5	C(37)-C(36)-H(36)	120.2
H(32A)-C(32)-H(32B)	109.5	C(38)-C(37)-C(36)	120.1(5)
C(29)-C(32)-H(32C)	109.5	C(38)-C(37)-H(37)	120.0
H(32A)-C(32)-H(32C)	109.5	C(36)-C(37)-H(37)	120.0
H(32B)-C(32)-H(32C)	109.5	C(37)-C(38)-C(33)	122.2(5)
C(34)-C(33)-C(38)	115.8(4)	C(37)-C(38)-H(38)	118.9
C(34)-C(33)-Si(2)	125.7(4)	C(33)-C(38)-H(38)	118.9
C(38)-C(33)-Si(2)	118.5(3)	C(44)-C(39)-C(40)	116.6(4)
C(35)-C(34)-C(33)	122.8(5)	C(44)-C(39)-Si(2)	120.5(3)
C(40)-C(39)-Si(2)	122.8(3)	C(41)-C(40)-H(40)	119.1
C(41)-C(40)-C(39)	121.9(4)	C(39)-C(40)-H(40)	119.1
C(42)-C(41)-C(40)	120.0(5)	C(42)-C(41)-H(41)	120.0

Table A3 (continued)

Angles			
C(40)-C(41)-H(41)	120.0	Cl(2)-C(45)-H(45A)	108.6
C(41)-C(42)-C(43)	120.0(4)	Cl(1)-C(45)-H(45A)	108.6
C(41)-C(42)-H(42)	120.0	Cl(2)-C(45)-H(45B)	108.6
C(43)-C(42)-H(42)	120.0	Cl(1)-C(45)-H(45B)	108.6
C(42)-C(43)-C(44)	119.6(5)	H(45A)-C(45)-H(45B)	107.5
C(42)-C(43)-H(43)	120.2	Cl(3)-C(46)-Cl(4)	116.5(4)
C(44)-C(43)-H(43)	120.2	Cl(3)-C(46)-H(46A)	108.2
C(43)-C(44)-C(39)	121.9(4)	Cl(4)-C(46)-H(46A)	108.2
C(43)-C(44)-H(44)	119.0	Cl(3)-C(46)-H(46B)	108.2
C(39)-C(44)-H(44)	119.0	Cl(4)-C(46)-H(46B)	108.2
Cl(2)-C(45)-Cl(1)	114.9(4)	H(46A)-C(46)-H(46B)	107.3

Symmetry transformations used to generate equivalent atoms:

#1 -x+1, -y+2, -z+1

Table A4 Anisotropic displacement parameters (Å^2 x 10^3) in **4·CH$_2$Cl$_2$**. The anisotropic displacement factor exponent takes the form: $-2\pi^2[h^2a^{*2}U^{11} + ... + 2hka^*b^*U^{12}]$

	U^{11}	U^{22}	U^{33}	U^{23}	U^{13}	U^{12}
Ta(1)	21(1)	21(1)	25(1)	-1(1)	-4(1)	0(1)
Ta(2)	22(1)	20(1)	24(1)	-2(1)	-4(1)	1(1)
Si(1)	26(1)	20(1)	28(1)	-3(1)	-5(1)	1(1)
Si(2)	26(1)	20(1)	26(1)	-2(1)	-4(1)	2(1)
Cl(1)	76(1)	63(1)	76(1)	-14(1)	-17(1)	24(1)
Cl(2)	62(1)	80(1)	62(1)	-10(1)	-19(1)	-2(1)
Cl(3)	110(2)	76(1)	67(1)	-10(1)	-22(1)	44(1)
Cl(4)	78(1)	102(2)	66(1)	3(1)	0(1)	-12(1)
O(1)	25(2)	21(1)	27(2)	-3(1)	-4(1)	0(1)
O(2)	23(1)	22(1)	22(2)	-3(1)	-3(1)	0(1)
O(3)	21(1)	19(1)	23(2)	0(1)	-2(1)	-4(1)
O(4)	30(2)	21(1)	28(2)	-2(1)	-4(1)	3(1)
N(1)	34(2)	31(2)	32(2)	1(2)	-4(2)	4(2)
N(2)	29(2)	38(2)	31(2)	-11(2)	-13(2)	4(2)
N(3)	32(2)	25(2)	36(2)	-8(2)	-12(2)	-1(2)
N(4)	28(2)	26(2)	36(2)	-9(2)	-7(2)	0(2)
N(5)	34(2)	30(2)	34(2)	-8(2)	-15(2)	6(2)

Table A4 (continued)

	U^{11}	U^{22}	U^{33}	U^{23}	U^{13}	U^{12}
N(6)	36(2)	33(2)	26(2)	1(2)	3(2)	8(2)
C(1)	28(2)	22(2)	33(2)	0(2)	0(2)	-1(2)
C(2)	43(3)	27(2)	46(3)	-10(2)	5(2)	-7(2)
C(3)	35(3)	35(3)	36(3)	7(2)	-5(2)	3(2)
C(4)	27(2)	35(3)	42(3)	-7(2)	-1(2)	-1(2)
C(5)	27(2)	20(2)	40(3)	-3(2)	-11(2)	2(2)
C(6)	43(3)	33(3)	38(3)	-7(2)	-6(2)	-8(2)
C(7)	58(3)	43(3)	46(3)	-17(3)	-11(3)	-5(3)
C(8)	43(3)	33(3)	67(4)	-18(3)	-22(3)	-3(2)
C(9)	38(3)	24(2)	55(3)	0(2)	-11(2)	-4(2)
C(10)	38(3)	28(2)	33(2)	-5(2)	-5(2)	1(2)
C(11)	26(2)	31(2)	28(2)	-1(2)	-6(2)	1(2)
C(12)	38(3)	35(3)	45(3)	-3(2)	-12(2)	4(2)
C(13)	39(3)	53(3)	68(4)	7(3)	-24(3)	10(3)
C(14)	46(3)	73(4)	48(3)	12(3)	-25(3)	-8(3)
C(15)	54(3)	71(4)	33(3)	-9(3)	-11(2)	-8(3)
C(16)	40(3)	46(3)	41(3)	-8(2)	-9(2)	1(2)
C(17)	55(3)	41(3)	41(3)	11(2)	-2(3)	9(3)
C(18)	45(3)	49(3)	36(3)	5(2)	6(2)	7(3)

Table A4 (continued)

	U^{11}	U^{22}	U^{33}	U^{23}	U^{13}	U^{12}
C(19)	48(3)	56(3)	38(3)	-14(2)	-23(2)	14(3)
C(20)	28(2)	32(2)	46(3)	-14(2)	-14(2)	-1(2)
C(21)	39(3)	48(3)	37(3)	-20(2)	-17(2)	12(2)
C(22)	50(3)	29(3)	62(3)	-9(2)	-19(3)	-5(2)
C(23)	47(3)	30(3)	60(3)	-13(2)	-14(3)	-4(2)
C(24)	30(2)	43(3)	36(3)	-18(2)	-12(2)	8(2)
C(25)	25(2)	35(3)	51(3)	-17(2)	-14(2)	3(2)
C(26)	54(3)	53(3)	42(3)	-17(3)	-25(3)	14(3)
C(27)	60(4)	40(3)	48(3)	15(2)	2(3)	12(3)
C(28)	56(3)	44(3)	38(3)	6(2)	10(2)	13(3)
C(29)	29(2)	24(2)	34(2)	0(2)	-3(2)	-2(2)
C(30)	42(3)	31(3)	53(3)	-11(2)	6(2)	-8(2)
C(31)	33(3)	39(3)	42(3)	12(2)	-1(2)	4(2)
C(32)	28(2)	37(3)	39(3)	0(2)	1(2)	-3(2)
C(33)	29(2)	25(2)	32(2)	-5(2)	-7(2)	3(2)
C(34)	59(3)	45(3)	36(3)	-13(2)	-4(2)	-11(3)
C(35)	76(4)	66(4)	49(4)	-27(3)	-3(3)	-19(4)
C(36)	48(3)	48(3)	84(5)	-38(3)	-20(3)	1(3)
C(37)	40(3)	30(3)	65(4)	-10(2)	-10(3)	-1(2)

Table A4 (continued)

	U^{11}	U^{22}	U^{33}	U^{23}	U^{13}	U^{12}
C(38)	34(3)	33(3)	45(3)	-8(2)	-5(2)	4(2)
C(39)	29(2)	32(2)	28(2)	-6(2)	-4(2)	4(2)
C(40)	35(3)	33(3)	36(3)	-5(2)	-6(2)	5(2)
C(41)	42(3)	43(3)	46(3)	-5(2)	-15(2)	12(2)
C(42)	50(3)	60(3)	35(3)	-3(2)	-18(2)	16(3)
C(43)	70(4)	64(4)	34(3)	-17(3)	-26(3)	22(3)
C(44)	55(3)	40(3)	38(3)	-14(2)	-14(2)	17(3)
C(45)	71(4)	68(4)	98(6)	-2(4)	-42(4)	11(4)
C(46)	73(5)	206(10)	62(5)	-2(6)	-16(4)	-19(6)

Table A5 Hydrogen coordinates (x 10^4) and isotropic displacement parameters ($Å^2$ x 10^3) in **4·CH_2Cl_2**

	x	y	z	U(eq)
H(2A)	9983	-665	1978	61
H(2B)	8647	-249	1916	61
H(2C)	9882	46	1240	61
H(3A)	7706	-666	886	56
H(3B)	8285	-1499	411	56
H(3C)	9015	-491	251	56
H(4A)	11013	-1173	516	54
H(4B)	10377	-2201	580	54
H(4C)	10936	-1938	1254	54
H(6)	8917	-3118	546	47
H(7)	8483	-4565	202	58
H(8)	7108	-5680	1066	54
H(9)	6206	-5342	2303	48
H(10)	6683	-3911	2651	41
H(12)	9900	-3826	2277	47
H(13)	11142	-4265	3107	64
H(14)	11102	-3394	4103	66

Table A5 (continued)

	x	y	z	U(eq)
H(15)	9967	-2013	4188	63
H(16)	8695	-1578	3360	51
H(17A)	5529	-2741	4562	74
H(17B)	6325	-2766	3704	74
H(17C)	4974	-3299	4011	74
H(18A)	3133	-2394	4353	71
H(18B)	3203	-1263	4129	71
H(18C)	3743	-1743	4820	71
H(19A)	7641	-83	4110	67
H(19B)	6755	-1015	4254	67
H(19C)	6158	-31	4476	67
H(20A)	7469	906	2481	40
H(20B)	7391	1197	3301	40
H(21A)	5491	1759	4032	58
H(21B)	4649	877	3962	58
H(21C)	4279	1939	3701	58
H(22A)	5537	2833	2523	68
H(22B)	6843	2410	2105	68

Table A5 (continued)

	x	y	z	U(eq)
H(22C)	6670	2718	2930	68
H(23A)	3480	-2834	2111	67
H(23B)	3424	-2544	2930	67
H(23C)	4686	-2965	2453	67
H(24A)	5915	-2050	1308	52
H(24B)	5513	-1000	1039	52
H(24C)	4689	-1902	987	52
H(25A)	2803	-1307	1710	42
H(25B)	2728	-1023	2532	42
H(26A)	3929	-108	547	70
H(26B)	3454	910	762	70
H(26C)	2473	28	941	70
H(27A)	5345	3190	973	82
H(27B)	3969	2725	1362	82
H(27C)	4621	2654	487	82
H(28A)	6438	1692	171	77
H(28B)	6940	1082	831	77
H(28C)	7113	2215	688	77

Table A5 (continued)

	x	y	z	U(eq)
H(30A)	141	-51	3659	67
H(30B)	1438	186	3022	67
H(30C)	182	714	2925	67
H(31A)	1044	324	4684	62
H(31B)	1880	1278	4565	62
H(31C)	2370	453	4061	62
H(32A)	-697	1965	3704	55
H(32B)	-126	2147	4394	55
H(32C)	-855	1163	4429	55
H(34)	1611	2793	4544	57
H(35)	2156	4126	5004	77
H(36)	3354	5364	4166	68
H(37)	3979	5256	2868	55
H(38)	3425	3926	2413	45
H(40)	584	3885	2660	42
H(41)	-546	4411	1782	52
H(42)	-664	3506	840	57
H(43)	324	2052	792	63

Table A5 (continued)

	x	y	z	U(eq)
H(44)	1502	1540	1657	52
H(45A)	2606	4606	1231	92
H(45B)	3248	4824	339	92
H(46A)	8090	4211	3263	139
H(46B)	8092	5226	3540	139

Table A6 Atomic coordinates (x 10^4) and equivalent isotropic displacement parameters ($Å^2$ x 10^3) in **10**. U(eq) is defined as one third of the trace of the orthogonalized U^{ij} tensor.

	x	y	z	U(eq)
C(1)	-56(10)	8293(6)	7152(2)	83
C(2)	-1037(8)	8624(5)	6782(3)	60
C(3)	2361(9)	8867(4)	6803(3)	76
C(4)	2783(9)	8049(5)	6988(3)	76
C(5)	-773(8)	6882(5)	6762(3)	78
C(6)	861(8)	6678(4)	6584(2)	55
C(7)	1376(6)	7888(4)	5582(2)	34
C(8)	221(6)	7936(4)	5561(2)	37
C(9)	4048(7)	8296(4)	6066(3)	74
C(10)	3897(7)	7152(5)	6245(3)	62
C(11)	3914(8)	7271(5)	5534(3)	64
C(12)	1572(8)	6004(4)	5778(3)	58
C(13)	-584(7)	6320(4)	5752(2)	52
C(14)	855(8)	6446(5)	5202(2)	60
C(15)	1743(6)	9432(4)	5976(2)	47
C(16)	-70(7)	9711(4)	6345(2)	46
C(17)	-261(7)	9417(4)	5607(2)	46

Table A6 (continued)

	x	y	z	U(eq)
C(18)	-2742(7)	8641(4)	6031(3)	56
C(19)	-2636(8)	7451(5)	6103(3)	78
C(20)	-2439(7)	7788(4)	5458(2)	53
C(21)	8158(9)	10054(4)	8092(3)	65
C(22)	8773(9)	9327(5)	7750(2)	62
C(23)	7979(6)	8150(4)	8335(2)	46
C(24)	9356(9)	7996(4)	7975(2)	56
C(25)	11248(9)	9900(4)	8102(3)	72
C(26)	11618(7)	9086(4)	8287(3)	53
C(27)	9539(6)	9613(4)	9419(2)	36
C(28)	8400(6)	9609(4)	9326(2)	34
C(29)	8287(6)	8029(3)	9217(2)	39
C(30)	10108(7)	7720(3)	8833(2)	37
C(31)	10381(7)	8141(4)	9571(2)	47
C(32)	12757(7)	8948(4)	9101(3)	56
C(33)	12137(8)	9651(4)	9702(2)	54
C(34)	12429(7)	10131(4)	9091(2)	52
C(35)	5807(6)	8884(3)	8830(2)	46
C(36)	5709(8)	9881(4)	8518(3)	65

Table A6 (continued)

	x	y	z	U(eq)
C(37)	5906(7)	10027(4)	9264(2)	52
C(38)	7861(9)	11192(4)	8865(3)	70
C(39)	10057(9)	10963(5)	8781(4)	96
C(40)	9147(9)	11079(4)	9449(3)	76
C(41)	7662(9)	3672(4)	8088(3)	79
C(42)	7123(8)	4492(5)	7974(3)	70
C(43)	8971(7)	5862(4)	8382(2)	46
C(44)	10668(7)	5732(4)	8243(3)	59
C(45)	10173(8)	4385(5)	7807(2)	61
C(46)	11055(7)	3962(4)	8164(2)	52
C(47)	9589(6)	4492(3)	9378(2)	30
C(48)	8431(5)	4522(3)	9333(2)	27
C(49)	8178(6)	3025(3)	8938(2)	44
C(50)	9958(7)	2789(4)	8554(2)	48
C(51)	10215(7)	3010(4)	9288(2)	50
C(52)	12660(6)	3897(4)	8948(3)	56
C(53)	12487(7)	5053(4)	8833(2)	48
C(54)	12313(7)	4777(4)	9510(2)	53
C(55)	5791(7)	4182(4)	8821(3)	55

Table A6 (continued)

	x	y	z	U(eq)
C(56)	6040(7)	5400(5)	8708(3)	60
C(57)	5904(7)	5182(4)	9392(2)	43
C(58)	10450(6)	6109(4)	9240(2)	52
C(59)	8995(8)	5919(4)	9786(2)	50
C(60)	8298(8)	6456(4)	9242(2)	48
C(61)	2986(7)	3700(5)	6771(3)	68
C(62)	1642(9)	4084(5)	7090(3)	91
C(63)	-663(12)	2695(7)	7151(4)	123
C(64)	-1207(8)	3339(5)	6863(3)	63
C(65)	2113(11)	2174(8)	6907(5)	156
C(66)	398(14)	1681(5)	6717(4)	130
C(67)	216(7)	2966(4)	5648(2)	44
C(68)	1360(7)	2956(4)	5652(2)	49
C(69)	4104(8)	3388(4)	5955(3)	60
C(70)	4173(7)	2371(5)	6266(2)	62
C(71)	3840(7)	2226(4)	5527(2)	49
C(72)	1761(8)	1111(4)	5897(3)	64
C(73)	-447(7)	1375(5)	5820(3)	74
C(74)	987(8)	1472(5)	5289(2)	62

Table A6 (continued)

	x	y	z	U(eq)
C(75)	1619(7)	4508(4)	6123(3)	60
C(76)	-409(8)	4458(4)	5744(2)	57
C(77)	-263(8)	4650(4)	6492(2)	57
C(78)	-2823(7)	3498(4)	6155(4)	81
C(79)	-2584(9)	2307(4)	6103(4)	80
C(80)	-2397(9)	2840(5)	5515(3)	76
C(81)	1563(7)	6260(4)	7401(2)	50
C(82)	1495(7)	6816(4)	7585(2)	49
C(83)	2401(8)	7575(5)	7996(3)	66
C(84)	3366(8)	7774(5)	8210(2)	60
C(85)	4464(8)	8345(4)	7880(3)	55
C(86)	5492(7)	8393(4)	7739(2)	54
C(87)	6386(7)	7949(4)	7339(3)	58
C(88)	6259(9)	7496(5)	7036(3)	74
C(89)	5934(12)	6485(7)	6864(4)	190
C(90)	5200(11)	6094(6)	6802(4)	129
C(91)	3404(8)	5857(5)	6802(2)	64
C(92)	2528(7)	5761(4)	7024(3)	51
C(93)	5805(7)	7053(4)	8370(2)	44

Table A6 (continued)

	x	y	z	U(eq)
C(94)	4950(6)	6576(4)	8421(2)	37
C(95)	3336(6)	6016(3)	8160(2)	40
C(96)	3661(7)	5450(4)	8057(2)	39
C(97)	4412(7)	4920(4)	7652(2)	46
C(98)	4958(8)	4956(4)	7333(3)	54
C(99)	5730(8)	4355(4)	6929(2)	55
C(100)	6868(7)	4526(4)	6969(3)	59
C(101)	8177(7)	5334(4)	7217(3)	59
C(102)	8276(7)	5937(4)	7370(3)	54
C(103)	7478(8)	6516(4)	7753(2)	50
C(104)	6732(8)	6473(4)	8028(2)	49
C(105)	2917(12)	2799(9)	8039(5)	182
C(106)	1878(14)	2409(10)	7933(5)	194
C(107)	1082(9)	1524(8)	7739(4)	116
C(108)	1256(9)	947(8)	7614(3)	124
C(109)	1935(12)	413(5)	7166(4)	118
C(110)	2474(11)	453(5)	6861(4)	106
C(111)	4118(13)	835(7)	6665(3)	118
C(112)	5152(12)	1146(9)	6782(3)	139

Table A6 (continued)

	x	y	z	U(eq)
C(113)	6040(10)	2073(11)	7038(4)	179
C(114)	5851(12)	2632(8)	7123(4)	148
C(115)	4978(13)	3211(5)	7489(4)	136
C(116)	4449(12)	3259(6)	7777(5)	134
C(117)	3992(7)	1033(4)	8132(2)	52
C(118)	4990(7)	1457(4)	8244(2)	47
C(119)	6039(7)	2278(4)	8116(2)	47
C(120)	7054(7)	2061(4)	8099(2)	47
C(121)	8020(7)	1556(5)	7733(3)	61
C(122)	7826(8)	1147(5)	7394(3)	74
C(123)	8640(9)	559(6)	7024(3)	87
C(124)	7997(11)	-1(5)	7000(3)	86
C(125)	6374(13)	-548(6)	6987(5)	163
C(126)	5455(11)	-542(6)	7072(3)	100
C(127)	4588(11)	18(5)	7447(3)	85
C(128)	4748(10)	400(5)	7768(3)	75
C(129)	5693(9)	6277(5)	10271(3)	72
C(130)	6675(9)	6538(4)	10151(3)	68
C(131)	7721(7)	7408(5)	10100(3)	66

Table A6 (continued)

	x	y	z	U(eq)
C(132)	7800(7)	8020(5)	10168(3)	61
C(133)	7009(10)	8758(4)	10054(3)	70
C(134)	6072(9)	8891(4)	9895(3)	63
C(135)	4265(9)	8783(5)	9914(3)	71
C(136)	3376(9)	8549(4)	10080(3)	70
C(137)	2305(7)	7689(5)	10138(3)	62
C(138)	2161(7)	7065(5)	10034(3)	59
C(139)	2951(9)	6303(4)	10056(2)	59
C(140)	3855(8)	6127(4)	10216(3)	60
C(141)	3570(6)	7182(3)	9152(2)	33
C(142)	2551(6)	7314(4)	9050(3)	55
C(143)	3620(7)	6665(3)	9224(2)	40
C(144)	4577(8)	6538(4)	9313(2)	52
C(145)	5474(7)	6942(5)	9321(2)	64
C(146)	5432(7)	7479(5)	9254(2)	56
C(147)	4500(6)	7577(4)	9173(2)	42
C(148)	4653(7)	7465(5)	10935(2)	54
C(149)	4499(8)	7955(5)	10853(2)	66
C(150)	5319(9)	8407(5)	10871(2)	62

Table A6 (continued)

	x	y	z	U(eq)
C(151)	3507(7)	2137(4)	8946(3)	47
C(152)	2446(8)	2194(5)	8836(4)	108
C(153)	3663(8)	1647(4)	9030(2)	56
C(154)	4367(7)	2580(4)	8960(2)	50
C(155)	2313(8)	5200(5)	4931(3)	65
C(156)	2324(8)	4329(4)	5073(3)	61
C(157)	2808(7)	3827(4)	4993(3)	61
C(158)	4424(9)	3540(4)	5050(3)	66
C(159)	5469(9)	3708(4)	5216(3)	60
C(160)	7055(8)	4341(5)	5226(3)	62
C(161)	6330(7)	5355(4)	6043(2)	42
C(162)	7368(7)	5296(5)	6199(3)	67
C(163)	5458(7)	4922(4)	6027(2)	52
C(164)	4522(9)	4984(5)	5906(3)	71
C(165)	4400(10)	5451(6)	5802(3)	77
C(166)	5316(11)	5881(5)	5824(3)	78
C(167)	6260(9)	5828(4)	5941(2)	57
C(168)	2524(7)	399(4)	4954(2)	53
C(169)	3194(7)	827(5)	4807(3)	58

Table A6 (continued)

	x	y	z	U(eq)
C(170)	4890(8)	1359(4)	4812(2)	54
C(171)	5948(9)	1476(4)	4982(3)	60
C(172)	7409(7)	1082(4)	5072(3)	56
C(173)	7802(7)	542(4)	4980(3)	56
C(174)	6285(7)	332(4)	5987(2)	46
C(175)	7368(8)	321(6)	6113(3)	81
C(176)	6073(8)	792(4)	5894(2)	50
C(177)	5068(10)	798(5)	5778(3)	69
C(178)	4274(9)	337(5)	5770(3)	60
C(179)	4504(7)	-123(4)	5863(2)	52
C(180)	5498(6)	-133(4)	5972(2)	45
Hf(1)	713(1)	7870(1)	6515(1)	30
Hf(2)	9398(1)	9227(1)	8425(1)	28
Hf(3)	9233(1)	4668(1)	8434(1)	27
Hf(4)	840(1)	2925(1)	6597(1)	30
K(1)	4440(1)	6836(1)	7583(1)	36
K(2)	3785(1)	1709(1)	7464(1)	33
K(3)	4998(1)	7523(1)	10080(1)	35
K(4)	5000	5000	5000	42

Table A6 (continued)

	x	y	z	U(eq)
K(5)	5000	0	5000	37
N(1)	-230(7)	8301(4)	6805(2)	55
N(2)	189(6)	7094(3)	6625(2)	45
N(3)	2093(6)	8247(3)	6780(2)	45
N(4)	8686(6)	9589(3)	8097(2)	42
N(5)	8958(5)	8385(3)	8232(2)	36
N(6)	10866(5)	9439(3)	8264(2)	42
N(7)	7909(5)	4269(3)	8148(2)	41
N(8)	9689(5)	5470(3)	8356(2)	33
N(9)	10280(5)	4300(3)	8146(2)	41
N(10)	1885(5)	3618(3)	6827(2)	45
N(11)	-450(6)	2975(4)	6872(2)	53
N(12)	1222(8)	2248(4)	6764(2)	76
O(1)	2456(4)	6295(2)	7210(1)	41
O(2)	2397(5)	7028(3)	7802(2)	50
O(3)	4273(5)	7846(3)	8023(2)	50
O(4)	5406(5)	7934(3)	7472(2)	47
O(5)	6011(5)	6954(3)	7129(2)	71
O(6)	4341(5)	6038(3)	6991(2)	51

Table A6 (continued)

	x	y	z	U(eq)
O(7)	6253(4)	6945(2)	8064(1)	37
O(8)	4171(4)	6486(2)	8161(1)	33
O(9)	4068(4)	5429(2)	7747(1)	41
O(10)	5242(5)	4422(3)	7232(2)	49
O(11)	7156(5)	5138(3)	7074(2)	48
O(12)	7592(5)	5963(3)	7627(2)	47
O(13)	3490(8)	2826(4)	7751(3)	125
O(14)	2057(6)	1872(5)	7825(2)	104
O(15)	1815(6)	945(3)	7316(2)	80
O(16)	3517(7)	780(3)	6942(2)	80
O(17)	5054(6)	1713(4)	6933(2)	86
O(18)	5265(6)	2704(3)	7419(2)	80
O(19)	3964(5)	728(3)	7809(2)	48
O(20)	5115(4)	1837(2)	8028(1)	40
O(21)	7071(5)	1752(3)	7781(2)	51
O(22)	8722(5)	924(4)	7344(2)	72
O(23)	6944(8)	25(4)	6968(2)	102
O(24)	5432(7)	-238(4)	7398(2)	88
O(25)	4826(6)	6407(3)	10115(2)	55

Table A6 (continued)

	x	y	z	U(eq)
O(26)	6808(5)	7148(3)	10213(2)	56
O(27)	6949(5)	8181(3)	10011(2)	52
O(28)	5164(6)	8657(3)	10044(2)	57
O(29)	3178(5)	7943(3)	10007(2)	59
O(30)	3032(5)	6873(3)	10159(2)	53
O(31)	2819(4)	4730(3)	4907(2)	47
O(32)	3882(5)	3979(2)	5122(2)	50
O(33)	6074(5)	4156(3)	5070(2)	53
O(34)	7147(4)	117(3)	5112(1)	41
O(35)	6387(5)	985(2)	4915(2)	46
O(36)	4223(5)	942(2)	4947(1)	46
Si(1)	1585(2)	7473(1)	5923(1)	26
Si(2)	3387(2)	7530(1)	5940(1)	40
Si(3)	842(2)	6543(1)	5662(1)	38
Si(4)	-201(2)	8255(1)	5991(1)	26
Si(5)	293(2)	9224(1)	5985(1)	31
Si(6)	-2035(2)	8044(1)	5896(1)	36
Si(7)	10126(2)	9161(1)	9069(1)	26
Si(8)	9728(2)	8245(1)	9174(1)	28

Table A6 (continued)

	x	y	z	U(eq)
Si(9)	11910(2)	9464(1)	9237(1)	36
Si(10)	8223(2)	9795(1)	8901(1)	26
Si(11)	6393(2)	9666(1)	8869(1)	34
Si(12)	8836(2)	10783(1)	9004(1)	44
Si(13)	10081(2)	4228(1)	8951(1)	24
Si(14)	9626(2)	3250(1)	8929(1)	29
Si(15)	11917(2)	4484(1)	9061(1)	29
Si(16)	8261(1)	4988(1)	9019(1)	22
Si(17)	6466(2)	4946(1)	8987(1)	33
Si(18)	9012(2)	5886(1)	9320(1)	30
Si(19)	1685(2)	2548(1)	5990(1)	32
Si(20)	3474(2)	2612(1)	5935(1)	38
Si(21)	992(2)	1606(1)	5750(1)	42
Si(22)	-213(2)	3247(1)	6074(1)	34
Si(23)	177(2)	4231(1)	6109(1)	38
Si(24)	-2033(2)	2989(1)	5965(1)	46

Table A7 Bond distances (Å) in **10**

Distances			
C(1)-N(1)	1.463(12)	C(15)-Si(5)	1.873(8)
C(2)-N(1)	1.457(11)	C(16)-Si(5)	1.878(9)
C(3)-N(3)	1.488(12)	C(17)-Si(5)	1.892(8)
C(4)-N(3)	1.448(11)	C(18)-Si(6)	1.900(8)
C(5)-N(2)	1.446(11)	C(19)-Si(6)	1.890(9)
C(6)-N(2)	1.470(11)	C(20)-Si(6)	1.842(9)
C(7)-C(8)	1.544(10)	C(21)-N(4)	1.456(11)
C(7)-Si(1)	1.945(7)	C(22)-N(4)	1.488(11)
C(8)-Si(4)	1.960(8)	C(23)-N(5)	1.418(10)
C(9)-Si(2)	1.885(10)	C(24)-N(5)	1.478(10)
C(10)-Si(2)	1.890(9)	C(25)-N(6)	1.448(10)
C(11)-Si(2)	1.899(10)	C(26)-N(6)	1.451(11)
C(12)-Si(3)	1.909(9)	C(27)-C(28)	1.528(10)
C(13)-Si(3)	1.913(9)	C(27)-Si(7)	1.940(8)
C(14)-Si(3)	1.888(9)	C(28)-Si(10)	1.932(7)
C(29)-Si(8)	1.884(8)	C(32)-Si(9)	1.874(9)
C(30)-Si(8)	1.889(8)	C(33)-Si(9)	1.908(9)
C(31)-Si(8)	1.924(8)	C(34)-Si(9)	1.872(8)
C(35)-Si(11)	1.907(8)	C(36)-Si(11)	1.907(9)

Table A7 (continued)

Distances			
C(37)-Si(11)	1.911(9)	C(53)-Si(15)	1.891(8)
C(38)-Si(12)	1.919(10)	C(54)-Si(15)	1.893(9)
C(39)-Si(12)	1.896(10)	C(55)-Si(17)	1.904(9)
C(40)-Si(12)	1.861(11)	C(56)-Si(17)	1.901(9)
C(41)-N(7)	1.417(12)	C(57)-Si(17)	1.902(8)
C(42)-N(7)	1.490(11)	C(58)-Si(18)	1.916(8)
C(43)-N(8)	1.472(10)	C(59)-Si(18)	1.929(9)
C(44)-N(8)	1.455(10)	C(60)-Si(18)	1.908(8)
C(45)-N(9)	1.478(11)	C(61)-N(10)	1.451(11)
C(46)-N(9)	1.444(11)	C(62)-N(10)	1.524(12)
C(47)-C(48)	1.541(10)	C(63)-N(11)	1.472(13)
C(47)-Si(13)	1.953(7)	C(64)-N(11)	1.469(12)
C(48)-Si(16)	1.936(7)	C(65)-N(12)	1.355(15)
C(49)-Si(14)	1.873(8)	C(66)-N(12)	1.566(16)
C(50)-Si(14)	1.871(8)	C(67)-C(68)	1.505(12)
C(51)-Si(14)	1.906(9)	C(67)-Si(22)	1.928(8)
C(52)-Si(15)	1.896(9)	C(68)-Si(19)	1.964(9)
C(69)-Si(20)	1.918(9)	C(71)-Si(20)	1.912(9)
C(70)-Si(20)	1.882(9)	C(72)-Si(21)	1.904(10)

Table A7 (continued)

Distances			
C(73)-Si(21)	1.908(9)	C(87)-O(4)	1.414(11)
C(74)-Si(21)	1.890(9)	C(87)-C(88)	1.502(15)
C(75)-Si(23)	1.875(9)	C(88)-O(5)	1.443(13)
C(76)-Si(23)	1.909(9)	C(89)-C(90)	1.204(16)
C(77)-Si(23)	1.905(9)	C(89)-O(5)	1.427(13)
C(78)-Si(24)	1.865(10)	C(90)-O(6)	1.394(11)
C(79)-Si(24)	1.899(11)	C(91)-O(6)	1.384(11)
C(80)-Si(24)	1.870(11)	C(91)-C(92)	1.509(14)
C(81)-O(1)	1.437(10)	C(92)-O(1)	1.420(10)
C(81)-C(82)	1.462(13)	C(93)-O(7)	1.424(9)
C(82)-O(2)	1.413(10)	C(93)-C(94)	1.510(11)
C(83)-O(2)	1.438(11)	C(94)-O(8)	1.419(9)
C(83)-C(84)	1.468(14)	C(95)-O(8)	1.429(9)
C(84)-O(3)	1.446(11)	C(95)-C(96)	1.531(12)
C(85)-O(3)	1.447(11)	C(96)-O(9)	1.411(9)
C(85)-C(86)	1.482(13)	C(97)-O(9)	1.411(10)
C(86)-O(4)	1.414(11)	C(97)-C(98)	1.540(12)
C(98)-O(10)	1.434(10)	C(99)-C(100)	1.463(13)
C(99)-O(10)	1.432(10)	C(100)-O(11)	1.462(11)

Table A7 (continued)

Distances			
C(101)-O(11)	1.402(11)	C(107)-C(108)	1.49(2)
C(101)-C(102)	1.483(13)	C(108)-O(15)	1.466(15)
C(102)-O(12)	1.423(10)	C(109)-O(15)	1.386(16)
C(103)-O(12)	1.407(10)	C(109)-C(110)	1.49(2)
C(103)-C(104)	1.539(11)	C(110)-O(16)	1.438(15)
C(104)-O(7)	1.415(10)	C(111)-O(16)	1.433(16)
C(105)-O(13)	1.44(2)	C(111)-C(112)	1.44(2)
C(105)-C(106)	1.50(2)	C(112)-O(17)	1.457(18)
C(106)-O(14)	1.39(2)	C(113)-C(114)	1.43(3)
C(107)-O(14)	1.386(15)	C(113)-O(17)	1.420(18)
C(114)-O(18)	1.477(19)	C(115)-O(18)	1.359(18)
C(115)-C(116)	1.40(2)	C(116)-O(13)	1.467(18)
C(117)-O(19)	1.411(11)	C(117)-C(118)	1.504(12)
C(118)-O(20)	1.410(10)	C(119)-O(20)	1.445(10)
C(119)-C(120)	1.529(12)	C(120)-O(21)	1.406(10)
C(121)-O(21)	1.428(10)	C(122)-O(22)	1.400(11)
C(121)-C(122)	1.557(15)	C(123)-O(22)	1.450(13)
C(123)-C(124)	1.454(17)	C(124)-O(23)	1.399(15)
C(125)-C(126)	1.269(17)	C(125)-O(23)	1.482(16)

Table A7 (continued)

Distances			
C(126)-O(24)	1.429(14)	C(133)-O(27)	1.390(12)
C(127)-O(24)	1.383(14)	C(133)-C(134)	1.500(16)
C(127)-C(128)	1.467(15)	C(134)-O(28)	1.431(11)
C(128)-O(19)	1.425(12)	C(135)-O(28)	1.396(12)
C(129)-O(25)	1.412(12)	C(135)-C(136)	1.454(15)
C(129)-C(130)	1.472(15)	C(136)-O(29)	1.439(12)
C(130)-O(26)	1.454(12)	C(137)-O(29)	1.376(11)
C(131)-O(26)	1.384(12)	C(137)-C(138)	1.492(14)
C(131)-C(132)	1.467(15)	C(138)-O(30)	1.438(11)
C(132)-O(27)	1.433(11)	C(139)-O(30)	1.375(11)
C(139)-C(140)	1.518(14)	C(144)-C(145)	1.377(15)
C(140)-O(25)	1.440(11)	C(145)-C(146)	1.419(15)
C(141)-C(143)	1.381(11)	C(145)-K(3)	3.352(9)
C(141)-C(147)	1.392(11)	C(146)-C(147)	1.338(13)
C(141)-C(142)	1.503(11)	C(146)-K(3)	3.494(10)
C(143)-C(144)	1.405(12)	C(148)-C(154)#1	1.375(13)
C(148)-C(149)	1.367(15)	C(149)-K(3)	3.331(10)
C(149)-C(150)	1.376(15)	C(150)-C(153)#1	1.423(14)
C(151)-C(153)	1.373(13)	C(151)-C(154)	1.398(12)

Table A7 (continued)

Distances			
C(151)-C(152)	1.492(14)	C(160)-O(33)	1.373(11)
C(153)-C(150)#1	1.423(14)	C(160)-C(155)#2	1.529(15)
C(154)-C(148)#1	1.375(13)	C(161)-C(167)	1.335(12)
C(155)-O(31)	1.438(11)	C(161)-C(163)	1.392(12)
C(155)-C(160)#2	1.529(15)	C(161)-C(162)	1.533(13)
C(156)-O(31)	1.383(11)	C(163)-C(164)	1.358(14)
C(156)-C(157)	1.492(14)	C(164)-C(165)	1.341(17)
C(157)-O(32)	1.442(11)	C(165)-C(166)	1.425(17)
C(158)-O(32)	1.402(12)	C(165)-K(4)	3.489(11)
C(158)-C(159)	1.460(15)	C(166)-C(167)	1.354(16)
C(159)-O(33)	1.472(11)	C(168)-O(34)#3	1.409(10)
C(168)-C(169)	1.477(13)	C(172)-O(35)	1.427(11)
C(169)-O(36)	1.407(11)	C(172)-C(173)	1.513(14)
C(170)-O(36)	1.428(11)	C(173)-O(34)	1.424(10)
C(170)-C(171)	1.487(14)	C(174)-C(176)	1.345(13)
C(171)-O(35)	1.428(11)	C(174)-C(180)	1.373(12)
C(174)-C(175)	1.505(13)	C(177)-K(5)	3.455(11)
C(176)-C(177)	1.391(15)	C(178)-C(179)	1.352(14)
C(177)-C(178)	1.377(15)	C(178)-K(5)	3.381(10)

Table A7 (continued)

Distances			
C(179)-C(180)	1.372(12)	Hf(4)-N(10)	2.023(7)
Hf(1)-N(3)	2.043(7)	Hf(4)-N(12)	2.067(8)
Hf(1)-N(2)	2.047(7)	Hf(4)-N(11)	2.084(7)
Hf(1)-N(1)	2.063(7)	Hf(4)-Si(22)	2.864(2)
Hf(1)-Si(1)	2.846(2)	Hf(4)-Si(19)	2.866(2)
Hf(1)-Si(4)	2.863(2)	K(1)-O(8)	2.722(6)
Hf(2)-N(5)	2.043(6)	K(1)-O(6)	2.837(6)
Hf(2)-N(6)	2.062(6)	K(1)-O(5)	2.853(7)
Hf(2)-N(4)	2.064(7)	K(1)-O(3)	2.855(6)
Hf(2)-Si(7)	2.864(3)	K(1)-O(4)	2.885(6)
Hf(2)-Si(10)	2.879(2)	K(1)-O(1)	2.925(6)
Hf(3)-N(8)	2.042(6)	K(1)-O(2)	2.955(6)
Hf(3)-N(7)	2.038(6)	K(1)-O(7)	2.998(6)
Hf(3)-N(9)	2.085(6)	K(2)-O(16)	2.805(7)
Hf(3)-Si(16)	2.841(2)	K(2)-O(20)	2.812(6)
Hf(3)-Si(13)	2.875(2)	K(2)-O(17)	2.813(7)
K(2)-O(14)	2.816(8)	K(2)-O(13)	2.901(8)
K(2)-O(15)	2.853(7)	K(2)-O(19)	3.084(6)
K(2)-O(18)	2.857(7)	K(3)-O(25)	2.754(7)

Table A7 (continued)

Distances			
K(3)-O(26)	2.788(7)	K(4)-C(165)#2	3.489(11)
K(3)-O(28)	2.798(6)	K(5)-O(36)	2.760(6)
K(3)-O(27)	2.800(6)	K(5)-O(36)#3	2.760(6)
K(3)-O(29)	2.814(7)	K(5)-O(34)#3	2.787(6)
K(3)-O(30)	2.821(6)	K(5)-O(34)	2.787(6)
K(4)-O(33)	2.789(6)	K(5)-O(35)#3	2.823(6)
K(4)-O(33)#2	2.789(6)	K(5)-O(35)	2.823(6)
K(4)-O(32)	2.800(6)	K(5)-C(178)#3	3.381(10)
K(4)-O(32)#2	2.800(6)	K(5)-C(177)#3	3.455(11)
K(4)-O(31)#2	2.802(6)	O(34)-C(168)#3	1.409(10)
K(4)-O(31)	2.802(6)	Si(1)-Si(2)	2.337(3)
Si(1)-Si(3)	2.347(3)	Si(10)-Si(11)	2.353(3)
Si(4)-Si(5)	2.357(3)	Si(10)-Si(12)	2.364(3)
Si(4)-Si(6)	2.362(3)	Si(13)-Si(14)	2.356(3)
Si(7)-Si(8)	2.347(3)	Si(13)-Si(15)	2.372(3)
Si(7)-Si(9)	2.350(3)	Si(16)-Si(17)	2.334(3)
Si(16)-Si(18)	2.341(3)	Si(19)-Si(20)	2.342(3)
Si(19)-Si(21)	2.338(4)	Si(22)-Si(24)	2.350(3)

Table A7 (continued)

Distances	
Si(22)-Si(23)	2.357(4)

Symmetry transformations used to generate equivalent atoms:

#1 -x+1, -y+2, -z+1

Table A8 Bond angles (deg) in **10**

Angles			
C(8)-C(7)-Si(1)	108.4(5)	O(2)-C(83)-C(84)	110.0(8)
C(7)-C(8)-Si(4)	111.1(5)	O(3)-C(84)-C(83)	111.4(8)
C(28)-C(27)-Si(7)	110.8(5)	O(3)-C(85)-C(86)	108.5(8)
C(27)-C(28)-Si(10)	111.9(5)	O(4)-C(86)-C(85)	107.2(8)
C(48)-C(47)-Si(13)	109.2(5)	O(4)-C(87)-C(88)	108.5(8)
C(47)-C(48)-Si(16)	109.8(5)	O(5)-C(88)-C(87)	108.7(8)
C(68)-C(67)-Si(22)	112.8(6)	C(90)-C(89)-O(5)	124.3(11)
C(67)-C(68)-Si(19)	108.3(6)	C(89)-C(90)-O(6)	123.5(11)
O(1)-C(81)-C(82)	110.9(7)	O(6)-C(91)-C(92)	109.0(8)
O(2)-C(82)-C(81)	108.6(7)	O(1)-C(92)-C(91)	107.4(7)
O(7)-C(93)-C(94)	113.5(7)	O(10)-C(98)-C(97)	105.6(8)
O(8)-C(94)-C(93)	107.0(7)	O(10)-C(99)-C(100)	113.3(8)
O(8)-C(95)-C(96)	112.7(7)	O(11)-C(100)-C(99)	108.8(8)
O(9)-C(96)-C(95)	108.5(7)	O(11)-C(101)-C(102)	107.0(8)
O(9)-C(97)-C(98)	106.8(7)	O(12)-C(102)-C(101)	107.4(7)
O(12)-C(103)-C(104)	106.1(7)	O(7)-C(104)-C(103)	107.5(7)
O(13)-C(105)-C(106)	107.6(13)	O(14)-C(107)-C(108)	106.9(12)
O(14)-C(106)-C(105)	107.8(13)	O(15)-C(108)-C(107)	109.1(10)
O(15)-C(109)-C(110)	109.1(10)	O(16)-C(110)-C(109)	109.5(10)

Table A8 (continued)

Angles			
O(16)-C(111)-C(112)	108.3(11)	O(22)-C(122)-C(121)	106.7(9)
C(111)-C(112)-O(17)	106.8(10)	O(22)-C(123)-C(124)	114.9(11)
C(114)-C(113)-O(17)	106.3(13)	O(23)-C(124)-C(123)	109.5(11)
C(113)-C(114)-O(18)	111.6(11)	C(126)-C(125)-O(23)	111.2(14)
O(18)-C(115)-C(116)	110.7(12)	C(125)-C(126)-O(24)	112.9(13)
C(115)-C(116)-O(13)	112.7(12)	O(24)-C(127)-C(128)	109.3(10)
O(19)-C(117)-C(118)	114.3(8)	O(19)-C(128)-C(127)	110.9(9)
O(20)-C(118)-C(117)	107.3(7)	O(25)-C(129)-C(130)	111.1(9)
O(20)-C(119)-C(120)	113.5(7)	O(26)-C(130)-C(129)	110.9(8)
O(21)-C(120)-C(119)	107.6(7)	O(26)-C(131)-C(132)	109.5(8)
O(21)-C(121)-C(122)	104.7(7)	O(27)-C(132)-C(131)	112.5(8)
O(27)-C(133)-C(134)	111.7(8)	O(30)-C(138)-C(137)	110.6(8)
O(28)-C(134)-C(133)	108.6(8)	O(30)-C(139)-C(140)	109.0(8)
O(28)-C(135)-C(136)	109.1(8)	O(25)-C(140)-C(139)	109.8(8)
O(29)-C(136)-C(135)	110.6(9)	C(143)-C(141)-C(147)	117.7(8)
O(29)-C(137)-C(138)	109.0(8)	C(143)-C(141)-C(142)	121.4(8)
C(147)-C(141)-C(142)	120.9(8)	C(144)-C(145)-C(146)	120.9(9)
C(141)-C(143)-C(144)	121.3(9)	C(144)-C(145)-K(3)	88.4(5)
C(145)-C(144)-C(143)	118.4(9)	C(146)-C(145)-K(3)	83.7(6)

Table A8 (continued)

Angles			
C(147)-C(146)-C(145)	118.1(9)	C(154)-C(151)-C(152)	120.5(9)
C(147)-C(146)-K(3)	95.1(6)	C(151)-C(153)-C(150)#1	120.3(10)
C(145)-C(146)-K(3)	72.5(5)	C(148)#1-C(154)-C(151)	121.1(10)
C(146)-C(147)-C(141)	123.5(9)	O(31)-C(155)-C(160)#2	110.4(8)
C(154)#1-C(148)-C(149)	120.1(10)	O(31)-C(156)-C(157)	107.7(8)
C(148)-C(149)-C(150)	120.8(10)	O(32)-C(157)-C(156)	109.0(8)
C(148)-C(149)-K(3)	91.6(6)	O(32)-C(158)-C(159)	110.4(8)
C(150)-C(149)-K(3)	88.0(6)	C(158)-C(159)-O(33)	108.3(8)
C(149)-C(150)-C(153)#1	119.0(10)	O(33)-C(160)-C(155)#2	110.1(9)
C(153)-C(151)-C(154)	118.6(9)	C(167)-C(161)-C(163)	120.9(10)
C(153)-C(151)-C(152)	120.9(9)	C(167)-C(161)-C(162)	120.0(9)
C(163)-C(161)-C(162)	119.0(9)	C(166)-C(165)-K(4)	85.7(7)
C(164)-C(163)-C(161)	119.4(11)	C(167)-C(166)-C(165)	122.8(11)
C(163)-C(164)-C(165)	122.4(12)	C(161)-C(167)-C(166)	118.5(11)
C(164)-C(165)-C(166)	116.0(11)	O(34)#3-C(168)-C(169)	111.0(7)
C(164)-C(165)-K(4)	95.5(7)	O(36)-C(169)-C(168)	110.3(8)
O(36)-C(170)-C(171)	108.6(8)	O(35)-C(172)-C(173)	107.1(8)
O(35)-C(171)-C(170)	110.1(8)	O(34)-C(173)-C(172)	108.1(7)
C(176)-C(174)-C(180)	119.5(9)	C(176)-C(174)-C(175)	121.0(9)

Table A8 (continued)

Angles			
C(180)-C(174)-C(175)	119.5(9)	N(3)-Hf(1)-N(1)	97.2(3)
C(174)-C(176)-C(177)	120.5(9)	N(2)-Hf(1)-N(1)	97.9(3)
C(178)-C(177)-C(176)	120.0(10)	N(3)-Hf(1)-Si(1)	96.8(2)
C(178)-C(177)-K(5)	75.4(6)	N(2)-Hf(1)-Si(1)	96.1(2)
C(176)-C(177)-K(5)	99.9(6)	N(1)-Hf(1)-Si(1)	155.7(2)
C(179)-C(178)-C(177)	118.5(10)	N(3)-Hf(1)-Si(4)	126.3(2)
C(179)-C(178)-K(5)	94.4(6)	N(2)-Hf(1)-Si(4)	123.5(2)
C(177)-C(178)-K(5)	81.4(6)	N(1)-Hf(1)-Si(4)	84.9(2)
C(178)-C(179)-C(180)	121.6(9)	Si(1)-Hf(1)-Si(4)	70.78(7)
C(179)-C(180)-C(174)	119.8(9)	N(5)-Hf(2)-N(6)	103.0(3)
N(3)-Hf(1)-N(2)	109.4(3)	N(5)-Hf(2)-N(4)	103.0(3)
N(6)-Hf(2)-N(4)	94.6(3)	N(6)-Hf(2)-Si(10)	133.9(2)
N(5)-Hf(2)-Si(7)	98.9(2)	N(4)-Hf(2)-Si(10)	84.9(2)
N(6)-Hf(2)-Si(7)	95.1(2)	Si(7)-Hf(2)-Si(10)	70.60(7)
N(4)-Hf(2)-Si(7)	153.3(2)	N(8)-Hf(3)-N(7)	109.8(3)
N(5)-Hf(2)-Si(10)	122.1(2)	N(8)-Hf(3)-N(9)	98.0(3)
N(7)-Hf(3)-N(9)	97.4(3)	N(9)-Hf(3)-Si(16)	155.9(2)
N(8)-Hf(3)-Si(16)	94.98(19)	N(8)-Hf(3)-Si(13)	125.34(19)
N(7)-Hf(3)-Si(16)	97.2(2)	N(7)-Hf(3)-Si(13)	123.9(2)

Table A8 (continued)

Angles			
N(9)-Hf(3)-Si(13)	85.3(2)	Si(22)-Hf(4)-Si(19)	70.12(7)
Si(16)-Hf(3)-Si(13)	70.61(7)	O(8)-K(1)-O(6)	120.19(19)
N(10)-Hf(4)-N(12)	106.7(4)	O(8)-K(1)-O(5)	138.3(2)
N(10)-Hf(4)-N(11)	101.8(3)	O(6)-K(1)-O(5)	58.45(18)
N(12)-Hf(4)-N(11)	96.3(4)	O(8)-K(1)-O(3)	77.53(18)
N(10)-Hf(4)-Si(22)	106.7(2)	O(6)-K(1)-O(3)	160.0(2)
N(12)-Hf(4)-Si(22)	144.1(3)	O(5)-K(1)-O(3)	115.8(2)
N(11)-Hf(4)-Si(22)	89.5(2)	O(8)-K(1)-O(4)	128.74(18)
N(10)-Hf(4)-Si(19)	105.6(2)	O(6)-K(1)-O(4)	108.67(19)
N(12)-Hf(4)-Si(19)	88.5(2)	O(5)-K(1)-O(4)	59.3(2)
N(11)-Hf(4)-Si(19)	149.5(2)	O(3)-K(1)-O(4)	58.26(19)
O(8)-K(1)-O(1)	102.17(16)	O(8)-K(1)-O(2)	72.15(17)
O(6)-K(1)-O(1)	58.37(18)	O(6)-K(1)-O(2)	114.88(19)
O(5)-K(1)-O(1)	107.8(2)	O(5)-K(1)-O(2)	149.4(2)
O(3)-K(1)-O(1)	111.47(19)	O(3)-K(1)-O(2)	58.91(19)
O(4)-K(1)-O(1)	116.53(17)	O(4)-K(1)-O(2)	101.64(19)
O(1)-K(1)-O(2)	56.57(18)	O(5)-K(1)-O(7)	83.8(2)
O(8)-K(1)-O(7)	58.72(15)	O(3)-K(1)-O(7)	79.92(17)
O(6)-K(1)-O(7)	116.40(18)	O(4)-K(1)-O(7)	87.23(17)

Table A8 (continued)

Angles			
O(1)-K(1)-O(7)	156.24(16)	O(14)-K(2)-O(15)	58.6(3)
O(2)-K(1)-O(7)	121.39(17)	O(16)-K(2)-O(18)	118.3(3)
O(16)-K(2)-O(20)	123.4(2)	O(20)-K(2)-O(18)	79.00(19)
O(16)-K(2)-O(17)	58.7(3)	O(17)-K(2)-O(18)	59.8(3)
O(20)-K(2)-O(17)	106.8(2)	O(14)-K(2)-O(18)	116.1(3)
O(16)-K(2)-O(14)	118.3(3)	O(15)-K(2)-O(18)	153.8(2)
O(20)-K(2)-O(14)	93.3(2)	O(16)-K(2)-O(13)	151.5(3)
O(17)-K(2)-O(14)	157.4(3)	O(20)-K(2)-O(13)	84.7(2)
O(16)-K(2)-O(15)	59.7(3)	O(17)-K(2)-O(13)	112.5(4)
O(20)-K(2)-O(15)	125.3(2)	O(14)-K(2)-O(13)	58.2(4)
O(17)-K(2)-O(15)	114.0(3)	O(15)-K(2)-O(13)	110.0(3)
O(18)-K(2)-O(13)	57.9(3)	O(15)-K(2)-O(19)	75.01(18)
O(16)-K(2)-O(19)	77.0(2)	O(18)-K(2)-O(19)	131.17(19)
O(20)-K(2)-O(19)	56.91(16)	O(13)-K(2)-O(19)	128.5(3)
O(17)-K(2)-O(19)	110.9(2)	O(25)-K(3)-O(26)	61.5(2)
O(14)-K(2)-O(19)	88.5(3)	O(25)-K(3)-O(28)	179.8(3)
O(26)-K(3)-O(28)	118.7(2)	O(28)-K(3)-O(27)	60.4(2)
O(25)-K(3)-O(27)	119.8(2)	O(25)-K(3)-O(29)	119.4(2)
O(26)-K(3)-O(27)	60.3(2)	O(26)-K(3)-O(29)	174.8(2)

Table A8 (continued)

Angles			
O(28)-K(3)-O(29)	60.4(2)	O(29)-K(3)-C(149)	77.7(2)
O(27)-K(3)-O(29)	120.0(2)	O(30)-K(3)-C(149)	74.1(2)
O(25)-K(3)-O(30)	60.6(2)	O(25)-K(3)-C(145)	77.5(3)
O(26)-K(3)-O(30)	119.9(2)	O(26)-K(3)-C(145)	79.6(2)
O(28)-K(3)-O(30)	119.2(2)	O(28)-K(3)-C(145)	102.6(3)
O(27)-K(3)-O(30)	179.0(2)	O(27)-K(3)-C(145)	78.6(2)
O(29)-K(3)-O(30)	59.7(2)	O(29)-K(3)-C(145)	105.6(2)
O(25)-K(3)-C(149)	96.0(3)	O(30)-K(3)-C(145)	102.4(2)
O(26)-K(3)-C(149)	97.2(2)	C(149)-K(3)-C(145)	173.4(3)
O(28)-K(3)-C(149)	84.0(3)	O(25)-K(3)-C(146)	101.1(2)
O(27)-K(3)-C(149)	104.9(3)	O(26)-K(3)-C(146)	93.7(2)
O(28)-K(3)-C(146)	79.0(2)	C(145)-K(3)-C(146)	23.8(3)
O(27)-K(3)-C(146)	69.2(2)	O(33)-K(4)-O(33)#2	179.999(2)
O(29)-K(3)-C(146)	91.1(2)	O(33)-K(4)-O(32)	61.1(2)
O(30)-K(3)-C(146)	111.7(2)	O(33)#2-K(4)-O(32)	118.9(2)
C(149)-K(3)-C(146)	162.7(3)	O(33)-K(4)-O(32)#2	118.9(2)
O(33)#2-K(4)-O(32)#2	61.1(2)	O(33)#2-K(4)-O(31)#2	119.2(2)
O(32)-K(4)-O(32)#2	180.00(14)	O(32)-K(4)-O(31)#2	120.38(19)
O(33)-K(4)-O(31)#2	60.8(2)	O(32)#2-K(4)-O(31)#2	59.62(19)

Table A8 (continued)

Angles			
O(33)-K(4)-O(31)	119.2(2)	O(33)-K(4)-C(165)	101.7(2)
O(33)#2-K(4)-O(31)	60.8(2)	O(33)#2-K(4)-C(165)	78.3(2)
O(32)-K(4)-O(31)	59.62(19)	O(32)-K(4)-C(165)	80.4(3)
O(32)#2-K(4)-O(31)	120.38(19)	O(32)#2-K(4)-C(165)	99.6(3)
O(31)#2-K(4)-O(31)	179.998(1)	O(31)#2-K(4)-C(165)	99.1(2)
O(33)-K(4)-C(165)#2	78.3(2)	O(31)-K(4)-C(165)	80.9(2)
O(33)#2-K(4)-C(165)#2	101.7(2)	C(165)#2-K(4)-C(165)	180.00(16)
O(32)-K(4)-C(165)#2	99.6(3)	O(36)-K(5)-O(36)#3	180.0(2)
O(32)#2-K(4)-C(165)#2	80.4(3)	O(36)-K(5)-O(34)#3	61.33(19)
O(31)#2-K(4)-C(165)#2	80.9(2)	O(36)#3-K(5)-O(34)#3	118.67(19)
O(31)-K(4)-C(165)#2	99.1(2)	O(36)-K(5)-O(34)	118.67(19)
O(36)#3-K(5)-O(34)	61.33(19)	O(34)-K(5)-O(35)#3	120.67(18)
O(34)#3-K(5)-O(34)	179.997(1)	O(36)-K(5)-O(35)	60.84(19)
O(36)-K(5)-O(35)#3	119.16(19)	O(36)#3-K(5)-O(35)	119.16(19)
O(36)#3-K(5)-O(35)#3	60.84(19)	O(34)#3-K(5)-O(35)	120.68(18)
O(34)#3-K(5)-O(35)#3	59.32(18)	O(34)-K(5)-O(35)	59.33(18)
O(35)#3-K(5)-O(35)	180.00(15)	O(34)#3-K(5)-C(178)	78.4(2)
O(36)-K(5)-C(178)	80.5(2)	O(34)-K(5)-C(178)	101.6(2)
O(36)#3-K(5)-C(178)	99.5(2)	O(35)#3-K(5)-C(178)	76.0(2)

Table A8 (continued)

Angles			
O(35)-K(5)-C(178)	104.0(2)	O(34)-K(5)-C(177)#3	93.4(2)
O(36)-K(5)-C(178)#3	99.5(2)	O(35)#3-K(5)-C(177)#3	81.1(2)
O(36)#3-K(5)-C(178)#3	80.5(2)	O(35)-K(5)-C(177)#3	98.9(2)
O(34)#3-K(5)-C(178)#3	101.6(2)	C(178)-K(5)-C(177)#3	156.8(2)
O(34)-K(5)-C(178)#3	78.4(2)	C(178)#3-K(5)-C(177)#3	23.2(2)
O(35)#3-K(5)-C(178)#3	104.0(2)	O(36)-K(5)-C(177)	72.3(2)
O(35)-K(5)-C(178)#3	76.0(2)	O(36)#3-K(5)-C(177)	107.7(2)
C(178)-K(5)-C(178)#3	179.999(1)	O(34)#3-K(5)-C(177)	93.4(2)
O(36)-K(5)-C(177)#3	107.7(2)	O(34)-K(5)-C(177)	86.6(2)
O(36)#3-K(5)-C(177)#3	72.3(2)	O(35)#3-K(5)-C(177)	98.9(2)
O(34)#3-K(5)-C(177)#3	86.6(2)	O(35)-K(5)-C(177)	81.1(2)
C(178)-K(5)-C(177)	23.2(2)	C(1)-N(1)-Hf(1)	112.5(6)
C(178)#3-K(5)-C(177)	156.8(2)	C(5)-N(2)-C(6)	111.2(8)
C(177)#3-K(5)-C(177)	180.000(2)	C(5)-N(2)-Hf(1)	129.0(7)
C(2)-N(1)-C(1)	106.5(8)	C(6)-N(2)-Hf(1)	119.7(6)
C(2)-N(1)-Hf(1)	141.0(6)	C(4)-N(3)-C(3)	113.0(8)
C(4)-N(3)-Hf(1)	133.0(6)	C(21)-N(4)-Hf(2)	140.1(6)
C(3)-N(3)-Hf(1)	113.3(6)	C(22)-N(4)-Hf(2)	112.9(5)
C(21)-N(4)-C(22)	106.9(7)	C(23)-N(5)-C(24)	114.0(7)

Table A8 (continued)

Angles			
C(23)-N(5)-Hf(2)	111.4(5)	C(46)-N(9)-C(45)	108.3(7)
C(24)-N(5)-Hf(2)	133.9(6)	C(46)-N(9)-Hf(3)	140.8(6)
C(25)-N(6)-C(26)	112.7(7)	C(45)-N(9)-Hf(3)	110.8(6)
C(25)-N(6)-Hf(2)	127.0(7)	C(61)-N(10)-C(62)	112.5(7)
C(26)-N(6)-Hf(2)	120.2(5)	C(61)-N(10)-Hf(4)	122.1(6)
C(41)-N(7)-C(42)	110.9(7)	C(62)-N(10)-Hf(4)	125.2(6)
C(41)-N(7)-Hf(3)	117.6(6)	C(64)-N(11)-C(63)	107.2(8)
C(42)-N(7)-Hf(3)	131.5(6)	C(64)-N(11)-Hf(4)	128.7(6)
C(44)-N(8)-C(43)	109.1(7)	C(63)-N(11)-Hf(4)	123.5(8)
C(44)-N(8)-Hf(3)	128.8(6)	C(65)-N(12)-C(66)	108.0(11)
C(43)-N(8)-Hf(3)	121.8(5)	C(65)-N(12)-Hf(4)	132.4(10)
C(66)-N(12)-Hf(4)	119.6(8)	C(82)-O(2)-K(1)	119.5(5)
C(92)-O(1)-C(81)	112.0(7)	C(83)-O(2)-K(1)	115.8(5)
C(92)-O(1)-K(1)	110.0(5)	C(85)-O(3)-C(84)	115.9(8)
C(81)-O(1)-K(1)	114.6(5)	C(85)-O(3)-K(1)	114.2(6)
C(82)-O(2)-C(83)	112.8(7)	C(84)-O(3)-K(1)	112.8(5)
C(86)-O(4)-C(87)	109.1(7)	C(89)-O(5)-C(88)	114.3(11)
C(86)-O(4)-K(1)	116.9(5)	C(89)-O(5)-K(1)	115.3(6)
C(87)-O(4)-K(1)	113.4(5)	C(88)-O(5)-K(1)	115.6(6)

Table A8 (continued)

Angles			
C(91)-O(6)-C(90)	112.6(10)	C(101)-O(11)-C(100)	113.7(7)
C(91)-O(6)-K(1)	118.7(6)	C(103)-O(12)-C(102)	112.5(7)
C(90)-O(6)-K(1)	117.5(6)	C(105)-O(13)-C(116)	118.3(12)
C(104)-O(7)-C(93)	112.8(7)	C(105)-O(13)-K(2)	109.3(10)
C(104)-O(7)-K(1)	115.4(5)	C(116)-O(13)-K(2)	112.7(8)
C(93)-O(7)-K(1)	102.4(5)	C(107)-O(14)-C(106)	106.0(12)
C(94)-O(8)-C(95)	114.0(6)	C(107)-O(14)-K(2)	121.4(9)
C(94)-O(8)-K(1)	125.8(4)	C(106)-O(14)-K(2)	120.7(11)
C(95)-O(8)-K(1)	116.3(5)	C(109)-O(15)-C(108)	113.2(11)
C(97)-O(9)-C(96)	109.6(6)	C(109)-O(15)-K(2)	111.0(8)
C(98)-O(10)-C(99)	114.9(7)	C(108)-O(15)-K(2)	109.3(7)
C(110)-O(16)-C(111)	114.2(10)	C(112)-O(17)-K(2)	111.8(8)
C(110)-O(16)-K(2)	116.7(8)	C(115)-O(18)-C(114)	113.4(12)
C(111)-O(16)-K(2)	118.1(8)	C(115)-O(18)-K(2)	119.0(9)
C(113)-O(17)-C(112)	112.0(12)	C(114)-O(18)-K(2)	112.7(8)
C(113)-O(17)-K(2)	109.6(8)	C(117)-O(19)-C(128)	112.3(7)
C(117)-O(19)-K(2)	96.7(5)	C(118)-O(20)-K(2)	123.6(5)
C(128)-O(19)-K(2)	126.0(6)	C(119)-O(20)-K(2)	123.6(5)
C(118)-O(20)-C(119)	112.6(7)	C(120)-O(21)-C(121)	112.1(7)

Table A8 (continued)

Angles			
C(122)-O(22)-C(123)	110.8(8)	C(132)-O(27)-K(3)	113.5(6)
C(124)-O(23)-C(125)	104.4(12)	C(135)-O(28)-C(134)	111.5(8)
C(127)-O(24)-C(126)	114.3(10)	C(135)-O(28)-K(3)	114.7(6)
C(129)-O(25)-C(140)	111.8(8)	C(134)-O(28)-K(3)	114.2(5)
C(129)-O(25)-K(3)	115.6(6)	C(137)-O(29)-C(136)	114.2(8)
C(140)-O(25)-K(3)	116.6(6)	C(137)-O(29)-K(3)	116.7(6)
C(131)-O(26)-C(130)	112.4(8)	C(136)-O(29)-K(3)	112.5(6)
C(131)-O(26)-K(3)	117.3(6)	C(139)-O(30)-C(138)	112.3(8)
C(130)-O(26)-K(3)	114.1(6)	C(139)-O(30)-K(3)	113.8(6)
C(133)-O(27)-C(132)	115.0(8)	C(138)-O(30)-K(3)	114.3(5)
C(133)-O(27)-K(3)	116.3(6)	C(156)-O(31)-C(155)	112.1(8)
C(156)-O(31)-K(4)	115.6(6)	C(160)-O(33)-C(159)	110.3(8)
C(155)-O(31)-K(4)	115.7(6)	C(160)-O(33)-K(4)	115.4(6)
C(158)-O(32)-C(157)	113.8(8)	C(159)-O(33)-K(4)	113.3(5)
C(158)-O(32)-K(4)	112.8(6)	C(168)#3-O(34)-C(173)	112.0(7)
C(157)-O(32)-K(4)	115.0(5)	C(168)#3-O(34)-K(5)	113.3(5)
C(173)-O(34)-K(5)	117.1(5)	C(172)-O(35)-K(5)	115.8(5)
C(171)-O(35)-C(172)	111.7(7)	C(169)-O(36)-C(170)	111.7(7)
C(171)-O(35)-K(5)	113.0(5)	C(169)-O(36)-K(5)	114.7(5)

Table A8 (continued)

Angles			
C(170)-O(36)-K(5)	115.8(5)	C(10)-Si(2)-Si(1)	114.6(3)
C(7)-Si(1)-Si(2)	102.0(2)	C(11)-Si(2)-Si(1)	115.1(4)
C(7)-Si(1)-Si(3)	101.8(3)	C(14)-Si(3)-C(13)	106.2(4)
Si(2)-Si(1)-Si(3)	105.39(12)	C(14)-Si(3)-C(12)	105.2(5)
C(7)-Si(1)-Hf(1)	112.9(2)	C(13)-Si(3)-C(12)	107.5(5)
Si(2)-Si(1)-Hf(1)	117.60(11)	C(14)-Si(3)-Si(1)	111.7(4)
Si(3)-Si(1)-Hf(1)	115.22(9)	C(13)-Si(3)-Si(1)	112.5(3)
C(9)-Si(2)-C(10)	106.5(5)	C(12)-Si(3)-Si(1)	113.2(4)
C(9)-Si(2)-C(11)	105.4(5)	C(8)-Si(4)-Si(5)	100.0(3)
C(10)-Si(2)-C(11)	106.5(5)	C(8)-Si(4)-Si(6)	101.2(3)
C(9)-Si(2)-Si(1)	108.0(3)	Si(5)-Si(4)-Si(6)	104.67(11)
C(8)-Si(4)-Hf(1)	112.8(2)	C(16)-Si(5)-C(17)	106.3(4)
Si(5)-Si(4)-Hf(1)	116.75(9)	C(15)-Si(5)-Si(4)	110.1(3)
Si(6)-Si(4)-Hf(1)	118.69(10)	C(16)-Si(5)-Si(4)	115.4(3)
C(15)-Si(5)-C(16)	106.2(4)	C(17)-Si(5)-Si(4)	112.9(3)
C(15)-Si(5)-C(17)	105.2(4)	C(20)-Si(6)-C(19)	105.3(5)
C(20)-Si(6)-C(18)	104.9(5)	C(19)-Si(6)-Si(4)	110.7(4)
C(19)-Si(6)-C(18)	106.6(5)	C(18)-Si(6)-Si(4)	117.1(3)
C(20)-Si(6)-Si(4)	111.4(3)	C(27)-Si(7)-Si(8)	104.6(3)

Table A8 (continued)

Angles			
C(27)-Si(7)-Si(9)	100.0(3)	C(32)-Si(9)-C(34)	108.7(5)
Si(8)-Si(7)-Si(9)	103.29(11)	C(32)-Si(9)-C(33)	105.1(5)
C(27)-Si(7)-Hf(2)	114.1(2)	C(34)-Si(9)-C(33)	105.7(4)
Si(8)-Si(7)-Hf(2)	113.19(9)	C(32)-Si(9)-Si(7)	116.2(3)
Si(9)-Si(7)-Hf(2)	119.74(10)	C(34)-Si(9)-Si(7)	109.1(3)
C(30)-Si(8)-C(29)	108.5(4)	C(33)-Si(9)-Si(7)	111.6(3)
C(30)-Si(8)-C(31)	106.0(4)	C(28)-Si(10)-Si(11)	97.8(2)
C(29)-Si(8)-C(31)	104.6(4)	C(28)-Si(10)-Si(12)	103.2(3)
C(30)-Si(8)-Si(7)	111.3(3)	Si(11)-Si(10)-Si(12)	104.89(11)
C(29)-Si(8)-Si(7)	110.2(3)	C(28)-Si(10)-Hf(2)	112.1(3)
C(31)-Si(8)-Si(7)	115.8(3)	Si(11)-Si(10)-Hf(2)	124.73(10)
Si(12)-Si(10)-Hf(2)	111.57(10)	C(35)-Si(11)-Si(10)	108.7(3)
C(37)-Si(11)-C(35)	105.0(4)	C(36)-Si(11)-Si(10)	119.1(4)
C(37)-Si(11)-C(36)	106.6(5)	C(40)-Si(12)-C(39)	108.6(6)
C(35)-Si(11)-C(36)	104.7(5)	C(40)-Si(12)-C(38)	105.3(5)
C(37)-Si(11)-Si(10)	111.7(3)	C(39)-Si(12)-C(38)	106.8(6)
C(40)-Si(12)-Si(10)	111.8(4)	C(47)-Si(13)-Si(14)	99.1(3)
C(39)-Si(12)-Si(10)	109.8(4)	C(47)-Si(13)-Si(15)	101.9(2)
C(38)-Si(12)-Si(10)	114.3(4)	Si(14)-Si(13)-Si(15)	106.00(10)

Table A8 (continued)

Angles			
C(47)-Si(13)-Hf(3)	113.2(2)	C(52)-Si(15)-C(54)	104.4(5)
Si(14)-Si(13)-Hf(3)	117.95(10)	C(53)-Si(15)-Si(13)	110.1(3)
Si(15)-Si(13)-Hf(3)	116.19(9)	C(52)-Si(15)-Si(13)	116.3(3)
C(50)-Si(14)-C(49)	104.8(4)	C(54)-Si(15)-Si(13)	112.4(3)
C(50)-Si(14)-C(51)	105.3(4)	C(48)-Si(16)-Si(17)	103.0(2)
C(49)-Si(14)-C(51)	105.7(4)	C(48)-Si(16)-Si(18)	101.2(3)
C(50)-Si(14)-Si(13)	116.2(3)	Si(17)-Si(16)-Si(18)	105.72(11)
C(49)-Si(14)-Si(13)	109.8(3)	C(48)-Si(16)-Hf(3)	111.9(2)
C(51)-Si(14)-Si(13)	114.1(3)	Si(17)-Si(16)-Hf(3)	118.70(10)
C(53)-Si(15)-C(52)	106.4(4)	Si(18)-Si(16)-Hf(3)	114.33(9)
C(53)-Si(15)-C(54)	106.5(4)	C(57)-Si(17)-C(55)	107.3(4)
C(57)-Si(17)-C(56)	104.4(4)	C(60)-Si(18)-C(58)	108.7(4)
C(55)-Si(17)-C(56)	108.5(5)	C(60)-Si(18)-C(59)	104.7(4)
C(57)-Si(17)-Si(16)	115.0(3)	C(58)-Si(18)-C(59)	105.6(4)
C(55)-Si(17)-Si(16)	107.7(3)	C(60)-Si(18)-Si(16)	113.5(3)
C(56)-Si(17)-Si(16)	113.6(3)	C(58)-Si(18)-Si(16)	111.7(3)
C(59)-Si(18)-Si(16)	112.1(3)	Si(21)-Si(19)-Si(20)	102.23(12)
C(68)-Si(19)-Si(21)	103.1(3)	C(68)-Si(19)-Hf(4)	112.1(3)
C(68)-Si(19)-Si(20)	99.8(3)	Si(21)-Si(19)-Hf(4)	113.86(11)

Table A8 (continued)

Angles			
Si(20)-Si(19)-Hf(4)	123.16(11)	C(67)-Si(22)-Hf(4)	113.6(3)
C(70)-Si(20)-C(71)	106.6(5)	Si(24)-Si(22)-Hf(4)	122.33(12)
C(70)-Si(20)-C(69)	106.9(5)	Si(23)-Si(22)-Hf(4)	111.85(10)
C(71)-Si(20)-C(69)	104.5(4)	C(75)-Si(23)-C(76)	105.8(5)
C(70)-Si(20)-Si(19)	114.4(3)	C(75)-Si(23)-C(77)	104.8(5)
C(71)-Si(20)-Si(19)	115.6(3)	C(76)-Si(23)-C(77)	106.7(5)
C(69)-Si(20)-Si(19)	108.0(3)	C(75)-Si(23)-Si(22)	111.3(4)
C(74)-Si(21)-C(73)	102.6(5)	C(76)-Si(23)-Si(22)	113.2(3)
C(74)-Si(21)-C(72)	107.1(5)	C(77)-Si(23)-Si(22)	114.3(3)
C(73)-Si(21)-C(72)	109.4(5)	C(80)-Si(24)-C(78)	106.0(6)
C(74)-Si(21)-Si(19)	112.3(4)	C(80)-Si(24)-C(79)	105.0(6)
C(73)-Si(21)-Si(19)	113.1(4)	C(78)-Si(24)-C(79)	105.1(6)
C(72)-Si(21)-Si(19)	111.8(3)	C(80)-Si(24)-Si(22)	111.1(4)
C(67)-Si(22)-Si(24)	99.6(3)	C(78)-Si(24)-Si(22)	117.5(3)
C(67)-Si(22)-Si(23)	102.7(3)	C(79)-Si(24)-Si(22)	111.1(4)
Si(24)-Si(22)-Si(23)	104.39(11)		

Table A9 Anisotropic displacement parameters ($Å^2 \times 10^3$) in **10**. The anisotropic displacement factor exponent takes the form: $-2\pi^2[h^2a^{*2}U^{11} + ... + 2hka^*b^*U^{12}]$

	U^{11}	U^{22}	U^{33}	U^{23}	U^{13}	U^{12}
C(1)	121	117	32	16	20	72
C(2)	61	79	57	19	30	45
C(3)	88	44	85	14	-27	-7
C(4)	72	73	86	33	-34	12
C(5)	68	82	87	34	42	5
C(6)	71	44	57	25	0	18
C(7)	38	47	28	18	12	22
C(8)	42	52	31	17	8	32
C(9)	31	51	129	6	2	-5
C(10)	44	91	63	35	-4	25
C(11)	58	75	76	32	39	36
C(12)	70	35	78	16	11	28
C(13)	40	59	49	1	5	1
C(14)	65	83	28	1	6	16
C(15)	34	52	47	9	-1	-5
C(16)	49	39	46	-3	2	11

Table A9 (continued)

	U^{11}	U^{22}	U^{33}	U^{23}	U^{13}	U^{12}
C(17)	54	43	43	21	-12	4
C(18)	32	46	93	3	9	24
C(19)	57	62	124	54	22	1
C(20)	45	45	59	-3	-19	2
C(21)	95	66	57	30	19	57
C(22)	99	76	26	21	15	42
C(23)	39	39	52	8	2	-7
C(24)	99	30	36	-5	18	15
C(25)	77	59	85	42	33	-1
C(26)	40	62	65	23	19	14
C(27)	38	49	27	2	0	24
C(28)	36	43	27	12	-5	14
C(29)	36	35	46	14	3	2
C(30)	54	31	28	2	-2	20
C(31)	49	49	43	18	-16	9
C(32)	36	46	87	8	5	15
C(33)	71	37	48	14	-35	-2
C(34)	52	33	66	20	-2	-10
C(35)	32	35	70	13	4	0

Table A9 (continued)

	U^{11}	U^{22}	U^{33}	U^{23}	U^{13}	U^{12}
C(36)	68	60	71	25	-29	16
C(37)	41	58	56	-1	11	15
C(38)	80	33	101	16	-12	24
C(39)	65	60	158	27	58	-9
C(40)	95	42	81	-18	-32	28
C(41)	73	39	117	13	-31	4
C(42)	66	59	84	26	-34	4
C(43)	49	50	48	22	10	20
C(44)	48	61	77	36	25	5
C(45)	78	82	32	14	21	35
C(46)	50	51	59	1	16	26
C(47)	33	37	26	6	9	20
C(48)	31	29	31	16	8	16
C(49)	33	31	66	5	15	3
C(50)	58	38	44	-4	15	12
C(51)	54	41	62	24	4	15
C(52)	28	52	89	4	6	17
C(53)	44	39	58	15	5	-5
C(54)	39	66	46	5	-5	1

Table A9 (continued)

	U^{11}	U^{22}	U^{33}	U^{23}	U^{13}	U^{12}
C(55)	31	47	77	3	3	-7
C(56)	43	87	66	41	5	29
C(57)	45	45	51	20	21	22
C(58)	35	52	58	10	9	-12
C(59)	64	51	34	4	6	16
C(60)	72	32	50	14	12	27
C(61)	36	81	68	-14	-3	-4
C(62)	73	86	76	-55	9	-4
C(63)	128	181	115	111	68	75
C(64)	52	85	59	17	25	24
C(65)	86	225	229	199	19	58
C(66)	222	50	107	26	-12	-2
C(67)	56	64	25	12	2	39
C(68)	60	60	43	24	16	34
C(69)	56	45	70	6	8	-7
C(70)	39	102	53	34	-1	18
C(71)	57	54	44	7	17	32
C(72)	72	42	80	25	-11	8
C(73)	45	97	57	-12	12	-14

Table A9 (continued)

	U^{11}	U^{22}	U^{33}	U^{23}	U^{13}	U^{12}
C(74)	71	92	24	-5	-1	34
C(75)	33	63	80	11	5	1
C(76)	71	52	45	13	-16	10
C(77)	53	54	53	-11	11	6
C(78)	38	33	167	-4	1	17
C(79)	58	46	136	23	6	3
C(80)	74	60	84	-12	-45	22
C(81)	35	70	48	28	-2	3
C(82)	35	66	44	-1	-2	14
C(83)	50	80	66	-13	16	34
C(84)	61	74	47	2	19	25
C(85)	60	44	63	15	-9	13
C(86)	55	50	54	6	-7	8
C(87)	49	48	80	24	15	0
C(88)	78	96	60	33	30	28
C(89)	134	157	183	-129	135	-67
C(90)	106	78	155	-52	100	-36
C(91)	78	62	42	-12	-12	13
C(92)	45	36	64	-6	1	3

Table A9 (continued)

	U^{11}	U^{22}	U^{33}	U^{23}	U^{13}	U^{12}
C(93)	39	49	38	-2	13	2
C(94)	31	42	33	6	-1	-1
C(95)	35	40	49	19	4	4
C(96)	46	45	23	9	10	0
C(97)	54	42	41	2	12	11
C(98)	63	43	59	3	13	22
C(99)	62	49	42	-5	14	-1
C(100)	50	43	74	-7	11	5
C(101)	34	65	69	-11	19	9
C(102)	40	47	65	-10	30	0
C(103)	59	38	52	2	22	9
C(104)	64	47	47	12	25	30
C(105)	101	259	144	-124	-14	99
C(106)	124	323	120	-89	6	137
C(107)	44	214	95	70	18	-1
C(108)	47	224	101	120	-22	-50
C(109)	144	42	159	47	-86	-15
C(110)	151	30	118	-14	-91	17
C(111)	197	143	43	-7	3	128

Table A9 (continued)

	U^{11}	U^{22}	U^{33}	U^{23}	U^{13}	U^{12}
C(112)	133	265	48	-6	26	140
C(113)	26	399	116	92	25	11
C(114)	92	237	96	117	-48	-83
C(115)	152	51	180	51	-123	-43
C(116)	121	54	194	-50	-100	31
C(117)	50	63	37	11	2	-2
C(118)	52	49	37	9	-1	5
C(119)	42	45	49	0	-3	5
C(120)	44	49	40	-2	-8	7
C(121)	38	82	64	3	2	26
C(122)	49	102	75	-2	11	42
C(123)	68	148	49	-1	17	51
C(124)	116	72	71	18	18	14
C(125)	132	72	226	-84	114	-31
C(126)	101	75	96	-42	-2	8
C(127)	137	61	63	1	-18	49
C(128)	101	85	45	3	-8	46
C(129)	94	56	77	16	-1	39
C(130)	99	55	65	7	18	53

Table A9 (continued)

	U^{11}	U^{22}	U^{33}	U^{23}	U^{13}	U^{12}
C(131)	38	102	57	2	6	23
C(132)	33	95	53	14	-5	7
C(133)	101	48	48	7	-2	-12
C(134)	100	26	61	15	22	-2
C(135)	105	56	63	28	-10	34
C(136)	90	59	72	5	-13	53
C(137)	40	93	59	15	3	31
C(138)	37	75	63	14	-14	10
C(139)	93	33	39	5	-5	-12
C(140)	62	49	70	29	6	-4
C(141)	33	28	39	2	12	11
C(142)	32	57	86	28	10	19
C(143)	55	34	36	10	17	15
C(144)	77	63	28	7	7	46
C(145)	45	121	24	-15	-4	40
C(146)	43	77	42	-4	5	11
C(147)	40	31	49	-1	15	0
C(148)	36	77	37	-7	3	1
C(149)	54	113	31	3	-1	32

Table A9 (continued)

	U^{11}	U^{22}	U^{33}	U^{23}	U^{13}	U^{12}
C(150)	87	73	35	9	10	37
C(151)	38	35	69	6	10	10
C(152)	32	76	218	24	14	25
C(153)	71	40	56	4	28	10
C(154)	56	33	58	2	24	5
C(155)	56	90	56	-7	3	49
C(156)	45	72	57	5	16	-3
C(157)	50	48	73	18	-6	-20
C(158)	103	34	65	13	-1	20
C(159)	96	39	58	26	-3	30
C(160)	53	65	72	11	-3	29
C(161)	46	35	41	-1	19	7
C(162)	44	84	76	16	2	19
C(163)	46	48	55	1	2	3
C(164)	68	78	56	-19	9	17
C(165)	81	98	56	-17	-9	60
C(166)	149	64	37	12	15	56
C(167)	82	44	58	20	27	32
C(168)	57	78	44	26	11	47

Table A9 (continued)

	U^{11}	U^{22}	U^{33}	U^{23}	U^{13}	U^{12}
C(169)	56	74	56	22	-2	33
C(170)	77	35	52	14	1	13
C(171)	91	28	55	3	-3	7
C(172)	36	49	75	16	-3	-12
C(173)	31	71	61	20	13	-9
C(174)	33	48	51	3	8	1
C(175)	37	103	98	23	-6	0
C(176)	68	39	40	6	14	6
C(177)	122	53	49	23	23	40
C(178)	66	63	52	6	13	21
C(179)	43	49	59	4	12	2
C(180)	34	47	51	4	8	8
Hf(1)	36	34	21	8	2	9
Hf(2)	35	24	25	7	5	5
Hf(3)	26	31	22	5	0	4
Hf(4)	32	34	24	4	0	6
K(1)	38	43	27	7	6	7
K(2)	36	32	27	3	3	3
K(3)	37	27	45	10	11	13

Table A9 (continued)

	U^{11}	U^{22}	U^{33}	U^{23}	U^{13}	U^{12}
K(4)	32	30	66	13	6	11
K(5)	30	29	56	11	7	11
N(1)	90	67	21	12	9	41
N(2)	60	48	34	25	18	13
N(3)	49	47	32	6	-18	-2
N(4)	63	41	32	16	11	20
N(5)	43	23	38	1	-4	5
N(6)	40	42	47	18	21	3
N(7)	35	45	36	1	-10	1
N(8)	27	41	34	18	6	4
N(9)	40	53	30	2	10	16
N(10)	41	52	30	-2	0	-7
N(11)	39	73	46	21	8	0
N(12)	134	78	38	22	19	65
O(1)	36	42	46	17	2	5
O(2)	39	69	45	9	11	19
O(3)	66	38	47	2	0	18
O(4)	50	49	40	10	-3	3
O(5)	63	62	64	-20	30	-20

Table A9 (continued)

	U^{11}	U^{22}	U^{33}	U^{23}	U^{13}	U^{12}
O(6)	47	46	53	-3	18	3
O(7)	36	34	39	5	8	3
O(8)	29	36	34	12	-2	4
O(9)	49	45	31	15	9	11
O(10)	52	38	54	2	4	7
O(11)	43	44	50	-2	9	3
O(12)	48	43	51	6	20	11
O(13)	121	65	170	-52	-78	59
O(14)	52	215	47	13	14	45
O(15)	61	75	103	58	-36	-19
O(16)	136	52	51	-15	-45	46
O(17)	51	169	58	57	20	36
O(18)	66	76	93	52	-36	-21
O(19)	55	47	37	9	-10	2
O(20)	36	41	39	4	-7	6
O(21)	51	57	45	0	-6	20
O(22)	47	101	76	18	7	32
O(23)	131	72	85	-10	47	-2
O(24)	104	98	71	5	9	51

Table A9 (continued)

	U^{11}	U^{22}	U^{33}	U^{23}	U^{13}	U^{12}
O(25)	93	44	37	14	-2	26
O(26)	67	74	37	9	7	38
O(27)	55	53	39	2	5	-7
O(28)	101	34	43	10	-1	32
O(29)	57	67	55	4	2	27
O(30)	56	57	41	13	1	-5
O(31)	39	56	43	2	7	8
O(32)	70	36	44	10	4	6
O(33)	66	63	36	3	-4	35
O(34)	35	61	34	16	8	17
O(35)	59	32	43	5	-4	0
O(36)	72	38	36	8	5	30
Si(1)	23	30	27	9	3	9
Si(2)	26	45	57	20	10	14
Si(3)	40	37	36	2	7	7
Si(4)	24	33	24	8	3	10
Si(5)	28	34	27	8	-4	1
Si(6)	25	32	52	12	2	5
Si(7)	28	21	30	5	0	8

Table A9 (continued)

	U^{11}	U^{22}	U^{33}	U^{23}	U^{13}	U^{12}
Si(8)	29	26	30	9	-2	6
Si(9)	30	24	51	6	-7	3
Si(10)	28	23	27	6	2	8
Si(11)	30	33	41	8	0	8
Si(12)	41	24	66	5	8	7
Si(13)	21	25	29	7	3	8
Si(14)	26	26	37	5	2	7
Si(15)	22	30	38	9	4	6
Si(16)	18	22	29	9	4	5
Si(17)	21	39	46	19	6	9
Si(18)	33	25	31	4	6	6
Si(19)	38	41	27	11	4	24
Si(20)	40	41	40	13	9	15
Si(21)	35	50	38	1	2	9
Si(22)	33	41	30	1	-1	20
Si(23)	25	41	44	1	-2	7
Si(24)	38	25	68	-7	-11	8

Table A10 Hydrogen coordinates (x 10^4) and isotropic displacement parameters ($Å^2$ x 10^3) in **10**

	x	y	z	U(eq)
H(1A)	215	8669	7271	124
H(1B)	435	8060	7178	124
H(1C)	-704	8143	7235	124
H(2A)	-1672	8435	6855	90
H(2B)	-1155	8657	6558	90
H(2C)	-818	8993	6916	90
H(3A)	2362	9054	7027	114
H(3B)	1855	8977	6671	114
H(3C)	3040	8971	6726	114
H(4A)	3490	8161	6934	114
H(4B)	2597	7645	6955	114
H(4C)	2720	8210	7213	114
H(5A)	-1127	6535	6624	116
H(5B)	-1210	7154	6776	116
H(5C)	-622	6817	6977	116
H(6A)	1097	6630	6795	82

Table A10 (continued)

	x	y	z	U(eq)
H(6B)	1452	6809	6469	82
H(6C)	473	6324	6462	82
H(7A)	1823	8261	5633	41
H(7B)	1552	7693	5374	41
H(8A)	-214	7565	5481	44
H(8B)	118	8173	5408	44
H(9A)	3845	8447	6278	111
H(9B)	3846	8501	5910	111
H(9C)	4791	8330	6075	111
H(10A)	4632	7178	6229	93
H(10B)	3545	6763	6199	93
H(10C)	3771	7324	6462	93
H(11A)	3645	7438	5368	96
H(11B)	3702	6868	5474	96
H(11C)	4662	7376	5553	96
H(12A)	1274	5638	5650	87
H(12B)	1515	5997	6006	87
H(12C)	2293	6107	5737	87

Table A10 (continued)

	x	y	z	U(eq)
H(13A)	-990	6554	5669	78
H(13B)	-633	6362	5984	78
H(13C)	-845	5934	5648	78
H(14A)	632	6054	5105	90
H(14B)	1549	6581	5145	90
H(14C)	390	6655	5123	90
H(15A)	1939	9830	5981	70
H(15B)	1959	9230	5779	70
H(15C)	2076	9344	6162	70
H(16A)	172	9619	6544	69
H(16B)	-814	9669	6338	69
H(16C)	247	10093	6338	69
H(17A)	-103	9819	5629	70
H(17B)	-1003	9282	5584	70
H(17C)	44	9247	5418	70
H(18A)	-2409	8967	5951	84
H(18B)	-2720	8729	6265	84
H(18C)	-3455	8527	5943	84

Table A10 (continued)

	x	y	z	U(eq)
H(19A)	-3383	7396	6080	117
H(19B)	-2403	7545	6331	117
H(19C)	-2429	7111	6002	117
H(20A)	-2076	7498	5370	80
H(20B)	-2274	8095	5344	80
H(20C)	-3177	7638	5431	80
H(21A)	8657	10381	8066	97
H(21B)	7837	10135	8294	97
H(21C)	7634	9952	7913	97
H(22A)	8105	9107	7657	93
H(22B)	9270	9088	7741	93
H(22C)	8999	9617	7628	93
H(23A)	7493	7995	8148	69
H(23B)	7723	8438	8478	69
H(23C)	8058	7857	8451	69
H(24A)	9410	7661	8053	84
H(24B)	10032	8177	7924	84
H(24C)	8886	7900	7782	84

Table A10 (continued)

	x	y	z	U(eq)
H(25A)	11799	10165	8238	107
H(25B)	10689	10084	8062	107
H(25C)	11507	9757	7897	107
H(26A)	11770	8922	8071	80
H(26B)	11334	8793	8400	80
H(26C)	12248	9312	8405	80
H(27A)	9585	9466	9617	44
H(27B)	9939	9998	9461	44
H(28A)	8154	9879	9490	40
H(28B)	7980	9238	9326	40
H(29A)	7904	8109	9038	59
H(29B)	8111	8235	9420	59
H(29C)	8110	7633	9216	59
H(30A)	10007	7357	8893	55
H(30B)	10829	7842	8796	55
H(30C)	9683	7693	8636	55
H(31A)	10107	7767	9605	70
H(31B)	10242	8412	9752	70

Table A10 (continued)

	x	y	z	U(eq)
H(31C)	11120	8190	9554	70
H(32A)	12637	8812	8869	84
H(32B)	12592	8638	9211	84
H(32C)	13476	9131	9153	84
H(33A)	12082	9312	9787	81
H(33B)	11622	9852	9792	81
H(33C)	12820	9883	9762	81
H(34A)	13160	10253	9156	78
H(34B)	12067	10417	9186	78
H(34C)	12326	10064	8857	78
H(35A)	6041	8756	9018	70
H(35B)	6025	8675	8636	70
H(35C)	5060	8826	8817	70
H(36A)	4971	9813	8541	98
H(36B)	5846	9664	8313	98
H(36C)	5965	10275	8522	98
H(37A)	5173	9881	9269	79
H(37B)	6027	10426	9272	79

Table A10 (continued)

	x	y	z	U(eq)
H(37C)	6274	9955	9449	79
H(38A)	7165	10973	8857	104
H(38B)	8008	11265	8651	104
H(38C)	7921	11543	9017	104
H(39A)	10345	11359	8843	144
H(39B)	9884	10864	8549	144
H(39C)	10559	10756	8839	144
H(40A)	9637	10891	9534	113
H(40B)	8520	11025	9562	113
H(40C)	9444	11475	9480	113
H(41A)	6940	3546	8121	118
H(41B)	8089	3541	8235	118
H(41C)	7791	3526	7866	118
H(42A)	7206	4415	7743	106
H(42B)	7223	4891	8051	106
H(42C)	6434	4313	8015	106
H(43A)	9266	6198	8539	68
H(43B)	8316	5687	8450	68

Table A10 (continued)

	x	y	z	U(eq)
H(43C)	8861	5957	8172	68
H(44A)	10530	5869	8049	89
H(44B)	11100	5460	8196	89
H(44C)	11021	6041	8411	89
H(45A)	10783	4640	7763	91
H(45B)	9569	4542	7779	91
H(45C)	10096	4031	7658	91
H(46A)	10820	3599	8025	78
H(46B)	11159	3917	8386	78
H(46C)	11701	4147	8095	78
H(47A)	9667	4235	9522	36
H(47B)	9999	4861	9476	36
H(48A)	8195	4680	9542	33
H(48B)	8012	4146	9257	33
H(49A)	7835	3206	8795	66
H(49B)	7983	3130	9157	66
H(49C)	7975	2624	8867	66
H(50A)	9746	2401	8570	72

Table A10 (continued)

	x	y	z	U(eq)
H(50B)	10698	2876	8535	72
H(50C)	9603	2853	8364	72
H(51A)	9935	2617	9276	74
H(51B)	10048	3223	9490	74
H(51C)	10959	3071	9280	74
H(52A)	12507	3729	8720	84
H(52B)	12454	3617	9078	84
H(52C)	13395	4050	8989	84
H(53A)	13226	5166	8887	72
H(53B)	12169	5372	8895	72
H(53C)	12357	4911	8602	72
H(54A)	13060	4880	9542	79
H(54B)	12057	4496	9635	79
H(54C)	12024	5104	9581	79
H(55A)	5955	3952	8969	83
H(55B)	6029	4056	8611	83
H(55C)	5050	4154	8802	83
H(56A)	5297	5360	8703	89

Table A10 (continued)

	x	y	z	U(eq)
H(56B)	6240	5281	8491	89
H(56C)	6370	5787	8789	89
H(57A)	5159	5056	9369	65
H(57B)	6077	5585	9452	65
H(57C)	6192	5023	9558	65
H(58A)	10506	6121	9012	77
H(58B)	10829	5841	9296	77
H(58C)	10736	6475	9370	77
H(59A)	9301	6294	9900	75
H(59B)	9388	5660	9847	75
H(59C)	8288	5818	9842	75
H(60A)	8710	6820	9339	72
H(60B)	7637	6405	9337	72
H(60C)	8188	6430	9010	72
H(61A)	3190	4033	6682	102
H(61B)	3111	3380	6619	102
H(61C)	3386	3742	6974	102
H(62A)	2062	4113	7288	136

Table A10 (continued)

	x	y	z	U(eq)
H(62B)	918	3997	7131	136
H(62C)	1794	4436	7017	136
H(63A)	-426	2961	7351	184
H(63B)	-304	2389	7134	184
H(63C)	-1400	2552	7150	184
H(64A)	-1896	3127	6877	95
H(64B)	-1177	3474	6661	95
H(64C)	-1043	3652	7044	95
H(65A)	1945	1908	7048	233
H(65B)	2488	2528	7033	233
H(65C)	2538	2033	6741	233
H(66A)	558	1418	6535	194
H(66B)	-285	1749	6676	194
H(66C)	416	1528	6912	194
H(67A)	-184	2587	5566	53
H(67B)	62	3201	5498	53
H(68A)	1772	3337	5699	59
H(68B)	1525	2769	5440	59

Table A10 (continued)

	x	y	z	U(eq)
H(69A)	4207	3584	6179	91
H(69B)	3656	3556	5835	91
H(69C)	4765	3413	5860	91
H(70A)	3846	1991	6275	92
H(70B)	4140	2613	6473	92
H(70C)	4889	2387	6220	92
H(71A)	4583	2315	5517	74
H(71B)	3510	2343	5350	74
H(71C)	3610	1827	5509	74
H(72A)	1471	730	5788	96
H(72B)	1724	1141	6129	96
H(72C)	2476	1211	5849	96
H(73A)	-851	1582	5712	111
H(73B)	-538	1448	6050	111
H(73C)	-675	979	5732	111
H(74A)	733	1078	5202	93
H(74B)	1683	1585	5227	93
H(74C)	542	1685	5204	93

Table A10 (continued)

	x	y	z	U(eq)
H(75A)	1871	4381	5915	91
H(75B)	1964	4373	6289	91
H(75C)	1762	4913	6173	91
H(76A)	-289	4862	5783	85
H(76B)	-1145	4304	5716	85
H(76C)	-86	4322	5550	85
H(77A)	110	4598	6682	85
H(77B)	-998	4521	6505	85
H(77C)	-122	5042	6482	85
H(78A)	-2654	3836	6069	122
H(78B)	-2670	3586	6388	122
H(78C)	-3551	3333	6106	122
H(79A)	-3325	2208	6053	121
H(79B)	-2436	2356	6335	121
H(79C)	-2270	2012	5991	121
H(80A)	-2990	2999	5475	114
H(80B)	-2568	2440	5434	114
H(80C)	-1821	3006	5405	114

Table A10 (continued)

	x	y	z	U(eq)
H(81A)	1613	6010	7552	60
H(81B)	934	6102	7258	60
H(82A)	1448	7068	7435	59
H(82B)	877	6787	7707	59
H(83A)	1804	7554	8128	79
H(83B)	2349	7838	7854	79
H(84A)	3340	8130	8351	72
H(84B)	3423	7504	8348	72
H(85A)	4461	8676	8047	66
H(85B)	3921	8316	7711	66
H(86A)	5678	8747	7665	65
H(86B)	6027	8380	7902	65
H(87A)	6887	7887	7497	70
H(87B)	6641	8315	7285	70
H(88A)	5703	7534	6888	89
H(88B)	6899	7530	6924	89
H(89A)	6019	6640	6667	228
H(89B)	6541	6326	6894	228

Table A10 (continued)

	x	y	z	U(eq)
H(90A)	5477	5756	6794	155
H(90B)	4930	6083	6581	155
H(91A)	3412	5510	6649	77
H(91B)	3300	6139	6678	77
H(92A)	1877	5584	6896	62
H(92B)	2673	5516	7169	62
H(93A)	5524	7391	8384	53
H(93B)	6350	7125	8545	53
H(94A)	5222	6237	8418	44
H(94B)	4662	6673	8630	44
H(95A)	2765	6033	8010	48
H(95B)	3085	6040	8377	48
H(96A)	4186	5412	8216	46
H(96B)	3064	5143	8046	46
H(97A)	3825	4602	7616	55
H(97B)	4895	4873	7821	55
H(98A)	4489	5024	7167	65
H(98B)	5572	5259	7371	65

Table A10 (continued)

	x	y	z	U(eq)
H(99A)	5465	4577	6790	65
H(99B)	5540	3963	6818	65
H(10D)	7138	4346	7132	71
H(10E)	7164	4409	6764	71
H(10F)	8676	5293	7053	71
H(10G)	8308	5121	7382	71
H(10H)	8989	6102	7455	65
H(10I)	8085	6143	7209	65
H(10J)	7189	6674	7583	60
H(10K)	8148	6755	7838	60
H(10L)	6208	6127	7973	59
H(10M)	7115	6474	8231	59
H(10N)	2820	3172	8139	218
H(10O)	3296	2658	8197	218
H(10P)	1437	2412	8115	233
H(10Q)	1531	2529	7758	233
H(10R)	715	1650	7571	139
H(10S)	668	1527	7928	139

Table A10 (continued)

	x	y	z	U(eq)
H(10T)	1661	833	7779	148
H(10U)	591	682	7568	148
H(10V)	1257	161	7115	142
H(10W)	2341	263	7313	142
H(11D)	2498	78	6743	127
H(11E)	2094	629	6722	127
H(11F)	3797	1032	6523	142
H(11G)	4149	465	6541	142
H(11H)	5599	1158	6601	167
H(11I)	5451	970	6940	167
H(11J)	6347	1969	7226	215
H(11K)	6511	2049	6864	215
H(11L)	5459	2710	6942	178
H(11M)	6512	2901	7160	178
H(11N)	4530	3249	7308	164
H(11O)	5594	3512	7515	164
H(11P)	4275	3629	7825	161
H(11Q)	4907	3230	7957	161

Table A10 (continued)

	x	y	z	U(eq)
H(11R)	3889	768	8279	62
H(11S)	3416	1227	8149	62
H(11T)	4955	1657	8466	57
H(11U)	5576	1270	8240	57
H(11V)	6000	2481	8336	57
H(11W)	6053	2542	7970	57
H(12D)	7649	2374	8148	56
H(12E)	7083	1822	8258	56
H(12F)	8169	1361	7904	73
H(12G)	8600	1868	7732	73
H(12H)	7220	848	7392	89
H(12I)	7706	1349	7222	89
H(12J)	9336	521	6966	104
H(12K)	8355	740	6865	104
H(12L)	8168	-255	6813	104
H(12M)	8133	-144	7195	104
H(12N)	6343	-796	6776	196
H(12O)	6748	-693	7145	196

Table A10 (continued)

	x	y	z	U(eq)
H(12P)	5077	-927	7055	121
H(12Q)	5100	-373	6922	121
H(12R)	3954	-266	7438	103
H(12S)	4515	227	7276	103
H(12T)	4729	183	7939	90
H(12U)	5429	649	7787	90
H(12V)	5627	5871	10230	87
H(12W)	5704	6410	10506	87
H(13D)	7256	6438	10259	82
H(13E)	6674	6396	9917	82
H(13F)	7724	7271	9866	80
H(13G)	8315	7318	10207	80
H(13H)	7816	8153	10402	74
H(13I)	8450	8200	10093	74
H(13J)	7632	8929	9961	84
H(13K)	7065	8920	10286	84
H(13L)	6143	9295	9922	76
H(13M)	6008	8731	9662	76

Table A10 (continued)

	x	y	z	U(eq)
H(13N)	4160	8623	9681	85
H(13O)	4340	9188	9943	85
H(13P)	3513	8683	10314	84
H(13Q)	2765	8675	10011	84
H(13R)	1697	7811	10063	74
H(13S)	2386	7794	10375	74
H(13T)	1524	6883	10115	71
H(13U)	2097	6963	9797	71
H(13V)	2966	6213	9820	71
H(13W)	2295	6100	10115	71
H(14D)	3847	6225	10453	72
H(14E)	3785	5722	10154	72
H(14F)	2208	7027	8870	83
H(14G)	2679	7672	8985	83
H(14H)	2115	7327	9231	83
H(143)	3009	6394	9214	48
H(144)	4603	6191	9364	62
H(145)	6131	6813	9293	77

Table A10 (continued)

	x	y	z	U(eq)
H(146)	6064	7714	9196	68
H(147)	4472	7929	9127	50
H(148)	4095	7161	10919	65
H(149)	3811	8044	10888	79
H(150)	5208	8742	10820	74
H(15D)	2136	1875	8669	162
H(15E)	2500	2533	8751	162
H(15F)	2019	2213	9019	162
H(153)	3100	1348	9022	67
H(154)	4275	2910	8898	60
H(15G)	2244	5353	5159	78
H(15H)	1620	5075	4821	78
H(15I)	1584	4227	5007	73
H(15J)	2409	4478	5307	73
H(15K)	2433	3523	5088	73
H(15L)	2770	3698	4758	73
H(15M)	4476	3443	4816	80
H(15N)	4045	3209	5121	80

Table A10 (continued)

	x	y	z	U(eq)
H(15O)	5805	3388	5191	72
H(15P)	5427	3846	5448	72
H(16D)	7407	4028	5210	74
H(16E)	7002	4490	5455	74
H(16F)	7931	5545	6126	101
H(16G)	7453	4914	6134	101
H(16H)	7369	5392	6433	101
H(163)	5515	4594	6098	62
H(164)	3946	4691	5894	85
H(165)	3734	5569	5835	92
H(166)	5264	6211	5755	94
H(167)	6845	6114	5950	68
H(16I)	2547	532	5189	63
H(16J)	1808	344	4866	63
H(16K)	3187	691	4573	69
H(16L)	2925	1170	4842	69
H(17D)	4618	1701	4841	65
H(17E)	4924	1224	4579	65

Table A10 (continued)

	x	y	z	U(eq)
H(17F)	6394	1784	4907	72
H(17G)	5904	1588	5216	72
H(17H)	7386	1183	5308	67
H(17I)	7867	1388	4999	67
H(17J)	7782	430	4744	67
H(17K)	8516	596	5068	67
H(17L)	7794	261	5932	121
H(17M)	7336	22	6232	121
H(17N)	7665	674	6256	121
H(176)	6602	1110	5907	60
H(177)	4877	1166	5798	83
H(178)	3566	403	5797	72
H(179)	3977	-440	5853	63
H(180)	5637	-454	6036	54
H(1)	-728	7980	6780	66
H(2)	-109	6956	6418	53
H(3)	2472	8179	6603	54
H(4)	8067	9348	8102	51

Table A10 (continued)

	x	y	z	U(eq)
H(5)	9318	8290	8395	43
H(6)	11109	9657	8463	51
H(7)	7531	4284	8328	49
H(8)	9931	5600	8569	39
H(9)	10778	4622	8202	49
H(10)	1764	3808	6667	54
H(11)	-864	2683	6730	64
H(12)	996	2368	6963	91

VITA

He Qiu was born in Changchun, Jilin Province, P. R. China. After completing his work at the High School of the Northeast Normal University, he was admitted to Jilin University where he studied chemistry and received his Bachelor of Science degree in July 2001. He conducted undergraduate research on the preparation of nanometer-scale polymer materials under the direction of Professor Wanjin Zhang. He Qiu began his graduate studies in chemistry department, The University of Tennessee at Knoxville, in August 2001 and joined Professor Ziling (Ben) Xue's group. He worked on synthesis, characterization and reactivities of Groups 4, 5 and 6 metal complexes.

His next position will be a research scientist at Headwaters Technology Innovation, LLC.